LOW-LATITUDE ELECTRON DENSITY PROFILES OBTAINED BY EMPIRICAL PROCEDURES

OLOGUNLEKO, AMOS OLUSEGUN

A THESIS IN THE DEPARTMENT OF PHYSICS

SUBMITTED TO THE SCHOOL OF POSTGRADUATE STUDIES

TOWARDS THE DEGREE OF

MASTERS OF TECHNOLOGY

FEDERAL UNIVERSITY OF TECHNOLOGY,

AKURE, NIGERIA.

JUNE, 1995

TABLE OF CONTENTS.

ABSTRACT.

A review of ionospheric studies is presented with a view to providing some theoretical background on the variations of the ionosphere with altitude, time of the day, season of the year, geographic or geomagnetic location and solar activity.

The conventional method for investigating the ionosphere is also discussed to show the interrelationship between the ionospheric parameters and to provide the background knowledge for interpreting the results.

The relevant theory on global phenomenological ionospheric models is examined including the International Reference Ionosphere (IRI) to facilitate the comparison of the results of electron density profiles obtained.

The study of low-latitude electron density profiles has been carried out on semi-empirical basis in order to compare the results of observed ionospheric parameters in this region with the International Radio Consultative Committee's (CCIR) predictions.

Ionospheric data from two low-latitude stations at different geographic/geomagnetic locations are drawn for the months of January/February, June and September representative of Winter and Summer seasons respectively. Electron density profiles are computed for different solar activities and time of the day with the relevant ionospheric data as inputs.

The spatial and temporal variations of the low-latitude ionosphere are investigated by a general consideration and evaluation of the experimental electron density profiles obtained. These results are compared with those obtained from

the International Radio Consultative Committee (CCIR) and the International Reference Ionosphere (IRI) models.

The results of the study revealed further the possibility of using simple analytic semi-empirical model to reproduce representative profiles of the equatorial ionosphere. The importance of further comparisons with additional sets of electron density profiles under different solar-geophysical conditions at more ionospheric stations is highlighted.

ACKNOWLEDGEMENTS.

I wish to express my profound gratitude to Prof. L.B Kolawole who suggested the subject of this thesis and provided a wholesome supervision to see it through. His constructive comments and suggestions have been invaluable. I appreciate very much his words of encouragement, assistance and the guidance offered me throughout the research work.

I acknowledge with thanks the assistance received from Dr M.T. Babalola and Mr M.O. Ajewole, both of the Department of Physics, Federal University of Technology, Akure. Their advice, comments and suggestions have been very invaluable.

I am very grateful to Profs P. Bradley of the Rutherford Appleton Laboratory, United Kingdom and D. Bilitza of the Goddard Space Flight Center, Greenbelt, United States of America for their assistance and encouragement during my visit to the International Centre for Theoretical Physics (ICTP), Trieste, Italy in the course of the present work.

The assistance rendered to me by Prof. S.M Radicella of the ICTP is also appreciated. He contributed immensely to the successful completion of the research work.

I acknowledge the immeasurable financial and moral support from my mother, Mrs E.O Ologunleko, without which my academic achievements would have been impossible.

Finally, I wish to express my profound thanks to Elder & Mrs S.B Adejuyigbe, Miss O.F Faseke, Mr F.O Sunmonu, Mrs A.O Famose and Mr S.M Odetokun for their moral support and encouragement.

CERTIFICATION BY SUPERVISOR.

I certify that this work has been carried out by Mr. A.O Ologunleko in the Department of Physics, Federal University of Technology, Akure.

L.B. Kolawole, B.Sc., Ph.D (Ibadan),
Professor, Department of Physics,
Federal University of Technology,
Akure, Nigeria.

June, 1995

DEDICATION.

I dedicate this work to my father, Late Mr E.A Ologunleko who departed this sinful world on 14th November, 1987.

INDEX OF FIGURES.

INDEX OF TABLES

CHAPTER ONE

1.0 INTRODUCTION.

1.1 Historical Survey.

The small daily variations of the earth's magnetic field had been known since the 18th century. Gauss suggested in 1839 that their origin might lie in atmospheric electric currents. In 1860, Lord Kelvin speculated the existence of a conducting layer in connection with the phenomenon of atmospheric electricity.

About 1860, James Clerk Maxwell predicted the existence of electromagnetic waves. The validity of this theory was established by Heinrich Hertz in 1887. By the time Hertz has verified the existence of radio waves, evidence for the existence of the ionosphere had been advanced by Balfour Stewart in 1878.

After some initial experiments in Italy, Guglielmo Marconi on getting to England in 1896 carried out several experiments. With each succcessive experiment, he increaced the distance of transmission. Long distance communication was initiated in 1901 when he achieved successful radio communication across the Atlantic.

In 1902, Kenelly and Heaviside independently suggested that the explanation of Marconi's trans-atlantic success was that the radio waves were returned to the earth's surface after reflection by an electrically conducting layer in the upper atmosphere.

In the meantime, Taylor in 1903 and Fleming in 1906, among others suggested that the conducting layer was produced by the ionizing action of ultraviolet light from the sun on the upper atmosphere. This implied the solar control of radio propagation, which was confirmed as soon as commercial communication links were set up across the Atlantic. The measured strength of the signals was also found to vary in a regular way

throughout the day, season and solar cycle, and to be affected when the earth's magnetic field was disturbed.

The discovery of high-frequency (HF) radio propagation in the early 1920s led to renewed interest in the properties of the Kenelly-Heaviside layer, as the ionosphere was then called. Experiments were carried out by Appleton and Barnett (1924) and Breit and Tuve (1926) to determine the height of the conducting layer. The experiment of Breit and Tuve showed direct evidence of the ionospheric layers and formed the basis for the ionosonde technique.

In the decade beginning in 1930, the ionosonde technique played an important role in the systematic study of the long-term variations in the ionosphere. These long-term studies were undertaken largely by laboratories that have played an important role in ionospheric research over the years. Such laboratories include the Radio Research Station and the Cavendich Laboratory in England, the National Bureau Of Standards and the Carnegie Institution in the United States.

During World War II, ionospheric studies relating to the methods used in applying ionospheric data to radio communication received considerable impetus. Many additional ionospheric sounding stations were set up in order to map the relevant ionospheric characteristics, e.g layer heights and critical frequencies. With this network of sounding stations the geomagnetic control of ionosphere was detected.

Since World War II, considerable progress has been made in the conversion of ionogram data to electron density profiles with much of the development made possible by the advent of high speed electronic computers. Extensive studies were also made of the spatial and temporal variations of different ionospheric layers.

The International Geophysical Year (1957 - 1958) saw the start of the Space Age

with the launching of Sputnik I. The introduction of rockets and satellites caused profound changes in ionospheric investigations by making possible direct measurement of the Sun's ionizing radiations, air density and composition, elecron density, and ion density and composition. Thus launchings of the topside ionosphere above the level of maximum electron density which cannot be observed by ground-based ionosondes are enhanced.

Finally, in the late 1970s advanced digital ionosondes that could serve as scientific research instruments and as routine monitoring devices became available.

1.2 The Ionosphere.

The ionosphere is that region of the earth's atmosphere lying approximately between 50km and about one earth radius (6370km), in which sufficient ionization exists to influence the propagation of radio waves. The presence of free electrons in the ionosphere produces the reflecting regions important to radio propagation.

For convenience in studies of radiowave propagation, the ionosphere is divided into three regions defined according to height and ion distribution - the D, E, and F regions. Each region is sub-divided into layers called C, D, E, F1 and F2, according to height and thickness.

These layers are not distinct but rather overlapping with a complete description being given by an electron density profile. The number of layers, their heights and electron densities vary geographically and with time. The approximate locations of these regions and the layers that may exist within them are given in Table 1

Little is known concerning the detailed distribution of electrons in the D-region. The so-called " C layer "(50 - 70km) is thought to be produced by cosmic rays, whereas the other layers E, F1 and F2 are produced by solar radiation (see section (1.2.2)).

1.2.1 Ionosonde and Ionogram.

Much of the current knowledge of the ionosphere comes from radio probing techniques, although some come from in-situ probe measurements made using artificial satellites. In this work, mention would be made of the use of ground-based swept high-frequency (HF) technique, simply known as the Ionosonde Technique.

An Ionosonde comprises a transmitting, receiving, monitoring and recording sections. The transmitter sends out pulses of electromagnetic energy, so that during an observation (usually lasting for about a minute) it covers a frequency range, e.g 0.5 to 20 MHz.

At the same time, the receiver is automatically held on tune to the swept frequency of the transmitter. The output of the receiver is coupled to a display (usually a cathode ray tube) which makes it possible to measure and record (on a photograph or a cine film) the time delay between the transmitted and returned pulses as a function of the swept frequency of the transmitter.

If the transmitted HF radio energy travels to and back from the reflection point at the same velocity, c, as does light in free space, the time delay, τ can be used to determine the virtual height of the ionized layer.

$$h' = \frac{3\times10^8\,\tau}{2} \quad (m) \qquad \ldots\ldots\ldots (1.1)$$

This height is called "virtual" because equation (1.1) ignores the fact that in an ionized atmosphere, radio pulses travel at the group velocity $u_g < c$.

A plot of the virtual height versus frequency generated from an ionosonde is known as an ionogram. There is a relationship between the critical frequencies (f_c) of each of the ionized layers and their respective maximum electron density (N_{max}) given by

Table 1: Approximate Location Of Ionospheric Regions And Layers And Their Electron Densities

Region	Height	Layer	Approximate Height, km	Approximate Daytime Electron Density, m^{-3}
D	50 to 90	C	65	10^8
		D	75 to 80	10^9
E	90 to 120-140	E_1	110	10^{11}
		E_2		
		Es	100	?
F	120-140 and up	F1, F1½	200	2×10^{11}
		F2	>250	10^{12}

Source: Davies K. (1969)

$$N_{max} = 1.24 \times 10^{10} f_c^2 \quad \ldots\ldots\ldots (1.2)$$

where f_c is measured in MHz.

Typical daytime ionograms from Lindau/Hartz, Germany (52°N , 10°E ; local time 15°E meridian) showing virtual height, h' (km) against frequency, f(MHz) is shown in Fig 1.1(a) and (b).

On the ionogram of 20th september, 1961, the ordinary critical frequencies are f_0E=3.1MHz, f_0F1=4.5MHz, f_0F2=6.0MHz, approximately. The corresponding extra-ordinary critical frequecies are 0.7MHz greater, for example, f_xF2=6.7MHz. There is an E_s (see section (1.4)) layer with f_0E_s=3.4MHz and f_xE_s=4.1MHz. Owing to "blanketing" by E_s (and to absorption), the F1 layer ordinary and extra-ordinary echoes are not seen at frequencies less than 3.4MHz and 4.3MHz, respectively.

On the ionogram of 24th August, 1960, f_0E=2.9MHz and f_0F2=8.3MHz, approximately. There is no dinstinct F1 layer. An E_s layer exists which "blankets" the F-layer ordinary echo between 2.9MHz and 3.3MHz, and the extra-ordinary echo between 3.6MHz and 4.0MHz approximately.

Also, some ionograms recorded from a standard network ionosonde located at Moggill (27.5°S , 152.9°E) in Australia are shown in Fig 1.2.

1.2.2 The Regular Ionospheric Regions.

Ionograms usually provide information on the E and F regions. Examples of ionograms showing normal E and F traces for Ibadan are shown in Fig (1.3). The variation of electron density with true height corresponding to the E and F traces is illustrated in Fig (1.4). The maximum ordinary mode frequencies reflected by the E and

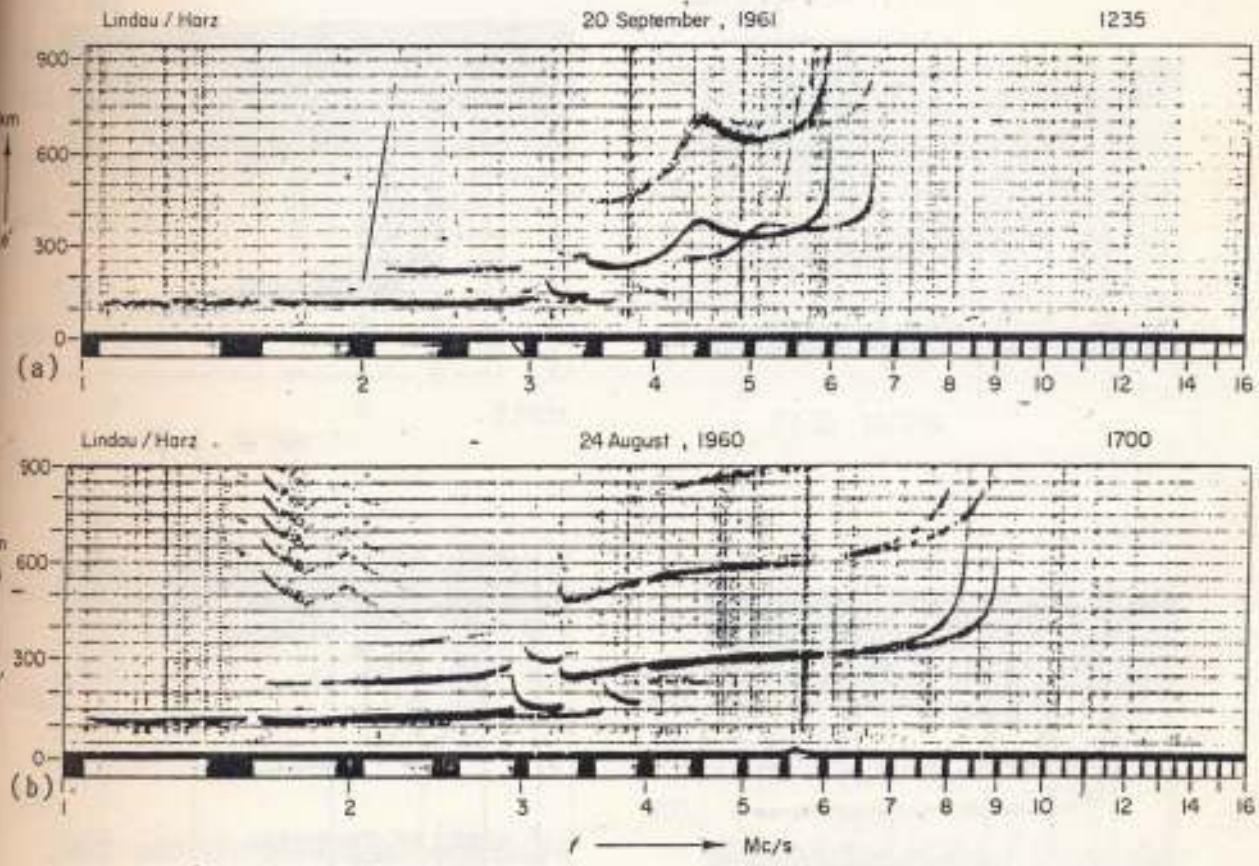

Fig 1.1

Daytime ionograms from Lindau/Hartz, Germany

Source: Rishbeth H. and Garriott O.K (1969)

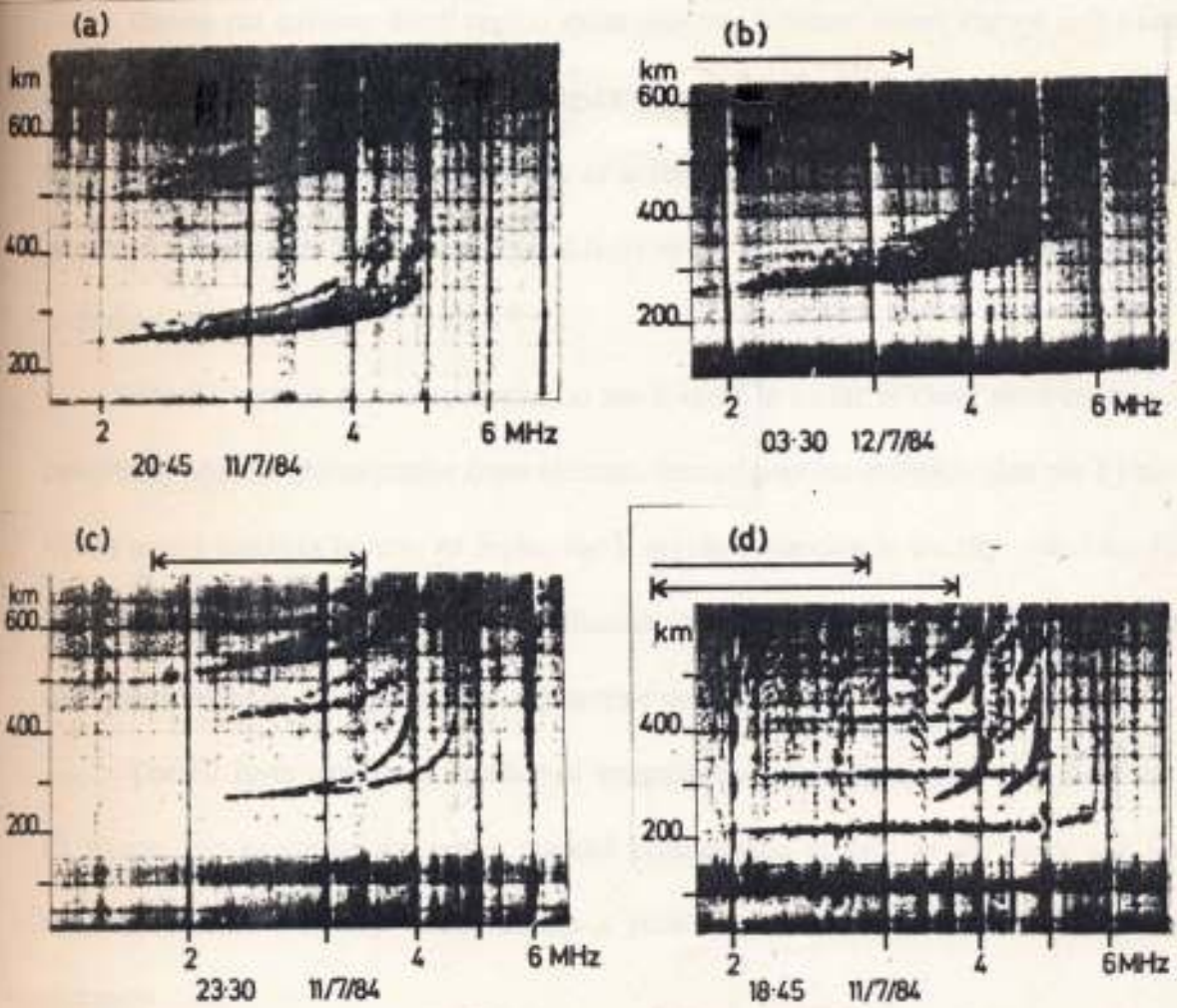

Fig 1.2 Some examples of standand Ionograms recorded at Mogill

Source: Bowman G. G et al (1986)

F regions otherwise known as critical frequecies are denoted by f_0E and f_0F2 respectively while their true heights are denoted by h_mE and h_mF2 respectively.

Historically, the first layer of the ionosphere discovered was the E layer. The E layer is always present by day at all seasons, and in all geographic locations, and its behaviour is subject to close solar control.

During the daytime the F region splits into two seperate layers known as F1 and F2 layers. At night , the D, E and F1 layers disappear almost completely while the F2 layer exists throughout the night though in a somewhat depleted fashion. This is one reason why F2 layer is the most important layer as far as high frequecy (HF) propagation is concerned.

The F1 layer is generally similar to the E layer in so far as close solar control is concerned. Most of the evidence from electron density profiles indicates that the F1 and F2 are rarely dinstinct layers. At night, the F region ionization is usually called the F2 layer, but this is often a matter of definition, since the night F-layer is sometimes continuous with the F1 layer across the sunrise period.

The F2 layer exhibits a number of irregularities when compared with the E and F1 layers. For example, there is a marked geomagnetic control of the layer and the maximum electron density often reaches a peak value, not at noon, but late in the afternoon.

In the D region, the pressure is large and collisions are dominant so that the usual techniques of studying the ionosphere are not applicable. For instance, ionosonde sounding is not possible because the collision frequency exceeds the critical frequency in general which means that absorption is heavy at all reflected frequencies. Consequently, rocket techniques have been particularly important in this region.

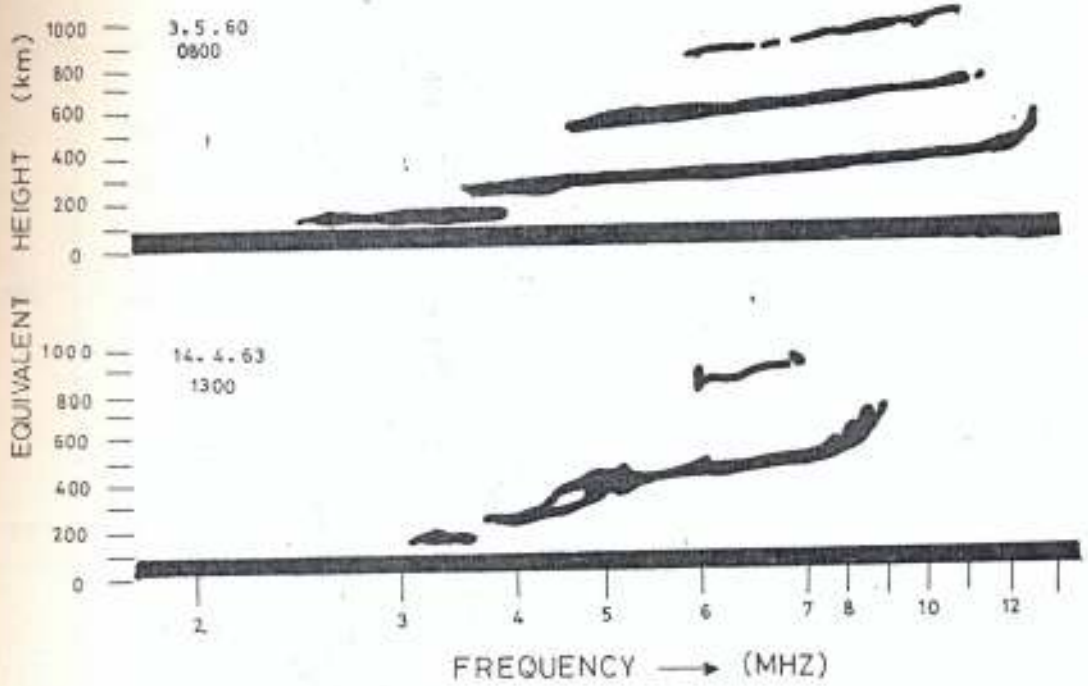

Fig. 1.3 Ionograms Showing Normal E and F Traces For Ibadan

Source: Oyinloye J.O (1978)

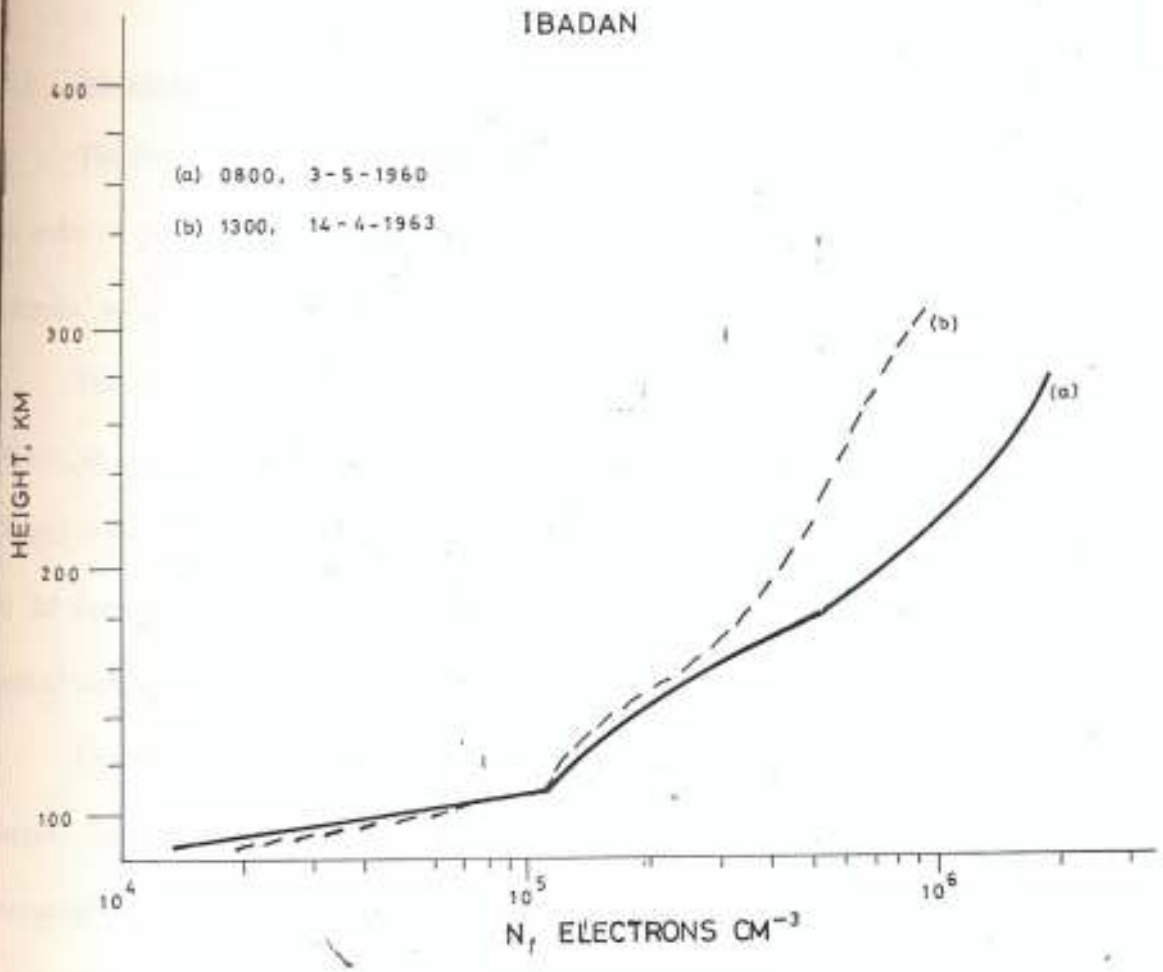

Fig. 1.4 Electron density profiles corresponding to the ionogram traces for Ibadan

Source: Oyinloye J.O (1978)

From the point of view of radio communication, the D region is of great importance because most of the absorption of medium and high frequency radio waves occurs in that layer.

1.3 Ionospheric Variations.

The five main variations of the ionosphere which must be taken into consideration in order to predict HF propagation conditions successfully are the diurnal, seasonal, location, solar activity and height variations.

The ionosphere varies with height ranging from D layer at the height range 50 - 90 km, up to the F layer at 140 to 600 km. The E layer lies between 90 and 140 km. The F layer is divided into F1 and F2 layers. Fig(1.5) shows the sketch of the various regions of the ionosphere as it appears during the day and night. The altitude regimes of the neutral atmosphere are also shown for comparison.

The diurnal variations of the critical frequencies of D, E and F1 layer is very simple. These layers are not there at night (Fig(1.5)) and during the day, their critical frequencies depends almost exclusively on the solar zenith angle (χ). However, the F2 layer differs from the F1 in that it exists during the nighttime.

The critical frequencies of the E and F1 layers are given by the following relationships

$$f_0E = 0.9[(180 + 1.44R)\cos\chi]^{1/4} \quad MHz \quad \ldots\ldots\ldots (1.3)$$

and

$$f_0F1 = (4.3 + 0.01R)\cos^{0.2}\chi \quad MHz \quad \ldots\ldots\ldots (1.4)$$

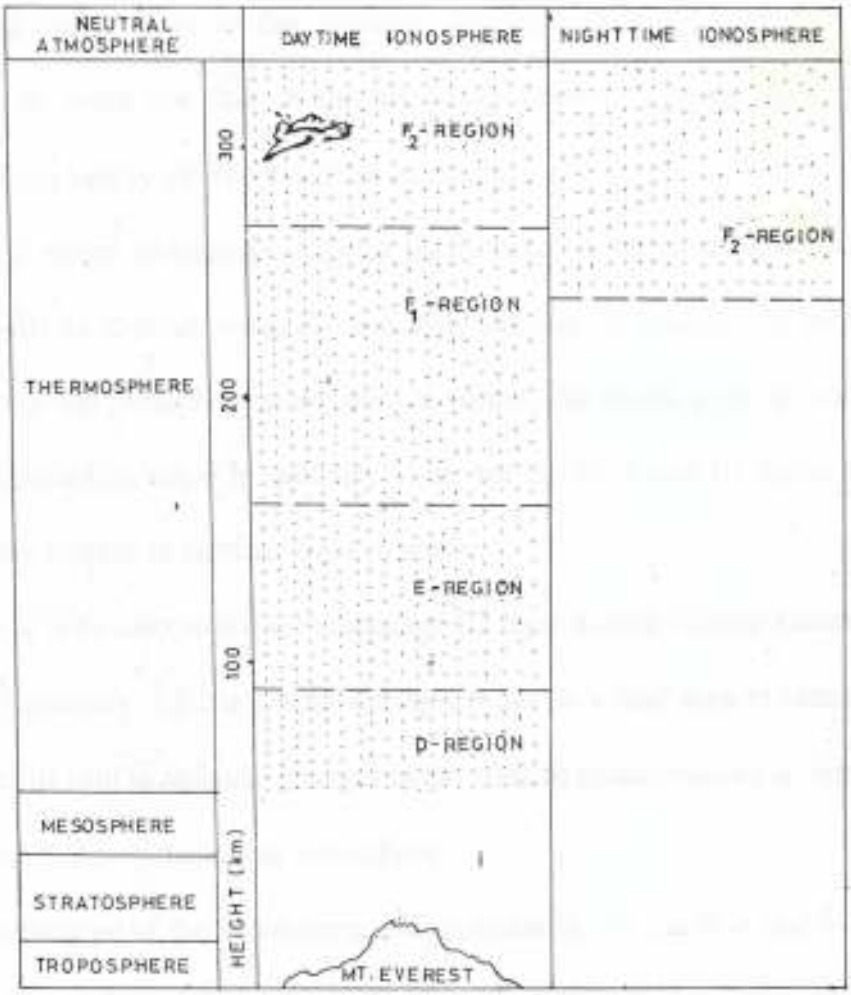

Fig 1. 5 Sketch of various ionospheric layers and their height regimes

Source: Mc Namara L.F (1991)

where R is the sunspot number.

These are empirical equations which fit the observations of f_oE and f_0F1 fairly well. In practice, somewhat complex formulas are used.

Consequently, the critical frequencies f_oE and f_oF1 reach their greatest value at noon and drop to zero at night. f_oF2 reaches its lowest value just before dawn, recombination having eaten away at the electrons at night. Also f_oF2 reaches its maximum value not at noon but late in the afternoon since f_0F2 rises rapidly as photoionization creates a supply of free electrons at sunrise.

The ionosphere varies throughout the year partly because the solar zenith angle has a seasonal as well as diurnal variation and also because of changes in neutral atmosphere from which the ionosphere is created. In winter, the zenith angle is always greater than the corresponding angle in summer. Thus, for the D, E and F1 layers, the critical frequencies are greater in summer than in winter.

However, there is an unexpected difference for F2 layer at mid-latitude known as mid-latitude seasonal anomaly. f_0F2 is greater during the day in winter than in summer. This phenomenon has its root in seasonal changes in the relative concentrations of atomic and molecular species that constitutes the ionosphere.

Part of the variations of the ionosphere with position on the earth is due to the variation with solar zenith angle (Fig 1.6(a)). Geomagnetic latitude and longitude are measured in the same way as the geographic latitude and longitude but using the geomagnetic poles and equator. The strength of the geomagnetic field is conveniently measured in terms of the electron gyrofrequency.

Another interesting feature of the geomagnetic field is the dip angle of the field which varies over the surface of the earth (Fig 1.6(b)). The behaviour of the ionosphere

at low latitudes depends to a large extent on the dip angle. At mid-latitudes there are significant differences between the ionosphere at geographically equivalent points in the northern and southern hemispheres simply because the geomagnetic field is different at the two points.

The ionosphere varies with changes in solar activity. The sunspot number is one of the parameters most widely used to describe the behaviour of the Sun as it affects the ionosphere. The relative sunspot number is given as,

$$R = C\,(\,10G + F\,) \qquad \ldots\ldots\ldots\ldots (1.6)$$

where F is the total number of spots including those in the group, G is the number of sunspot groups and C is a constant adjusted over a long period of time to give as good a fit as possible to a standard observing point.

The sunspot number varies as the Sun rotates and also varies from zero to a value around 100 every 11 years, known as a solar cycle. It is found that the monthly median value of the critical frequencies of the ionosphere for a particular month is linearly related to the monthly average value of the sunspot number smoothed or averaged over 12 months, R_{12}.

1.4 Ionospheric Irregularities.

Very often, the ionosphere departs from an equilibrum state described in theory. Such phenomenon as spread-F irregularities, electrojet irregularities and travelling ionospheric disturbances (TID's) are manifestations of the non-equilibrum state of the ionosphere. Studies of ionospheric irregularities are important for several reasons:

_ irregularities influence radio communications.

FIGURES 1.6 (a) & (b)

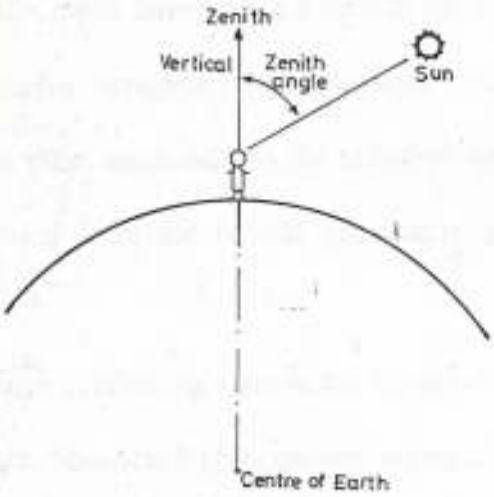

(a) Variation of ionosphere with Zenith angle

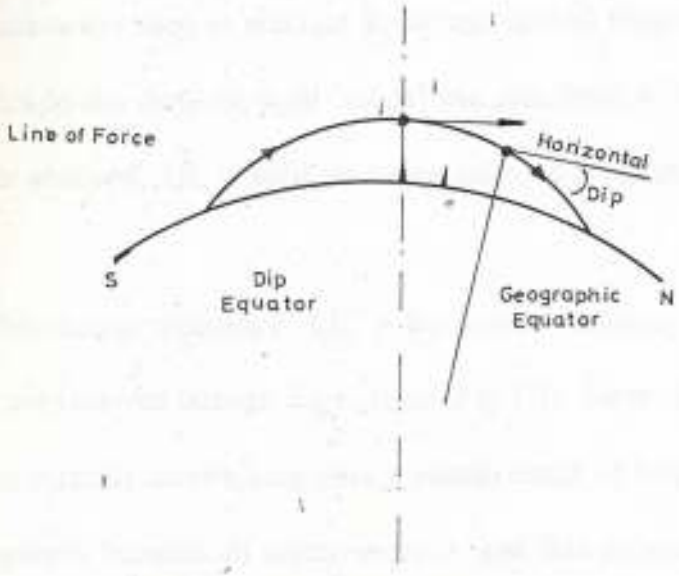

(b) Variation of dip angle over the surface of the Earth

Source : Mc Namara L.F (1991)

_ irregularities affect the gross dynamics of the ionosphere through the re-distribution of plasma, energy and momentum.

_ irregularities can be used as a diagnostic for equilibrum ionospheric conditions.

_ basic plasma physics could be tested in a neutral environment.

At the D-region heights, irregular plasma structure is related to the neutral atmosphere turbulence. The main mechanism is the turbulent mixing in the presence of the electron gradient different from the neutral air density gradient or temperature gradients.

Ionosondes often detect a reflecting layer in the ionosphere which comes and goes sporadically at E-layer height. Sporadic E (E_s) consists largely of relatively dense patches of electrons of the order of a few tens of kilometers in horizontal extent and occurs at altitudes between 90 and 130km. E_s is most often observed in summer season, in areas near the magnetic equator and in auroral zones.

The parameters used to describe E_s include critical frequencies f_0E_s and f_xE_s. E_s ionogram traces do not show the usual "cusps" and sometimes a "top frequency" at which reflections are obtained, f_tE_s is used. In many cases, it is assumed that f_tE_s is equal to f_xE_s.

The "blanketing frequency" f_bE_s is the lowest frequency at which echoes from higher layers are received through the E_s layer (Fig 1.7). Generally, $f_bE_s < f_tE_s$, so that the E_s layer is partially transmitting over a (small) range of frequency. Sometimes, the E_s layer completely blankets all layers above it, and thus prevents observation of the F layer.

Another parameter is the virtual height $h'E_s$ which is usually independent of frequency over most of the trace in which case it should be nearly equal to the actual

height of the E_s layer. It is however pertinent to note that all E_s cannot be explained by a single grand theory.

Mid-latitude E_s is essentially a daytime summer phenomenon, occuring most often at these times and with the highest critical frequencies. Mid-day values of f_0E_s during the summer reach about 10MHz. At least some mid-latitude E_s are thought to be caused by high altitude winds blowing in opposite directions and compressing the very fine debris of meteors into a narrow sheet.

Low-latitude E_s is essentially a daytime phenomenon with little seasonal variation and the initial frequencies are higher than at mid-latitudes. Near the geomagnetic equator, the critical frequency f_0E_s exceeds 5MHz for 90% of the time during daytime (McNamara,1991).

Near the geomagnetic equator, a dinstinctive type of "equatorial" E_s is observed which is patchy and transparent to waves reflected from higher layers. It is strongly associated with the "electrojet" current which flows along the geomagnetic equator by day. The equatorial E_s irregularities appear to be aligned with the geomagnetic field and may be caused by plasma instabilities arising from the flow of large electrojet current. Vertically incident signals are little affected by Equatorial E_s.

High latitude E_s associated with aurora also has little seasonal variation but it occurs most often at night. Critical frequencies greater than 5MHz are observed for more than 50% of the time prior to midnight and somewhat less often from midnight to dawn.

As if the F-region were not complicated enough, nature conspired to make it even more complicated at night by sometimes causing the ionization to break into small branches of electron, rather than stay in a uniform, homogeneous sea of electron. These bunches of electrons are known as irregularities because when they exist, the distribution

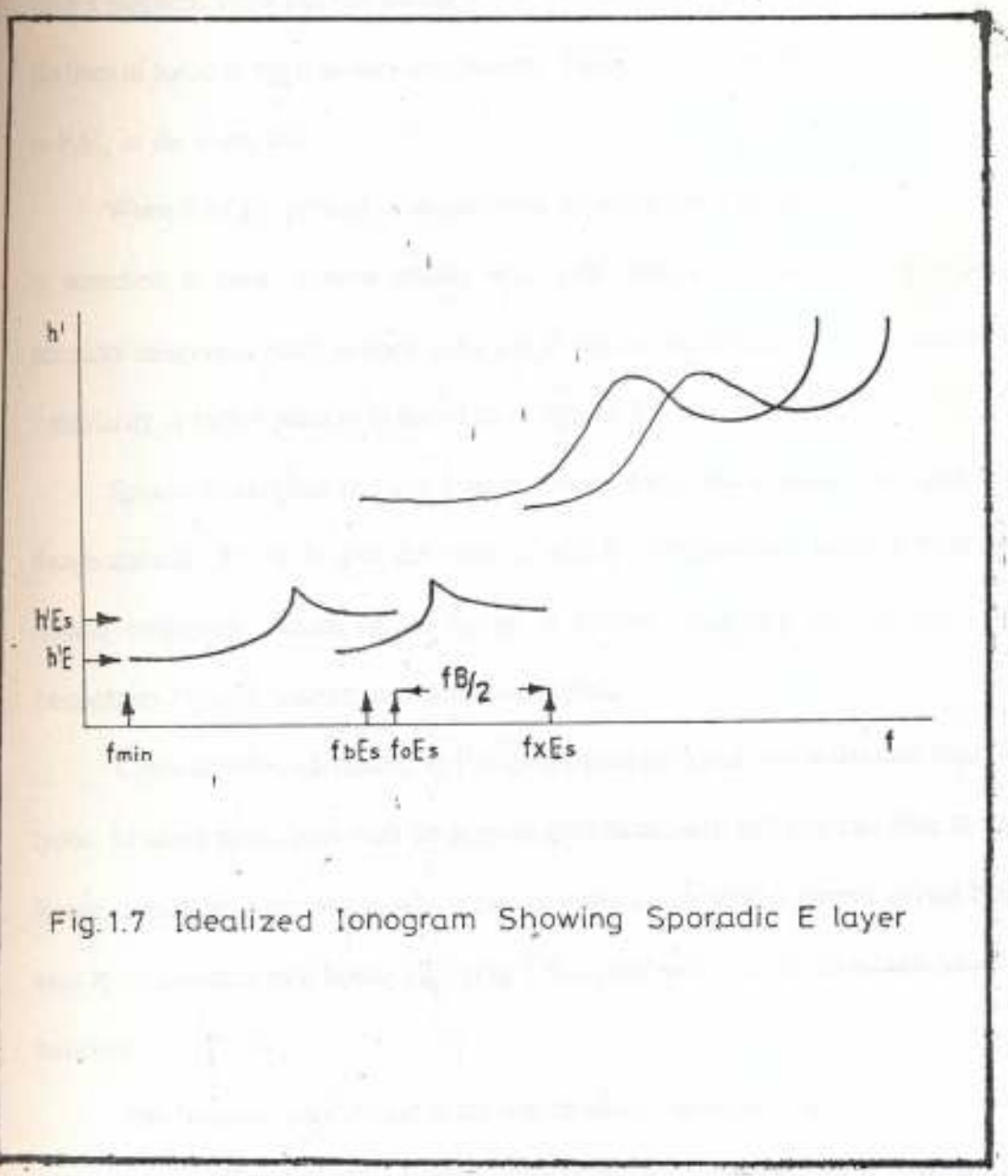

Fig.1.7 Idealized Ionogram Showing Sporadic E layer

Source: Piggott W.R and Rawer K.(1979)

of ionization in the F-region is no longer a regular phenomenon.

Since electrons are free to move at will up and down along lines of force of the earth's magnetic field but not across them, the irregularity become stretched out along the lines of force as soon as they are created. This is known as Field Alined Irregularities or FAI, in the F-region.

When FAI are present, a single pulse reflected from the ionosphere will be spread or stretched in time, echoes arising with time delay significantly longer than those normally observed. Such echoes from the F region are called spread-F echoes and the irregularity is rather loosely referred to as spread-F.

Spread-F irregularities can lead to echoes which are stretched in range known as Range Spread. There is also the case in which irregularities cause spreading at the critical frequency, which is no longer a simple frequency but covers a band of frequencies. This is known as Frequency Spread.

Consequently, spreading of F region traces on ionogram is divided into two main types. In some cases both may be present simultaneously and one can lead to the other. Range spreading is the one in which two or more traces with different virtual heights are seen at frequencies well below f_0F2 (Fig 1.8(a)) and which seems to be prevalent at lower latitudes.

The frequency spreading is the one in which the high frequency ends of the traces are blurred or branched (Fig 1.8(b)). This is the type mostly seen at high latitudes and the range Δf of frequency covered by the "spreading" is related to the fractional deviation of electron concentration within the irregularity as,

$$\frac{\Delta f}{f_0 F2} \approx \frac{1}{2}\frac{\Delta N}{N} \qquad \ldots\ldots\ldots\ldots (1.7)$$

In general, Spread-F at low and mid-latitudes occur at night, whereas at high latitudes it can occur during the day. Range spreading and Frequency spreading of echoes seem to have different causes in that they have different variations with location on earth, level of solar activity, season and time of the day.

Another feature of the ionospheric F-region is the presence of travelling ionospheric disturbances (TIDS) which are the ionospheric response to atmospheric gravity waves (AGWs). In other words, TIDs are wavelike motions of the ionosphere attributed to the passage of waves through the neutral atmosphere and coupling between the ionosphere and neutral atmosphere.

TIDS are present to some degree at all times of the day and night, but are particularly noticeable during daylight hours. TIDs have wavelengths of the order of 500km and travel apparently in a horizontal direction at speeds of 5 - 10km per minute.

TIDs are divided into two groups namely: Large scale TIDs (LSTIDs) and medium scale TIDs (MSTIDs). Auroral generated LSTIDs have periods in the range 0.5 - 0.3hr and speeds exceeding 400m/s while MSTIDs have periods in the range 0.25 - 1hr and speeds of 100 - 250m/s. TIDs usually have well-defined direction of travel which varies diurnally and seasonally in reasonably predictable ways.

1.5 The Scope Of The Present Work.

Ionosondes are employed as probes of the E- and F-regions of the ionosphere. Unfortunately, they do not directly give the distribution of electron concentration as a function of the true height but in terms of the virtual height of reflection of the probing waves. However, true height data are needed for morphological studies and for investigation of radio propagation phenomenon.

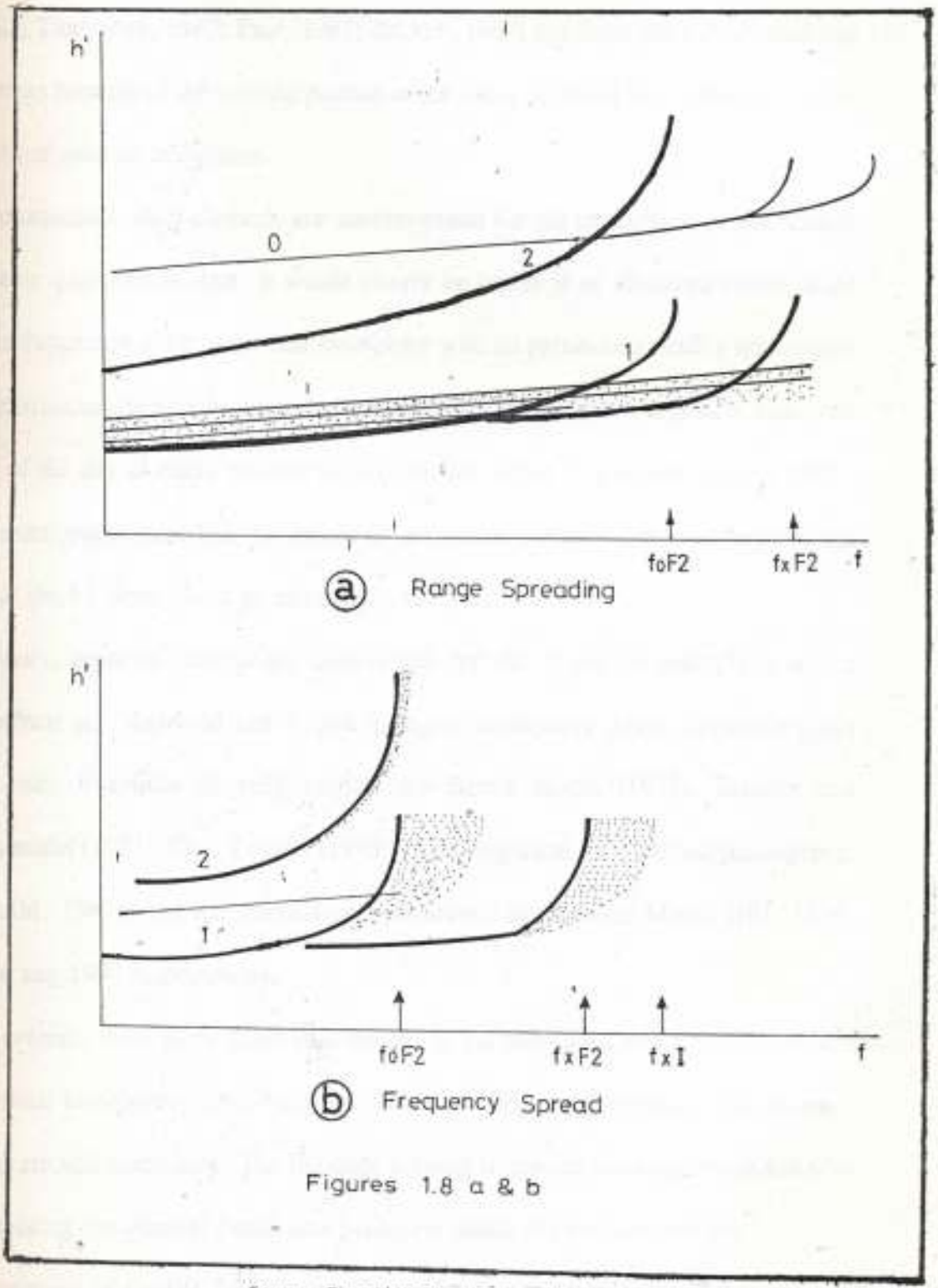

Figures 1.8 a & b

Source : Piggott W. R and Rawer K. (1978)

A number of procedures have been developed to convert virtual to true height profiles (E.g Titheridge, 1967; Paul, 1967; Becker, 1967) but these are complicated and liable to errors because of the missing portion of the ionograms and time consuming even with the aid of modern computers.

Consequently, such methods are uneconomical for the production of statistically representative quantities of data. It would clearly be useful if an idealized model could be developed approximating to the real ionosphere with its parameters readily determined from the internationally agreed ionospheric characteristics which are regularly measured each hour of the day at many stations throughout the world (Pigott and Rawer, 1972). Thus important parameters like the height of maximum electron concentration and the thickness of the F2 layer could be estimated.

Usually, separate models are constructed for the D region ionosphere where dynamic effects are neglected and E and F region ionosphere where dynamics plays important role. Examples of such models are Bent's model (1972), Bradley and Dudeney's model (1973), Chiu's model (1975), Semi-empirical Low Latitude Ionospheric Model (SLIM, 1987), and the International Reference Ionospheric Model (IRI, 1976, 1979, 1986 and 1990 respectively).

At present, there is no doubt that the IRI is the most advanced empirical model of the terrestial ionosphere. Over the years, there had been improvements and reviews. Discussions are still continuing. The IRI code is being improved more and more and new options are being introduced. Some new problems which are encountered are discussed at yearly meetings of the IRI Task Group. For example, the most recent IRI meeting on "Low and Equatorial Latitudes in IRI" was held at the National Physical Laboratory in New Delhi, India from 9th to 13th January, 1995.

The objective of the present work is to compare the electron density profiles obtained using the experimental values of the F2 peak electron density and height as inputs into the IRI90 model with the profiles obtained using the CCIR coefficients of f_0F2 and M(3000)F2.

The comparison would provide information on the correction needed to improve CCIR predictions and electron density profile estimates through the IRI model. The CCIR coefficients are incorporated into the IRI model so as to be used in all cases where there are dearths of ionosonde or where the values of ionospheric parameters f_0F2 and h_mF2 are not available.

CHAPTER TWO

2.0 ELECTRON DENSITY PROFILES AND MODELS.

2.1 Electron Density Distribution.

Considerable analysis is needed to obtain the vertical electron distribution, N(h) profile from h'(f) curves. The virtual height (or group height), h' and the real height h at which a signal of frequency f is refracted are connected by an equation that depends on the electron distribution below the refraction point;

$$h' = \int_0^h \mu'(f, N)\, dh \qquad \ldots\ldots\ldots\ldots (2.1)$$

since the group refractive index $\mu' \geq 1$,the group height $h' \geq h$. The equation is solved to obtain N(h) by writing it as an integral with respect to the plasma frequency instead of height (which assumes that N and f_N vary monotonically with height).

$$h'(f) = \int_0^f \mu'\left(\frac{dh}{df}_N\right) df_N + h(0) \qquad \ldots\ldots\ldots (2.2)$$

where h(0) is the height of the base of the ionosphere below which it is assumed that $f_N = 0$. At this base the real and virtual heights are equal.

The availability of electronic computers has made obsolete the earlier methods in which a special form, such as a parabola, is assumed for the N(h) profile. The methods of solving the integral equation (2.2) fall into two main classes; "lamination" and "polynomial" methods.

For a method of N(h) analysis to be suitable for recommendation to users other than the originator, it must satisfy, at least, the following conditions:

(1.) It should have been found reliable in all the tests conducted, these being

assumed representative of typical ionospheric conditions.

(2.) The corresponding computer program should be

(a) readily available in a standard computer language

e.g. FORTRAN.

(b) well documented,

(c) well commented throughout,

(d) easy to use,

(e) fast,

(f) as small as possible,

(g) provided with a complete set of test data and

results.

(3.) The method should have well-defined and automatic default procedures for use when there is insufficient information in the ionogram (such as no suitable X traces for use in starting and valley corrections).

2.1.1 Lamination Method.

Lamination method, represented by the "matrix method" of Budden (1955) replaces the integration in (2.2) by a summation over a number of thin slabs, each corresponding to a discrete interval of plasma frequency. For this purpose, some simplifying assumptions are made, the simplest being the gradient dh/df_N is constant within each slab so that the function $h(f_N)$ is represented by a series of linear-segments.

Suppose there are n slabs, and that h'(f) is the virtual height for the frequency f_i reflected at the top of the i^{th} slab, at a real height h_i, we can then form a set of $n+1$ equations such as

$$h'(0) = h(0)$$

$$h'(f_1) = h(0) + \frac{h(f_1) - h(0)}{f_1 - 0} \int_0^{f_1} \mu'(f_1, f_N)\, df_N$$

$$h'(f_j) = h(0) + \sum_{i=1}^{j} \frac{h(f_i) - h(f_{i-1})}{f_i - f_{i-1}} \int_{f_{i-1}}^{f_i} \mu'(f_j, f_N)\, df_N \quad \ldots (2.3)$$

Additional equations are written up to j = n (note that $f_{i-1} = 0$ for i = 1). By using the abbreviation,

$$M_{ji} = (f_i - f_{i-1})^{-1} \int_{f_{i-1}}^{f_i} \mu'(f_j, f_N)\, df_N \quad \ldots . (2.4)$$

we can write the equations compactly in the form,

$$h'(f_j) - h(0) = \sum_{i=1}^{j} [\, h(f_i) - h(f_{i-1}]\, M_{ji} \quad \ldots \ldots \ldots \ldots (2.5)$$

or

$$h^{*'} = \sum_{i=1}^{j} (\Delta h_i) M_{ji} \quad \ldots \ldots \ldots \ldots \ldots \ldots (2.6)$$

$h^{*'}$ is the virtual height at frequency f_i measured from h(0), the base layer; Δh_i is the real width of the i^{th} slab; while M_{ji} is the average value of μ' within the i^{th} slab for waves of frequency f_j. This equation can obviously be written in matrix form,

$$h^{*'} = M \,.\, \Delta h$$

its solution being,

$$\Delta h = M^{-1} \cdot h^{*'}$$

From the inverted equation, which gives the width of each slab, the height is obtained as,

$$h_j = h(0) + \sum_{i=1}^{j} \Delta h_i \qquad \ldots\ldots\ldots\ldots\ldots\ldots\ldots\ldots (2.7)$$

Given the necessary data to evaluate the matrix elements for the required location, equations (2.6) and (2.7) may be solved conveniently with the aid of a computer to obtain the real height h_j for the plasma frequencies f_j.

2.1.2 Polynomial Method.

In the polynomial method of Titheridge (1961), it is assumed that the function $h(f_N)$ can be represented by a polynomial in f_N. Using h^* and $h^{*'}$ to denote real and virtual heights measured from the base level h(0), we write,

$$h - h(0) \equiv h^* = \sum_{i=1}^{n} \alpha_i f_N^{i-1} \qquad \ldots\ldots\ldots\ldots\ldots\ldots\ldots\ldots (2.8)$$

The first set of sampling frequencies $f_1, f_2, ----, f_n$ is chosen. Then the heights h_i^* at which the plasma frequency takes the values f_i can be included in a matrix equation,

$$h^* = A \cdot \alpha$$

in which each element of the column matrix α is the coefficient appearing in equation (2.8), and the element A_{ij} is equal to f_i^{j-1}. Now the set of virtual heights at frequencies f_i can be written as,

$$h^{*'} = B \cdot \alpha$$

in which the elements of B contain integrals with respect to frequency of the group refractive index . Hence,

$$h' = AB^{-1} \cdot h''$$

The elements of the matrix AB^{-1} depend on the frequencies f' and the parameters of the geomagnetic field and can be computed for a given location and a given set of sampling frequencies. Thus sets of values of h' and h are connected by a matrix equation, as in the lamination method.

Whereas the lamination method represents the function $h(f_N)$ by a series of linear or other specially shaped segments, the polynomial method assumes that a smooth polynomial of degree $(n+1)$ in f_N can be drawn to pass through n sampling points (h_i, f_i), although the coefficients of this polynomial are not required to be known.

For a given method of sampling points, the polynomial method gives greater accuracy than the lamination method.

2.2 Problems in N(h) Analysis.

Even when very accurate virtual heights are available, there exist two fundamental problems in real-height or N(h) analysis. These are referred to as the "starting" problem and the "valley" problem and both are manifestations of incomplete data.

2.2.1 The Starting Problem.

Conventional ionosondes have a lower frequency limit, usually about 0.5 - 1.0 MHz, and record no echoes below this limit. Thus with practical ionograms, the accuracy of a calculated N(h) profile may be severely restricted because reflections are not obtained below some limiting frequency f_{min}.

This limit is set by choice, the broadcast station interference, the output power of the ionosonde, the antenna system, or by the rapid increase of absorption towards the

lower frequencies. Each of these effects leads to what is known as the "starting problem" in N(h) analysis.

2.2.2 The Valley Problem.

The "valley" or decrease of electron density between the E- and F- layers of the ionosphere has long been a problem in the analysis of ground-based ionograms. The simpler ionogram reduction techniques have generally ignored the valley, assuming that the electron density increases monotonically with height.

This assumption, or the use of some assumed valley size is necessary if only ordinary-ray virtual data are available, since there is an infinite number of valleys that can satisfy the data. More sophisticated techniques involve analysing the ionogram by normal monotonic methods up to the E layer, followed by a special restart procedure.

The valley problem is essentially a daytime problem, since at night $foE < f_{min}$ for most ionogram and any valley problem is subsumed by the starting problem. The techniques used to overcome the valley problem are usually quite similar to those used for the starting problem and depend on the use of X-ray data above f_xE.

In the absence of such data, it is necessary to assume that there is no valley (that is, the profile is monotonic) or to assume some synoptic value of the valley shape.

2.3 Models Of Electron Density In The Ionosphere.

The actual distribution with height of ionospheric electron density is very complicated and cannot in general be expressed in terms of simple mathematical functions. Even in the case of relatively simple layers, it is almost impossible to find analytical solutions to radio propagation integrals. For many purposes, especially those

of academic interest, it is preferable to employ models of electron density profiles which results in integrable expressions when combined with propagation equations. Model layers are used in the calculation of ray paths, phase and group paths, absorption, polarization and so on. Some sample model layers are shown in Fig 2.1.

In addition, some phenomenological electron density models and profiles are presented in this section.

2.3.1 Linear Layer.

Over sufficiently small height ranges, except near the peak, any electron density profile can be approximated by linear segments of the form,

$$N - N_0 = a(h-h_0) \qquad \text{------(2.9)}$$

where a is the electron density gradient and N_0 is the density at the reference height (see Fig 2.1a).

The linear layer is useful in practice because a more realistic layer can be divided into a large number of thin linear slabs. Each slab can then be dealt with successively.

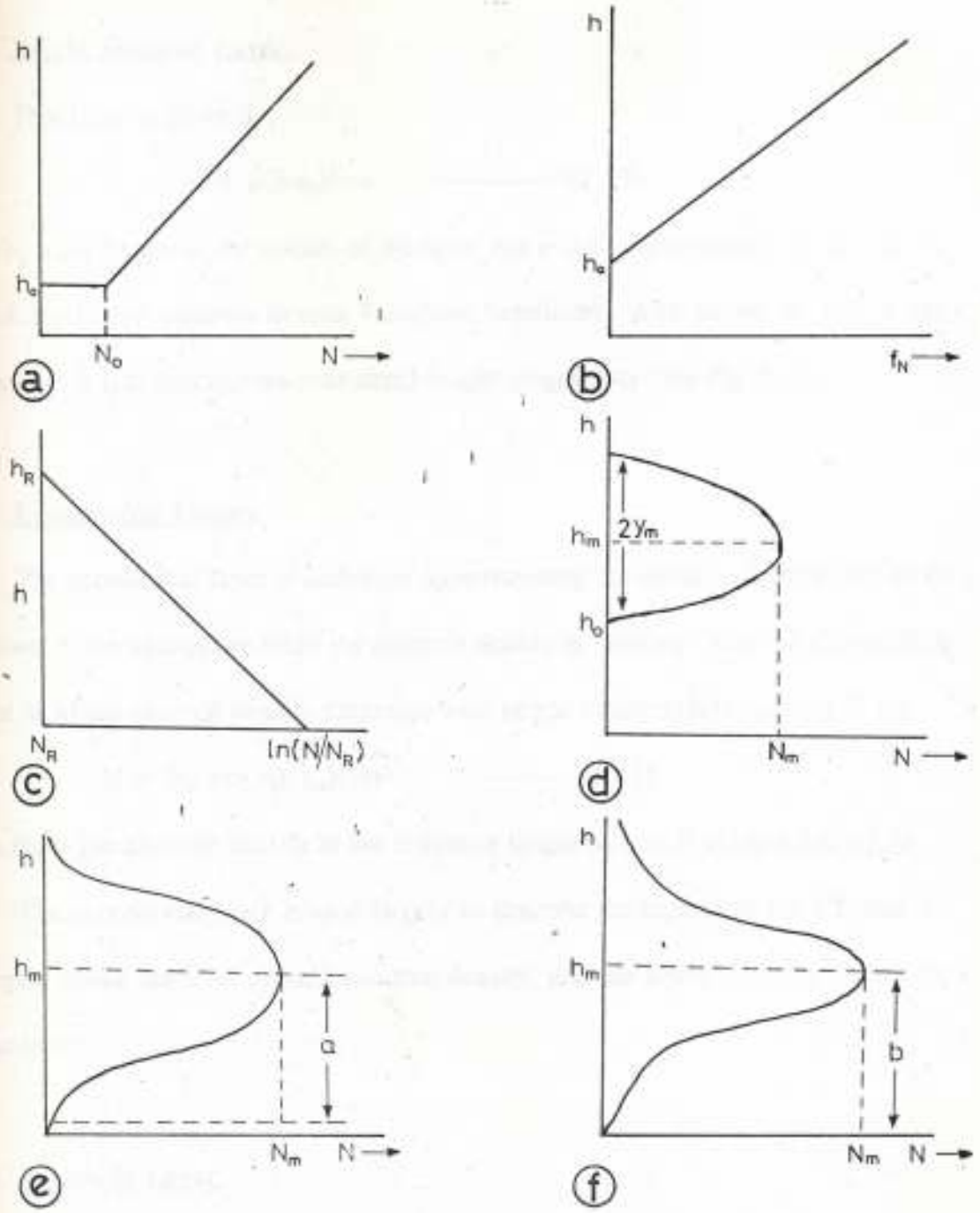

Fig. 2.1 Sample Of Some Ionospheric Model - Layers

Source: Davies K. (1969)

2.3.2 Height Squared Layer.

This layer is given by,

$$N = \alpha(h-h_0)^2 \qquad \text{----------(2.10)}$$

where h_0 is the height of the bottom of the layer and α is a proportionality factor. In this type of layer, the electron density increaces indefinitely with height so that it can approximate a real distribution over small height ranges only (see Fig 2.1b).

2.3.3 Exponential Layer.

The exponential layer is useful for approximating the electron density high up or low down in the ionosphere when the electron density is "trailing" away. An example is a layer in which electron density decreases with height exponentially (see Fig 2.1c).

$$N = N_R \exp -(h-h_R)/2H \qquad \text{----------(2.11)}$$

where N_R is the electron density at the reference height h_R and H is the scale height.

The exponential layer is used largely to describe the topside of the F2, that is , the region above the level of peak electron density, and the lower E region (below the 100km level).

2.3.4 Parabolic Layer.

This approximation is of great value in describing the profile near the maximum of electron density, the so-called "nose" of the layer (see Fig 2.1d). Its of the form,

$$N = N_0 [\ 1 - ((h-h_0)/2H)^2\ ] = N_0 [\ 1 - ((h-h_0)/y_m)^2\ ] \text{-------(2.12)}$$

where $y_m = 2H$ is the semi-thickness of the parabola, that is, half the distance between the heights at which the electron density is zero. N_0 is the maximum electron density of the layer at height h_0. However, it is common to express parabolic distribution in terms

of the height h_0 of the bottom of the layer and the maximum electron density N_m as follows:

$$N = N_m [2(h-h_0)^2/y_m - ((h-h_0)/y_m)^2] \quad \text{--------(2.13)}$$

2.3.5 Cosine Layer.

For some purposes, the parabolic profile is unsatisfactory because it has discontinuities of electron density gradient at the top and bottom of the layer (see Fig 2.1e). The cosine layer is given by,

$$N = 1/2 [N_m (1 + \cos\pi(h-h_m)/a)] \quad \text{---------(2.14)}$$

where a is the half-thickness of the layer. The top and bottom of the layer are at $h_m \pm a$.

2.3.6 Sech-squared Layer.

This layer also is free from discontinuities in electron density gradient at the top and bottom of the layer (see Fig 2.1f). The profile is given by,

$$N = N_m \, \text{sech}^2 ((h-h_m)/2b) \quad \text{----------(2.15)}$$

where b is a scale factor. This profile has no zero of electron density.

2.3.7 Bent's Model (Bent et al., 1972).

This is purely a phenomenological electron density model deduced from satellite measurements. F2 peak layer models and profiles are obtained from ground stations (only in the American sector).

The model covers the altitude range from 150 to 1000km. The F2 peak density is computed from the CCIR f_oF2 maps and h_m from M(3000)F2 predictions. In fig 2.2,

$y_t = y_m$ for $f_0F2 \leq 10.5MHz$ ----------(2.16a)

$y_t = y_m [1 + 0.133333 (f_0F2 - 10.5)]$

for $f_0F2 > 10.5MHz$ ----------(2.16b)

The constants K_1, K_2, and K_3 vary with season, latitude, altitude, solar flux and f_0F2. Half thickness y_t and y_m vary with season, f_0F2 and strongly with local time. The E and F1 layers are not seperately modeled but included into the combined profile below h_mF2.

2.3.8 Bradley & Dudeney's Model (1973).

This ionospheric model is employed to determine the propagation models involving reflection from the E and F-layers using parameters which depend on f_0F2, f_0E, M(3000)F2 and h'F2. h'F,F2 is the minimum virtual height of signal reflection from the F2-layer. It is equal to h'F by night and h'F2 when f_0F1 is observed by day. The model consists of :

(i.) a parabolic E-layer below its height of maximum electron concentration h_mE, with semi-thickness y_mE. h_mE is taken as constant at 110km and y_mE as 20km.

(ii.) a parabolic F2-layer with height of maximum electron concentration h_mF2 and semi-thickness y_mF2.

(iii.) a linear increase of electron concentration with height between h_mE and the point on the parabolic F2-layer where the plasma frequency f_t is $1.7f_0E$. This value was derived empirically to give results consistent with measured F-layer heights. Thus the model is specified in terms of the four variables parameters f_0F2, f_0E, h_mF2 and y_mF2 (Fig 2.3).

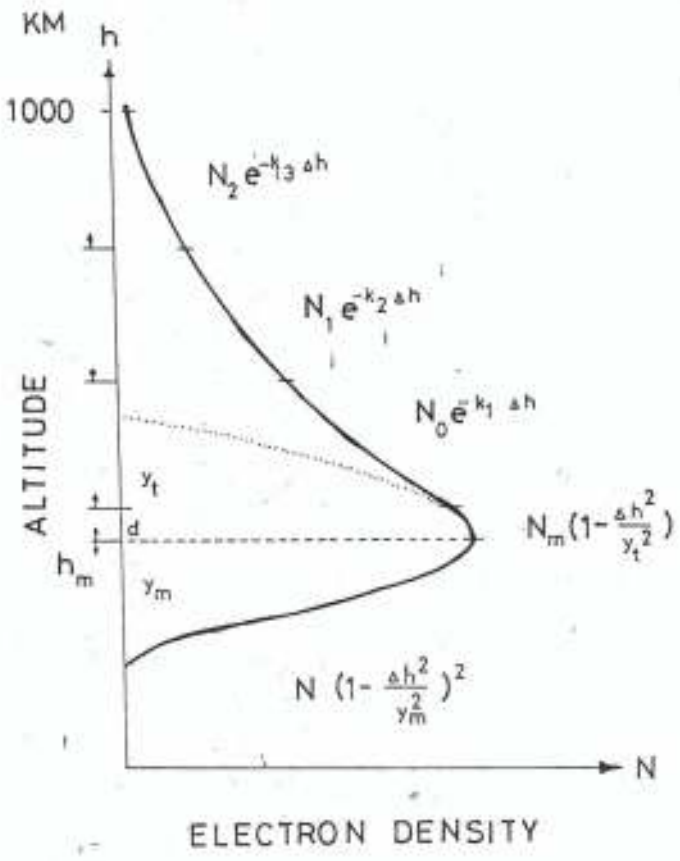

Fig 2.2 Bent's electron density model

The height increments Δh are measured from the starting point of the various layers

Source: Wernik A.W (1991)

Fig. 2.3 Bradley and Dudeney's electron density model

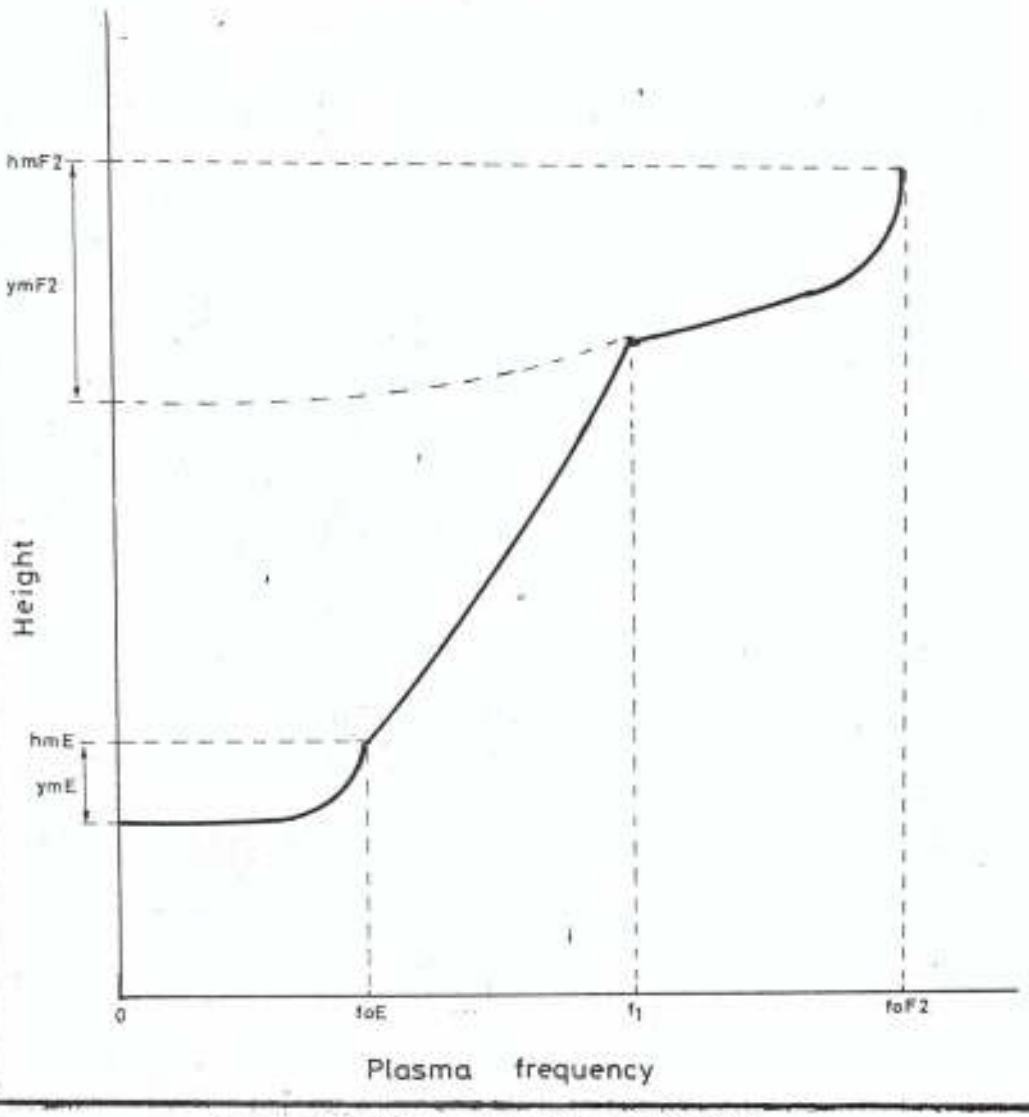

Source: Bradley P.A and Dudeney J.R (1973)

The model parameters h_mF2 and y_mF2 are given from the empirical equations;

(i.)

$$h_mF2 = \frac{1490}{M(3000)F2 + \Delta M} - 176 \qquad \ldots\ldots\ldots\ldots (2.17)$$

with

$$\Delta M = 0.18/(x - 1.4)$$

where

$x = f_0F2/f_0E$ or 1.7 whichever is the larger.

(ii.)

$$y_mF2 = h_mF2 - (h'F, F2 - \Delta h') \qquad \ldots\ldots\ldots\ldots (2.18)$$

where

$$\Delta h' = \left[\frac{0.613}{x - 1.33}\right]^{0.86} (h_mF2 - 104)$$

y_mF2 has a preset minimum value of 35km and a maximum value of ($h_mF2 - h_mE$). This model gave an improved match to measured ionization profiles in the F1-region. It also provides a more accurate representation of the F2 layer height of maximum ionization and semi-thickness.

2.3.9 Chiu's Model (1975).

This is a global phenomenological model of electron density in the altitude range 110 to 1000km. The input parameters of the model are :

z - altitude in km,

t - annual time (days of year) in units of months as measured from 15 December

of previous year,

λ_m- geomagnetic latitude in radians,

λ - geographic latitude in radians,

l_m- geomagnetic longitude in radians measured eastward,

δ_m- geomagnetic dip angle in radians,

Φ - local time in radians measured from local midnight,

ρ - monthly smoothed zurich sunspot number R

(where ρ = R/100).

In Fig 2.4, peak altitudes and scale heights are kept fixed at 110km and 10km and at 180km and 34km, respectively for the E and F1 layers.

The electron density N is the sum of the E-, F1-, and F2-layer densities, N_i, where the subscript i runs from 1 to 3 denoting the above layers in order. Each layer density, N_i, is the product of an amplitude parameter A_i, profile function Z_i and layer peak function V_i.

$$N(z, t, \lambda, \lambda_m, \phi, \rho) = \sum_{i=1}^{3} N_i(z, t, \lambda, \lambda_m, \phi, \rho) \qquad \ldots\ldots\ldots (2.19)$$

where

$$N_i = A_i\, Z_i(z,\lambda_m,\phi)\, V_i(t,\lambda,\lambda_m,\phi,\rho)$$

A_i takes the values 1.36, 2.44, 0.66 for i=1, 2 and 3 respectively. The function Z_i is given as

$$Z_i = Exp\{\alpha_i[\,1 - r_i - \exp(-r_i)\,]\} \qquad \ldots\ldots\ldots\ldots (2.20)$$

while function V_i consists of a polar function p_i, a non-polar function u_i and a folding factor f_i.

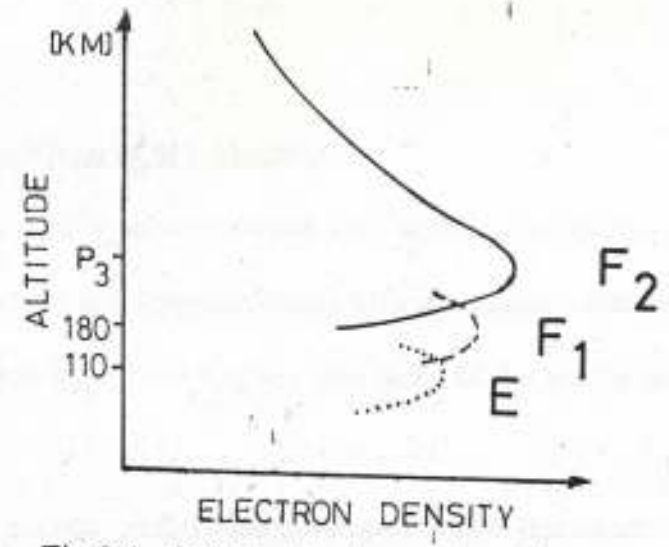

Fig.2.4 Chiu's electron density

Peak altitudes and scale heights are kept fixed at 110 and 10 km and at 180 and 34 km, respectively for the E and F1 layers.

Source: Wernik A.W (1991)

The data base for the model consists of ionosonde data from 50 stations with additional data from 18 stations which include complete available chronologies in the epoch 1958 - 1971. To model polar ionosphere, data from 9 antarctic and 9 arctic stations are included. The model is continuous at the north pole, but not at the south pole. The model poorly represents the details of the equatorial anomaly as well as the night-time conditions.

2.3.10 Anderson et al's Models.

Anderson et al's semi-empirical low latitude ionospheric model (SLIM) was developed to generate in a computationally efficient manner, electron density profiles at low latitudes which were more realistic than those of the widely used empirical models of Chiu or Bent.

In 1989, another model was developed which reproduces SLIM by means of analytic functions. This model is simply called a Fully Analytic Low- and Middle-Latitude Ionospheric Model (FAIM).

2.3.10.1 Semi-Empirical Low-Latitude Ionospheric Model(SLIM, 1987)

SLIM produces F region electron and ion (O^+) density profiles in the altitude range 180 - 1000km every 2^0 latitude (24^0N to 24^0S) and every half hour local time over the 24-hour day. SLIM consists of functions and coefficients which reproduce nine sets of theoretically calculated low-latitude electron density profiles corresponding to the three seasons (equinox, June solstice, and December solstice) for three levels of solar activity (solar minimum ($F_{10.7}$ = 70), moderate solar activity ($F_{10.7}$ = 125) and solar maximum ($F_{10.7}$ = 185)).

The electron density profiles are approximated by a modified Chapman function below and above F2 peak.

$$N_e(z) = n_mF2 \exp\{c[1 - z - \exp(-z)]\} \quad \ldots\ldots\ldots\ldots (2.21)$$

Thus the profiles are determined by the six parameters n_mF2, h_mF2, H_{UP}, H_{LO}, C_{UP} and C_{LO}. Where n_mF2 is the peak plasma density, h_mF2 is the altitude , $N_e(z) = n_mF2$, $z = (h - h_mF2) / H$, and the subscripts UP and LO refer respectively to those regions above and below h_mF2.

The drawback of the model is that only O_+ ions are considered, thus it is not realistic below F layer and above the transition height where H^+ ions dominate.

2.3.10.2 Fully Analytic Low-Latitude Ionospheric Model(FAIM, 1989)

In developing the low-latitude portion of FAIM, new analytic formulations for the parameters f_0F2, h_mF2, H_{UP} and H_{LO} in the Chiu model based on the SLIM profiles were derived. The local time variation at a given dip latitude is expressed as a series of sines and cosines with amplitudes a_n and b_n with the series going from n=0 to n=6.

$$f(\lambda, \phi) = \sum_{n=0}^{6} [a_n(\lambda) \sin(n\phi) + b_n(\lambda) \cos(n\phi)] \quad \ldots\ldots (2.22)$$

where ϕ is local from midnight in radian. A seperate function $f_s(\lambda,\phi)$ is found for each of the four defining parameters, s=1 to 4.

In reality, for f_0F2 and h_mF2 values equation (2.6) was used to fit the difference between the Chiu and the SLIM values so that in this new analytic model, Chiu values were simply calculated and added to the analytically formulated differences to provide the final f_0F2 and h_mF2 quantities specified by FAIM.

In FAIM, seperate topside and bottomside F-region scale height was found which reproduced each SLIM profile density to within 0.5MHz, assuming the expression for $N_e(z)$ given by equation (2.5). These scale heights H_{UP} and H_{LO} are different from those specified in SLIM because the values C_{UP} and C_{LO} are assumed to be unity. Once values of H_{UP} and H_{LO} were determined by this method, the analytic functions given by (2.6) were derived.

Next, appropriate functions and coefficients which reproduce the seperate sets of a_n and b_n values as a function of dip latitude were found. The modified harmonic oscillator function $H_k(\psi)e^{-\psi^2}$ where H_k is the Hermite polynomial of order k and $\psi = \lambda_m/14$, (ψ_m in degrees) was found to be ideally suited for this purpose:

$$a_n(\lambda_m), b_n(\lambda_m) = \sum_{k=0}^{4} c_k H_k(\psi) e^{-\psi^2} \qquad \ldots\ldots\ldots\ldots\ldots\ldots (2.23)$$

The report by Forbes et al (1989) contains a tabulation of the c_k values as well as the FORTRAN code for FAIM.

The middle-latitude correction to the h_mF2 specification of the Chiu model is based on an examination of equinox ionosonde data as detailed in an Air Force Geophysics Laboratory (AFGL) report (Forbes et al.,1989). Thus, significant improvements are obtained in FAIM over previous comparable analytic models.

2.4 International Reference Ionosphere (IRI).

The International Reference Ionosphere (IRI) is the empirical reference model of ionospheric densities and temperatures (electrons and ions) recommended for international use by the Committee On Space Research (COSPAR) and the International Union Of Radio Science (URSI). It was established in a world-wide collaboration starting in the late

sixties as a joint project of URSI (subcommission 6.4) and COSPAR study group C.

Upon a proposal by Sid Bowhill "to create an ionospheric pendant to COSPAR International Reference Atmosphere (CIRA)", COSPAR decided in her study group C the project "International Reference Ionosphere" with a special task group chaired by K. Rawer (Oyama, 1994). The task group chaired since 1988 and 1992 by Lucien Bossy and Dieter Bilitza respectively developed an important activity with yearly meetings the proceedings of which normally appear in the COSPAR periodicals "Advances In Space Research".

IRI project initiated a particularly intense and fruitful international cooperation. The first exchange of views among scientists revealed that in spite of decades of pure and applied ionospheric research, by far not all data needed in the project were available.

While in a few fields an enourmous number of measured data existed -mainly taken in view of propagational applications- reliable worldwide information was almost completely missing in others. For example, few ionograms had been reduced to "true" electron density profiles and for plasma temperatures and composition most rocket or satellite positive ion data had been reduced by rules that excluded them from being introduced into a consistent project.

A very first set of provisional tables was presented to URSI in 1975. Thereafter, URSI requested that IRI be presented in a form readily applicable by workers in the field. A computerized approach was adopted to and published by URSI.

In 1981, a considerably improved code was published by World Data Center-A (Solar-Terrestial Relationship) in Boulder, Colorado, U.S.A. Later, it was decided that the IRI code be available on magnetic tape or diskette. This allowed a quicker incorporation of changes that had been decided at the yearly group meetings. At present,

the code is available on the worldwide computer network from the National Aeronautics And Space Administration (NASA)/ National Space Science Data Center (NSSDC) site.

When work on IRI started, there existed a very complete computerised set of monthly average ionization maps. The Gallet-Jones algorithm was with a few improvements taken up by the International Radio Consultative Committee (CCIR) in 1967. For any point on the Earth, the CCIR code gives as a function of hour, monthly averages of the peak density (N_mF2) and M(3000)F2 (a parameter used in propagational applications) that is closely related to the peak height (h_mF2). An empirically established connecting relation is used to deduce h_mF2 from M(3000)F2. The CCIR code was incorporated into the IRI by the task group so as to be used in all cases where actual peak data are not available.

The main aim of the IRI is to establish a compedium of height profiles through the ionosphere for the four plasma parameters, namely: plasma density, plasma temperatures of electrons and ions and ion composition. The emphasis of IRI is to summarize reliable experimental data when available; hence, the development of IRI76 with subsequent improvements and reviews - IRI79, IRI86 and IRI90 respectively. Thus, IRI -the most advanced empirical model- is a computer program which produces profiles.

IRI allows prediction of electron density, electron temperature, ion temperature and ion composition (IRI90 also specifies ion drifts) for:

_ specified altitude,

_ location (geographic or geomagnetic),

_ time (local or universal time or solar zenith angle),

_ month,

_ solar activity (12-month running mean solar sunspot number).

The following data sources are used:

_ ionosonde,

_ incoherent scatter,

_ topside sounder,

_ Langmuir probe,

_ retarding potential analyzer,

_ rocket composition data (in the D-region).

Restrictions are as follows:

_ auroral latitudes are not considered,

_ ionospheric irregularities (e.g spread-F, sporadic-E and winter anomaly) are not included,

_ mean values : the actual data can deviate up to 30% ; quasi-actual profiles can be obtained by introducing measured F peak values,

_ solar activities below R_{z12} = 150. For higher solar activities the model is independent of R_{z12}.

The task group has been responsible for subsequent reviews and improvements in the IRI. In fact, IRI is being updated bi-yearly by the task group during special IRI workshops to incorporate newly available measurements. For example, the prime objective of the 1995 meeting held at the National Physical Laboratory, New Dehli, India from January 9 - 13 was to evolve substantial improvements and extensions of the IRI model at low and equatorial latitudes. Of particular interest were:

_comparative studies of IRI with data, simulations and other models;

_investigations that could lead to better representation of ionospheric parameters in IRI;

_regional mapping of E and F peak parameters;

_occurrence statistics for Spread-F and other ionospheric irregularities;

_applications of IRI in science, engineering, and education.

The IRI electron density profile is divided into six sub-regions as shown in Fig 2.5, including the topside, the F2 bottomside, the F1 layer, the intermediate region, the E-valley, and the bottomside and the D region.

The topside ionosphere (region 1 in Fig 2.5) model is based on topside ionosonde data compiled by Bent et al. (1970) and uses the LAY-functions. The LAY-function combines the Epstein transition function with a linear term.

$$LAY(h;h_m,HX,SC) = EPS_{.5}(h;HX,SC) - EPS_{.5}(h_m;HX,SC) - (h - h_m)\, EPS_0(h_m;HX,SC)/SC$$

$$LAY(h; h_m, HX, SC) = \ln(1+e^{x}) - \ln(1+e^{x_m}) - (x - x_m)/(1+e^{x}) \quad \ldots (2.26)$$

with

$$x = (h - HX)/SC \qquad \text{and} \qquad x_m = (h_m - HX)/SC$$

In the IRI86 and IRI90 the plasmasphere diffusive equilibrum model is smoothly coupled at 650km with the topside ionospheric model.

The bottomside F2 region (region 2) is represented by :

$$N(h) = N_mF2 \exp(-x^{B_1}) / \cosh(x) \quad \ldots\ldots\ldots (2.27)$$

with

$$x = (h_mF2 - h)/B_0)$$

N_mF2 and h_mF2 are the electron density and height of the F2-peak, and $B_1 = 3$ in most cases. While both N_mF2 and h_mF2 are obtained from CCIR maps of f_0F2 and M(3000)F2,

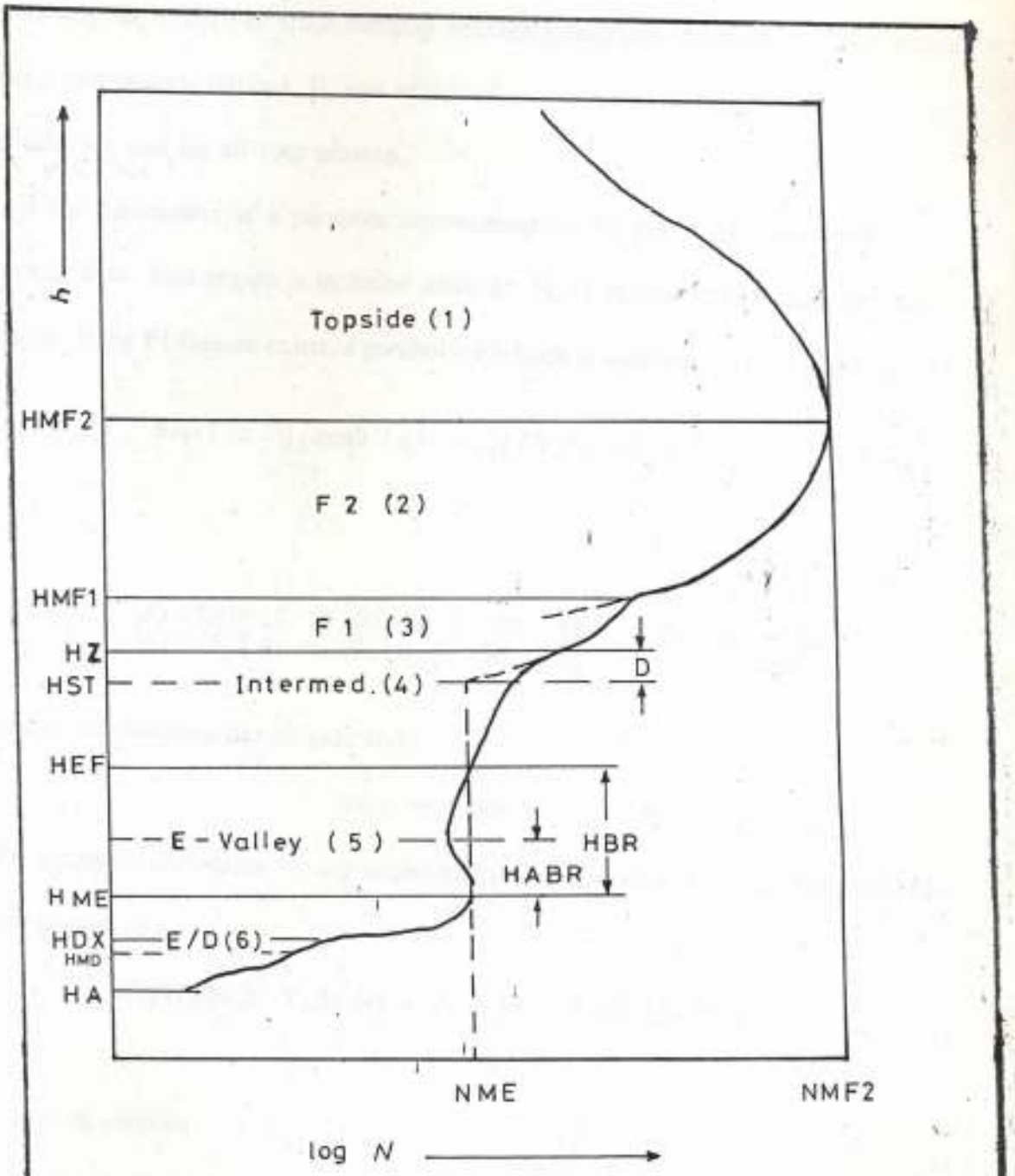

Fig 2.5 Electron density profile in International Reference Ionosphere (IRI)

Source: Bilitza D. (1990)

respectively, B_0 is derived from monthly average ionograms recorded at 2 low latitude and at 1 mid latitude stations. B_0 was evaluated for noon and midnight, for low and high solar activity, and for all four seasons.

The parameters of a parabola representing the F1 region (3), are based on the ionosonde data. This region is included when the N_mF1 model predicts the existence of this layer. If the F1 feature exists, a parabolic F1-layer is added to the bottomside profile.

$$N(h) / N_mF2 = \exp(-x^{B_1}) / \cosh(x) + C_1((h_mF1 - h) / B_0)^{1/2} \quad \ldots\ldots (2.27)$$

with

$$C_1 = \begin{cases} EPSTEP(18;\ 0.09,\ 0.2,\ 30,\ 10) & for\ |\mu| < 18 \\ EPSTEP(\mu;\ 0.09,\ 0.2,\ 30,\ 10) & else \end{cases}$$

where μ is the modified dip latitude and,

$$\tan \mu = \Psi / \cos^{1/2} \varphi$$

Ψ is the magnetic inclination (or dip angle) and φ is the geodetic latitude. The EPSTEP function is given by :

$$EPSTEP(h, Y_1, Y_2, hs, ds) = Y_1 + (Y_2 - Y_1) EPS_0(h; hs, ds)$$

where

$$x = (h - hs)/ds$$

In the intermediate region (4), the profile is constructed rather artificially and starts slightly above the heights where the bottomside density profile is equal to the N_mE and bends downward to meet the valley top. The boundary of the intermediate region is defined by;

$$HZ = (h_x + HST)/2 \qquad \ldots\ldots\ldots\ldots (2.28)$$

$$h_x = \begin{cases} h_mF1 & \text{if } F1 \text{ layer is present} \\ h_mF2 & \text{else} \end{cases}$$

starting from HZ, the profile is bent downward parabolically such that it meets the E-valley top h_{vT}. This is accomplished with the altitude transformation,

$$h' - HZ = T/2 \pm (T^2/4 - T(h - HZ))^{1/2}$$

where

$$T = (HZ - HST)^2 / (HST - h_l)$$

and

$$h_l = \begin{cases} h_{vT} & \text{if valley is present} \\ h_mE & \text{else} \end{cases}$$

h_{vT} is the height at the top of the valley and h_mE is the height of the E-peak.

The E-peak critical frequency is obtained from the CCIR model. It consists of four factors;

$$f_0E^4 = A \cdot B \cdot C \cdot D \qquad \ldots\ldots\ldots\ldots (2.29)$$

depending on the 12-month running mean of the solar 10.7cm radio flux (COV_{12}) on season (χ_{noon} is the solar zenith angle at noon), on geodetic latitude (ψ) and on the solar zenith angle (χ).

$$A = 1 + 0.0094 (COV_{12} - 66)$$

$$B = \cos^m \chi_{noon}$$

$$m = \begin{cases} -193 + 1.92 \cos \varphi & \text{for } |\varphi| < 32^0 \\ 0.11 - 0.49 \cos \varphi & \text{for } |\varphi| \geq 32^0 \end{cases}$$

$$c = \begin{cases} 23 + 116 \cos \varphi & \text{for } |\varphi| < 32^0 \\ 92 + 35 \cos \varphi & \text{for } |\varphi| \geq 32^0 \end{cases}$$

$$D = \cos^{n}\chi_{s}$$

$$n = \begin{cases} 1.2 & for \quad |\varphi| > 12^{0} \\ 1.31 & for \quad |\varphi| \leq 12^{0} \end{cases}$$

Different from CCIR (1973), a modified zenith angle was introduced to improve the nighttime variation (Rawer and Bilitza, 1990).

$$\chi_{s} = \chi - 3\ EPS_{.1}(\chi;\ 89.98,\ 3)$$

[Note that $EPS_{.1}(h;\ HX,\ SC) = \ln(1 + e^{x})$; where $x = (h - HX)/SC$]

During all times f_0E is kept above or equal to the observed minimum value,

$$f_0E_{min} = 0.121 + 0.0015\ (COV_{12} - 66) \quad \text{.....(2.30)}$$

A constant height $h_mE = 105$km is assumed for all conditions.

The F-region peak and valley profile is described by a fifth order power series,

$$N(h)/N_mE = 1 + E_1x^2 + E_2x^3 + E_3x^4 + E_4x^5 \quad \text{....(2.31)}$$

with

$$x = h - h_mE$$

parameters E_1, E_2, E_3, and E_4 are determined from the valley width, HBR, the valley depth, DP, the distance between valley base and h_mE, HABR, and the logarithmic derivative at the valley top DLN.

$$DP = 100\ (N_mE - N_{vB})/N_mE$$

where N_{vB} is the density at the valley base.

Also,

$$DLN = \frac{d\ln N}{dh}\Big|_{h\ =\ h_{vT}}$$

The lower ionospheric model is based on a selection of rocket measurements. Most D-region profiles exhibit a characteristic inflection point with the height h_mD and

the density N_mD. The density profile starts at height HA and is represented by a third order polynomial,

$$N(h)/N_mD = \exp (F_1x + F_2x^2 + F_3x^3) \quad \text{.....(2.32)}$$

with

$$x = h - h_mD$$

Somewhat arbitrarily, an exponential function is used to connect the D-region profile with the E-layer peak density N_mE and height h_mE.

$$N(h)/N_mE = \exp (-D_1 (h_mE - hDX)^k) \quad \text{.....(2.33)}$$

The parameters D_1 and k are determined such that the function agrees with the D-region profile function and its first derivative at the height hDX.

$$k = -DN (h_mE - hDX)/(NDX \ln (NDX/N_mE))$$

$$D_1 = DN / (NDX \cdot k(h_mE - hDX)^{k-1})$$

NDX is the electron density at hDX and DN the derivative dN/dh at that height.

CHAPTER THREE

3.0 RESULTS AND ANALYSIS.

3.1 Data Base.

The primary data used for the study were the recorded median values of f_0F2 and h_mF2 obtained for Ibadan (7.4°N,3.9°E) and Tsumeb (19.2°S,17.7°E) and published by the department of Scientific and Industrial Research, Radio Research Station, Slough, England.

Basically, the published median values of f_0F2 and h_mF2 measured at Ibadan between December 1959 and March 1975 and Tsumeb between August 1964 and March 1973 were used in the study. Tables 2 and 3 show typical values of ionospheric data recorded by ionosondes at Ibadan.

The smoothed monthly observed Zurich relative sunspot number (R_{Z12}) compiled from April 1954 to December 1976 was used in the study. Since the 10.7cm solar flux ($F_{10.7}$) and sunspot number are quite correlated, $F_{10.7}$ was obtained by means of an empirical relation given by

$$COV = 63.75 + R(0.728 + 0.00089\ R) \qquad \ldots\ldots\ldots\ldots\ldots (3.1)$$

where

$$R_{Z12} = R \qquad \text{and} \qquad F_{10.7} = COV$$

such that,

$$R_{Z12} = 150 \text{ for } R > 150$$

and

$$F_{10.7} = 193 \text{ for } COV > 193.$$

CHARACTERISTIC foF2 UNIT 0.1MHz FEBRUARY 1964

OBSERVED AT IBADAN

IONOSPHERIC DATA. Table I HOURLY VALUES.

DATE	0° MEAN TIME												DATE
	00	01	02	03	04	05	06	07	08	09	10	11	
1	027	027	024	020		S	031	062 J S	C	079	072	067	1
2	056	051	044 - V	034	020		030	060	067	059	060	065	2
3		S	087 Q F	065 Q F	043	022		S	027	057	068	064	059	062	3
4	065 Q F	065 Q F	062 Q F	037 Q F	023	013 - S	028	056	066	059	052	059	4
5	062 Q F	042 Q F	051 Q F	043 S F	036 U F	023 - V	030	053	073	080	054 - H	058 - H	5
6	062 Q F	043 Q F	052 Q F	051 Q F	030 Q F	025 - V	030	057	076 - R	079	087	R	6
7	062 J S	065	045	035	027 U R	B	080 - R	060 U S	073 J R	081	081	070	7
8	056	054	043	032	030	027 - F	037	057	070	082	083	073 - R	8
9	061 J S	059 J S	052 Q F	049	R	030	034	060	079 U S	073 I R	075 U R	075 I R	9
10	057 U S	058 Q F	S	045 U S	028	018 J S	030 - S	059	070	075 J R	072 U R	068	10
11	061 U F	047	032	031 - F	063 Q F	025	033	059	077	080	084	088	11
12	043	031 U F	027 U F	026 U R	023	OK - S	030	058	C	070	062	057	12
13	065 J S	065	046 U S	031		A	B	033	064	075 J R	088	089	078 - R
14	061 J S	049	030	024	019		F	032	064	079 U R	083 - R	067	068
15	065 Q F	063 Q F	063 Q F	043 J S	027 J S		S	031	063	080	085	070	065
16	059 U S	046	036	020	014 U S		B	031 U H	060	076	080	070	066
17	067 U S	060 J S	048	040 U F	039 U S	032 J C	034 - S	058	065	075	074 J R	C	
18	059 - F	044 - F	039 - F	031 - V	023 - V	016 U R	032	061 - S	069	078	079 J R	065	
19	070 U F	062 Q F	055 Q F	044 J S	087	029	036	057	066	080	079	072 - R	
20	058 Q F	056 - F	048 Q F	039 Q F	032 J S	022 J S	033 U S	C	076 J R	078	078	077	
21	066 Q F	047 Q F	065 Q F	063 Q F	042 U F	040 Q F	044 U F	066	077	085	088	074 U R	
22	067	063 J S	049	040	036	027 Q F	038	064	065	072 J R	079 U R	086	
23	063 Q F	059 J S	067 U S	043 U F	036 Q R	026	036	067	R	R	067	065	
24	052 Q F	063 Q F	048 Q F	036 - F	034 U F	021	035	066 - S	080	079	082	R	
25		053 Q F	049 - S	047 U S	025 - V	021	033 - S	065 - S	079	080 U R	078 - R	076 U R	
26	052 U S	055	055 Q F	038 - F	027	S	034	063	080 - R	079	073 J R	077 U R	
27	070	C	C	C	C	C	C	C	C	C	C	081	
28	C	C	C	C	C	C	C	C	C	R	075 U R	067	070
29	S	069 - S	052 J S	033 J S	015 J S	038	070	082	085	070	070		
30													
31													
COUNT	26	27	26	27	24	18	27	26	24	27	28	26	COUNT
MEDIAN	061	055	048 - F	039	029	024	033	060	074	079	074	070	MEDIAN
QUARTILE RANGE	009	016	012	013	011	009	005	006	010E	007	012E	011	QUARTILE RANGE

DATE	0° MEAN TIME												DATE
	12	13	14	15	16	17	18	19	20	21	22	23	
1	074	081	084	084	083	080 U S	S	S	079 - R	080 J S	065 J S	057	1
2	064	062	065	070 J C	073 U S	084	075 J S	C	072 J S	067	065 J S	067 U S	2
3	059	066	066	070	080	076	C	074 J S	078 J S	067 U F	057 Q F	064 Q F	3
4	068	C	065	067	074 J S	084	087	085	076 J R	065	086 Q F	086 Q F	4
5	065	C	C	C	C	087	089	069	S	065 J S	062 Q F	065 Q F	5
6	070 U R	068	070	068	068 J S	073 J S	076 J S	073 J S	062 J S	057 U F	062 Q F	065 Q F	6
7	067	068	062	061	068	080 U S	083 J S	079	081 U S	081 J S	075 J S	086 Q F	7
8	066	070	075	071 - S	070 - S	059 - S	062 J S	065 J S	068 U S	065 Q F	067 Q F	063 Q F	8
9	075 U R	079	084	075	072 J S	076 J R	080	070 U S	088 Q F	088 Q F	088 Q F	088 Q F	9
10	065	066	071 - S	076	078	078 - S	071 J S	S	065 J S	086 Q F	086 Q F	062 Q F	10
11	070	071	070	069	070 - S	S	071 J S	063 J S	088 Q F	086 Q F	086 Q F	062 Q F	11
12	070	066	071 U S	076	088	083 U S	081 U S	S	081 J S	088 Q F	086 Q F	S	12
13		A	077 - R	082	073	C	070 J S	070 J S	070 U S	092	C	076 J S	070 J S
14	067		A	C	070 J R	066	079 U S	088	062 Q F	088 Q F	088 Q F	087 Q F	086 Q F
15	066	063 - S	067	075	080	093 U S	088	081 U S	070 Q F	082 Q F	062 Q F	065 J S	15
16	065	068	070	070	073 J R	S	086 U S	083 U R	070 J S	071 - S	067 J S	064 U F	16
17		C	C	065	070	079	080	S	087 U S	065 Q F	086 Q F	087 Q F	086 Q F
18	062	065	062	063	068	070 U S	075 J S	072 U R	067	088 Q F	065 Q F	065 Q F	18
19	072	066	069	075	081	093 U S	096 J S	082	070 U S	069 U S	065 Q F	056 U F	19
20		R	077 U R	070	078	084	086	080 - R	076 J R	086	S	C	
21	071	070	070	070	077	065	072	086	076 J S	086 Q F	109 Q F	081	21
22	088	081	071	069	079	084	083	077 - S	074 J S	068 J S	088 Q F	088 Q F	22
23	069	068	065	063	066	S	067 J S	062 J S	086 Q F	062 Q F	062 Q F	061 Q F	23
24	076 U R	070 U S	088 - R	072	092	085	082	070 J S	070 U S	065 Q F	063 Q F	062 J S	24
25		C	C	088	095	101 U S	096 U S	092	079 U S	088 Q F	088 Q F	087 Q F	085 Q F
26	070	075 U R	086	071	088	089	095	068	065 Q F	070 J S	065 Q F	070 J S	
27		C	C	C	C	C	C	C	C	C	C	089 U S	C
28	070	080	093	095	091 J S	077 U S	101 J S	085 U S	S	077 U S	070 J S	071	
29	069	075 U R	080 - R	089	092 J R	098 U S	095	086	080	088 Q F	088 Q F	065 Q F	
30													
31													
COUNT	24	23	26	27	26	25	25	24	26	27	28	26	COUNT
MEDIAN	069	070	070	073 U	080	085 - S	086 U S	077 U S	076 U	084 U F	086 Q F	065 Q F	MEDIAN
QUARTILE RANGE	007E	011	016	017E	018E	014	014	015	018E	021	023E	024	QUARTILE RANGE

CHARACTERISTIC foF2 UNIT MHz FEBRUARY 1964

OBSERVED AT IBADAN

Table 2

IONOSPHERIC DATA. HOURLY VALUES.

0° MEAN TIME

DATE	00	01	02	03	04	05	06	07	08	09	10	11	12	13	14	15	16	17	18	19	20	21	22	23	DATE
1	295	290	300	280	S	A	295	S	C	345	335	315	295	305	290	295	325	340	S	S	S	S	S	290	1
2	310	270	310-V	290	270	H	345	275	325	370	375	345	345	365	370	C	310 U S	315	S	C	S	305	S	335 U S	2
3	S	F	F	270	R	B	280	280	305	370	340	335	370	345	315	310	320	310	C	S	S	F	F	F	3
4	F	F	F	F	F	S	B	275	325	320	365	370	380	C	335	320	S	300	275	285	R	335	F	F	4
5	F	F	F	F	S	305	230	235	280	370-H	410-H	320	C	C	C	C	275	295	290	S	S	F	F	5
6	F	F	F	F	275-V	270	250	275-R	280	320	R	325 U R	360	350	390	S	S	S	S	S	F	F	F	6
7	S	290	290	300	R	S	285-R	310 U S	R	285	390	335	380	385	390	A	A	A	S	A	A	S	S	F	7
8	290	270	260	300	310	270-F	270-F	265	280	295	325	310-R	365	325	310	325-S	390-S	310-S	S	S	340 U S	F	F	F	8
9	S	S	F	280	R	260	305	295	285	R	320	A	310 U R	335	345	320	A	A	365	430	F	F	F	F	9
10	255 U S	F	S	290 U S	245	S	290-S	270	280	R	295 U R	260	295	300	270-S	280	260	255-S	S	S	S	F	F	F	10
11	230 U F	235	260	245-F	F	220	235	225	285	275	290	275	295	305	300	280	265-S	S	S	S	F	F	F	F	11
12	220	F	220 U F	215 U R	245	225-S	245	235	C	270	260	280	255	300	275	270	265	240 U S	235 U S	S	S	F	F	S	12
13	S	215	285 U S	230	A	B	230	215	R	245	280	355-R	A	290-R	280	235	C	S	S	230 U S	235	C	S	S	13
14	S	285	245	255	250	B	245	190	250 U R	285-R	310	A	295	A	C	R	A	275 U S	285	F	F	F	F	F	14
15	F	F	F	F	S	S	B	230	210	230	265	305	295	320	260-S	295	275	255	255 U S	270	295 U S	F	F	F	S	15
16	245 U S	230	220	220	240 U S	B	225 U-R	210	230	270	285	330	290	275	255	275	R	S	295 U S	310 U R	S	270-S	S	F	16
17	265 U S	S	245	255 U F	250 U F	C	200-S	210	210	245	R	C	C	C	270	270	255	255	S	280 U S	F	F	F	F	17
18	245-F	230-F	255-F	240	235	245 U R	220	235-S	225	250	R	315	360	255	295	270	275	240 U S	S	280 U R	300	F	F	F	18
19	310 U F	F	F	S	280	275	270	245	240	290	340	345-R	325	295	255	315	320	315 U S	S	315	365 U S	405 U S	F	F	19
20	F	275-F	F	F	S	S	250 U S	C	R	305	340	335	F	405 U R	285	255	250	235	235	260-R	R	235	S	C	20
21	F	F	F	F	F	F	285 U F	275	275	300	305	345 U R	245	290	400	270	230	225	240	255	S	F	F	285	21
22	270	S	325	305	300	F	255	245	245	R	305 U R	320	260	415	250	265	255	220	225	270-S	S	S	F	F	22
23	F	S	315 U S	300 U F	285 U R	295	260	280	R	R	260	315	265	250	405	210	255	S	S	S	E	F	F	F	23
24	F	F	F	280-F	275	285	265	270-S	265	290	260	R	B	R	260-R	255	245	265	210	S	240 U S	F	F	S	24
25	285	F	300-S	260 U S	265-V	295	265-S	290-S	300	350 U R	260-R	240 U R	C	C	C	245	230 U S	270 U S	205	205 U S	F	F	F	F	25
26	330 U S	325	F	305-F	295	B	290	280	220-R	285	R	240 U R	250	245 U R	250	C	275	215	235	295	F	S	F	R	26
27	320	C	C	C	C	C	C	C	C	C	C	255	C	C	C	C	C	C	C	C	C	C	285 U S	C	27
28	C	C	C	C	C	C	C	C	C	R	335 U R	340	365	A	240	235	240	S	260 U S	S	280 U S	S	230 U S	S	275	28
29	S	310-S	320	S	S	S	305	265	290	250	275	305	375	A	230-R	S	B	210 U S	215	275	210	F	F	F	29
30																									30
31																									31
COUNT	14	12	15	19	14	10	26	25	21	24	25	24	22	21	25	22	18	21	14	16	6	6	1	4	COUNT
MEDIAN	280	270	260	280	270	270	270	265	275	290	340	335	335	340	335	320	330	315	320	365	370	330-S	285 U S	290	MEDIAN
QUTILE RANGE	065	060 E	060	055	040	040	045	050	060	050	050)	035	070	075	070 E	075	090	065	070	100 E	070	030	—	025)	QUTILE RANGE

R_{Z12} is the 12-months-running mean of solar sunspot number.

Typically, data recorded in the months of January or February, June and September for years with low ($F_{10.7} < 80.0$), moderate ($100.0 < F_{10.7} < 130.0$) and high ($F_{10.7} > 150.0$) solar activities were used in the analysis.

For Ibadan, consideration was given to data of the median values of parameters f_0F2 and h_mF2 obtained at LT: 00.00hr (LT=Local Time) and LT: 12.00hr for chosen months. Furthermore, due to missing ionogram data for Tsumeb, mostly during night-time and early hours of the day, data recorded between LT: 09.00hr and LT: 15.00hr were used to obtain the required electron density profiles.

The observed f_0F2 and h_mF2 values (hereafter referred to as "experimental" data) at these two typical low-latitude stations are compared with the CCIR-67 predictions for f_0F2 and M(3000)F2 using the IRI90 model. h_mF2 values are determined from M(3000)F2 empirically (Bilitza et al,1990).

$$h_mF2 = \frac{1490}{(M(3000)F2 + DM)} - 176 \qquad \ldots\ldots\ldots (3.2)$$

with the correction factor,

$$DM = f_1 f_2 / (f_0F2/f_0E - f_3) + f_4$$

and the solar activity functions,

$$f_1 = 0.00232\ R_{Z12} + 0.222$$

$$f_2 = 1 - R_{Z12} / 150 \exp (- (\Psi / 40)^2)$$

$$f_3 = 1.2 - 0.0116 \exp (R_{Z12} / 41.84)$$

$$f_4 = 0.096 (R_{Z12} - 25) / 150$$

Ψ is the magnetic dip latitude where,

$$\tan\Psi = \tfrac{1}{2} \tan\psi$$

and ψ is the magnetic inclination of the Earth,s magnetic field at 300 km altitude.

A more detailed description of IRI and explanations of the equation as well as the CCIR option has been given in section (2.4).

3.2 Analysis.

There are three basic criteria that must be taken into account in order to ascertain the success of an ionospheric model. They are: 1) how well the model matches the range of "experimental" profiles; 2) the ease of obtaining the external data required to specify the profile, and 3) the simplicity of the mathematical expressions used to derive the profile.

At present, the most widely used empirical model in terms of standard ionospheric characteristics and parameters is the multi-segment model known as the International Reference Ionosphere, IRI (designated as IRI-90 in its current form). This model appears to satisfy all these aforementioned criteria but there is still the need for widespread profile testings, proper assessments and analysis of results so as to test the efficacy of the empirical relations.

Since the IRI depends on the monthly CCIR numerical maps prediction of f_0F2 and M(3000)F2, it simply describes monthly median profiles. Hence, comparisons of IRI profiles with monthly median observations of ionospheric parameters is expedient to judge the success of the model.

Consequently, this present work discusses these comparisons for a typical equatorial station (Ibadan) and a low-latitude station (Tsumeb) and offers some explanations for the results based on appropriate data analysis. The emphasis here is to assess how well the CCIR predictions apply to or matches the range of ionospheric

characteristics observed experimentally in these regions.

3.2.1 Results.

Comparisons of the IRI profiles for Ibadan for the three chosen months revealed that the F2-layer peak density is lowest in the month of June for the three different solar activities during night-time (Figs 3.1a - 3.3a). This peculiarity is quite in agreement with the observed profiles for Tsumeb at all solar activities (Figs 3.4 - 3.6) and could therefore be inferred to be typical of low-latitude F2-layer during June solstices. The result is that the peculiarity observed is due to the well known seasonal variations of the ionosphere at low latitudes.

In addition, there are marked differences between the F2 peak and the E-region peak densities and their height regimes for all the three solar activities during daytime (Figs 3.1 - 3.6). In general, the F2 peak densities are higher in magnitude and greater than those occuring in the E-region. This result confirmed the well known close inter-relationship between the peak heights and the peak electron densities at each of the regions or layers of the ionosphere. Typically, the E-region is about 20km thick while the topside is about 500km and above to the cut-off heights.

During the daytime, the F1 layer appeared in most of the profiles as small gradient discontinuites (Figs 3.1b - 3.6b). This result is a reflection of the well known cusp-like trace structures of F1 layer normally observed on ionograms during daytime at low-latitudes.

As evident from the electron density profiles, the valley is always present at night (Figs 3.1a - 3.3a). The result is that the F1 and E layer are 'almost' not present during nighttime at low latitudes. The absence of E and F1 layers during nighttime is a well

known characteristic feature of the diurnal variation of low latitude ionosphere.

Also, the F2 peak electron densities are observed to increase consistently for all the months during low, moderate and high solar activities respectively (Figs 3.1 - 3.6). This result confirmed the solar activity dependence of the peak electron densities at these low latitude ionospheric stations.

In general, no precise seasonal dependence or trend was observed in the structures of the peak heights and peak densities of the profiles obtained from the CCIR/IRI based predictions for Ibadan and Tsumeb during daytime (Figs 3.7b - 3.12b).

However, during the nighttime, the profiles follow a 'consistent' trend in that the F2 peak densities for the month of June are quite lesser than those obtained for the months of February and September respectively for all solar activities (Figs 3.10a - 3.12a). This result is similar to that obtained for the experimental profiles and could be attributed to the well known dependence of ionospheric parameters at these regions on seasonal variations of the ionosphere.

Deductions based on diurnal observations of these profiles showed that F1 and E layers are present during the day whereas during nighttime they are seen to be absent. This result is in agreement with the well known characteristic feature of the diurnal variations of low latitude ionosphere.

For example in Figs 3.10a to 3.12a, representing nighttime profiles, valley is observed always at heights below 200km confirming the absence of F1 and E layers. However,in Figs 3.7b to 3.12b, F1 layers are seen in most of the profiles as small gradient discontinuities while the E layers are also represented by the E peak densities during daytime.

As evident on the profiles (Figs 3.7b - 3.12b), there are marked differences

between the F2 peak densities and the E region peak densities and their height regimes respectively. The result is that the CCIR/IRI profiles reproduced the well known correlation and close inter-relationship between the peak heights and the peak electron densities at each of the regions (or layers) of the ionosphere.

Incidentally, the CCIR/IRI profiles from the above deductions have been found to reproduce most of the features observed on the experimental profiles.

The electron density profiles obtained from the IRI and CCIR predictions were compared in order to see how the two procedures differ from each other. The study covers the months of February, June and September for low, moderate and high solar activities during nighttime and noontime respectively.

The comparisons show that the best agreement between the experimental profiles and the CCIR/IRI predicted profiles was found for February, 1964 and September, 1968 during nighttime (Figs 3.13a & 3.21a). Also, the agreement during nighttime for the month of September, 1964 was found to be good (Fig 3.19a).

In most cases, the CCIR profiles show too large electron densities near the F2 peak and at topside during daytime (Figs 3.13b - 3.21b). However, better agreements were generally observed during daytime at the bottomside of the F2 layers.

In general, the agreement at nighttime was found to be better than at noontime for all the three solar activities (Figs 3.13, 3.19 & 3.20). However, the divergence at nighttime - when observed - are found to be significant (Figs 3.15, 3.16 & 3.18).

It is worth noting that the agreement of all comparisons for experimental and predicted electron density profiles during nighttime and noontime was found for the month of September (Figs 3.19, 3.20 & 3.21). The divergence of the profiles for the month of June was found to be too large most especially during nighttime for all the three

solar activities (Figs 3.16, 3.17 & 3.18). However, the agreement for the topside profiles during nighttime and noontime respectively for the month of June, 1968 was found to be good (Fig 3.17).

Also, both profiles represent the F2 peak region satisfactorily but show significant differences mostly at greater heights. Furthermore, the divergence or agreement tendencies of the experimental and predicted profiles' curvature was found to depend mainly on the value of the ionospheric parameters f_0F2 and h_mF2.

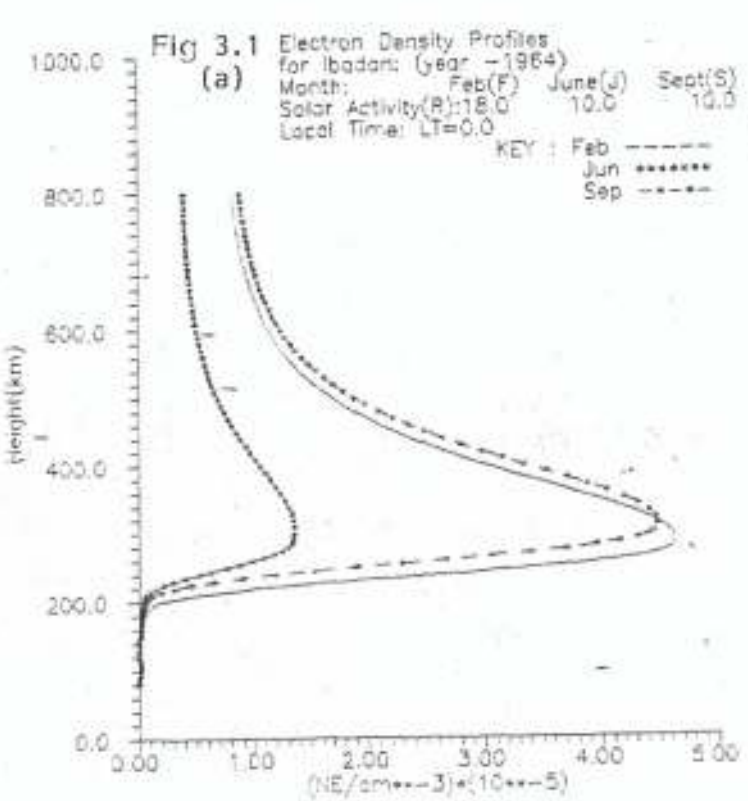
Fig 3.1 (a)
Electron Density Profiles
for Ibadan: (year -1964)
Month: Feb(F) June(J) Sept(S)
Solar Activity(R):18.0 10.0 10.0
Local Time: LT=0.0
KEY : Feb
Jun
Sep
1000.0
800.0
600.0
400.0
200.0
0.0
Height(km)
0.00
1.00
2.00
3.00
4.00
5.00
(NE/cm**-3)*(10**-5)

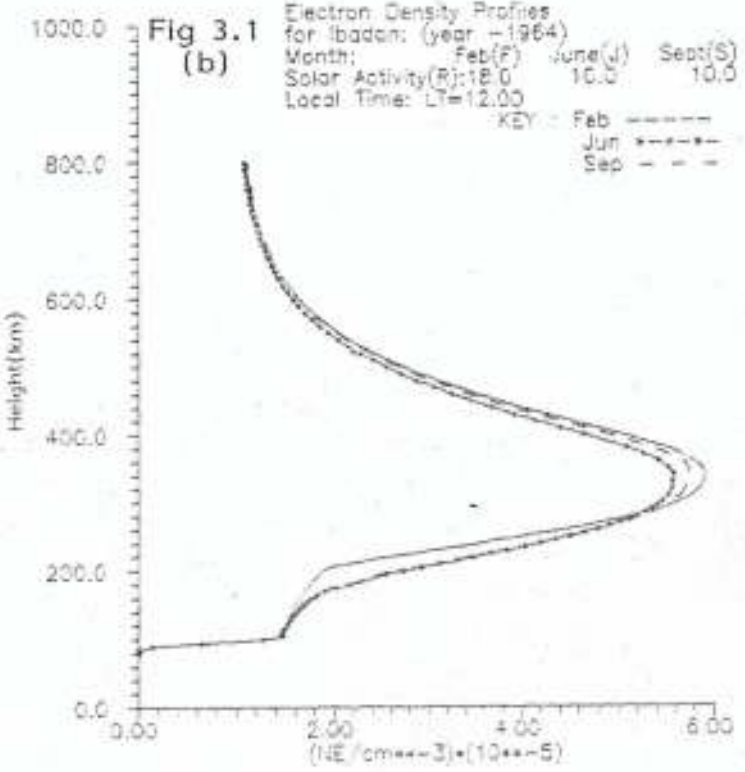
Fig 3.1 (b)
Electron Density Profiles
for Ibadan: (year -1964)
Month: Feb(F) June(J) Sept(S)
Solar Activity(R):18.0 10.0 10.0
Local Time: LT=12.00
KEY : Feb
Jun
Sep
1000.0
800.0
600.0
400.0
200.0
0.0
Height(km)
0.00
2.00
4.00
6.00
(NE/cm**-3)*(10**-5)

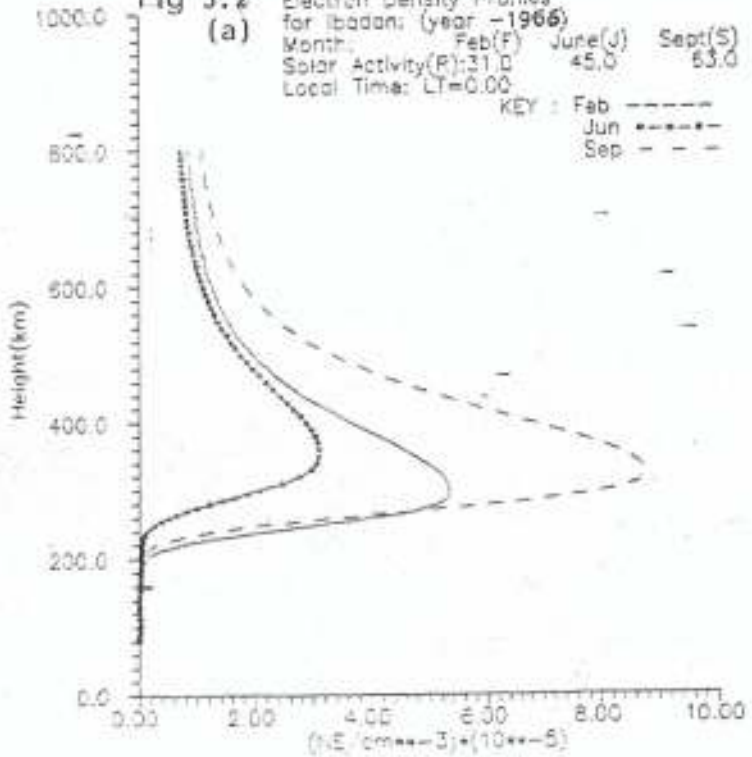
Fig 3.2
(a)
Electron Density Profiles
for Ibadan: (year -1966)
Month: Feb(F) June(J) Sept(S)
Solar Activity(R):31.0 45.0 63.0
Local Time: LT=0.00
KEY : Feb
Jun
Sep
Height(km)
1000.0
800.0
600.0
400.0
200.0
0.0
0.00
2.00
4.00
6.00
8.00
10.00
(NE/cm**-3)*(10**-5)

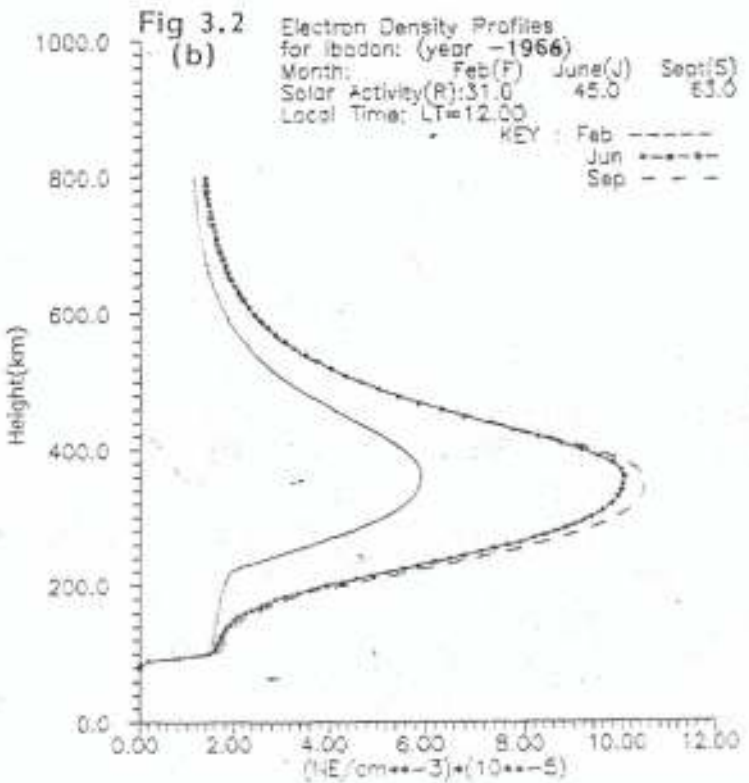
Fig 3.2
(b)
Electron Density Profiles
for Ibadan: (year -1966)
Month: Feb(F) June(J) Sept(S)
Solar Activity(R):31.0 45.0 63.0
Local Time: LT=12.00
KEY : Feb
Jun
Sep
Height(km)
1000.0
800.0
600.0
400.0
200.0
0.0
0.00
2.00
4.00
6.00
8.00
10.00
12.00
(NE/cm**-3)*(10**-5)

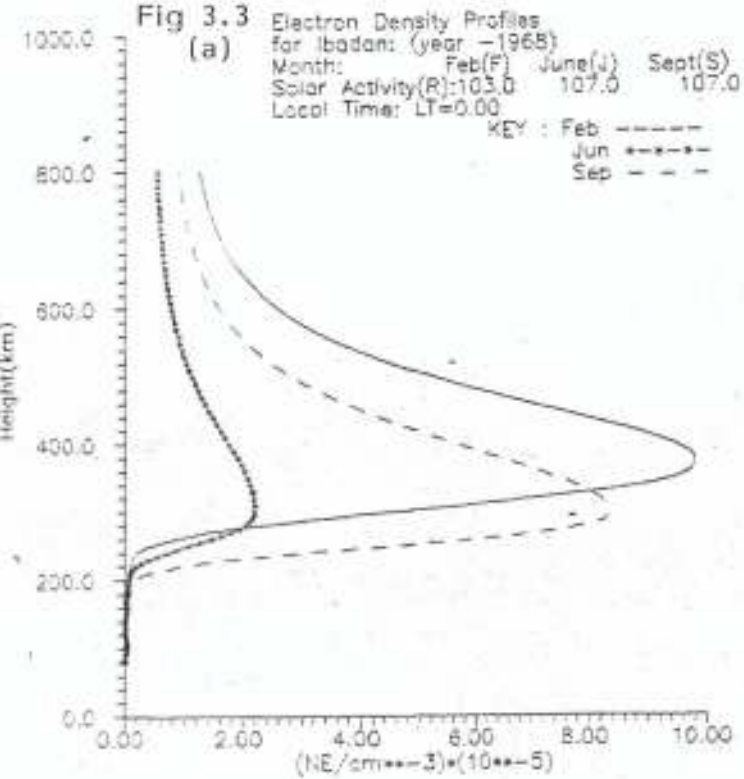
Fig 3.3 (a)
Electron Density Profiles
for Ibadan: (year -1968)
Month: Feb(F) June(J) Sept(S)
Solar Activity(R): 103.0 107.0 107.0
Local Time: LT=0.00
KEY : Feb ------
Jun *-*-*-
Sep - - -
Height(km)
1000.0
800.0
600.0
400.0
200.0
0.0
0.00
2.00
4.00
6.00
8.00
10.00
(NE/cm**-3)*(10**-5)

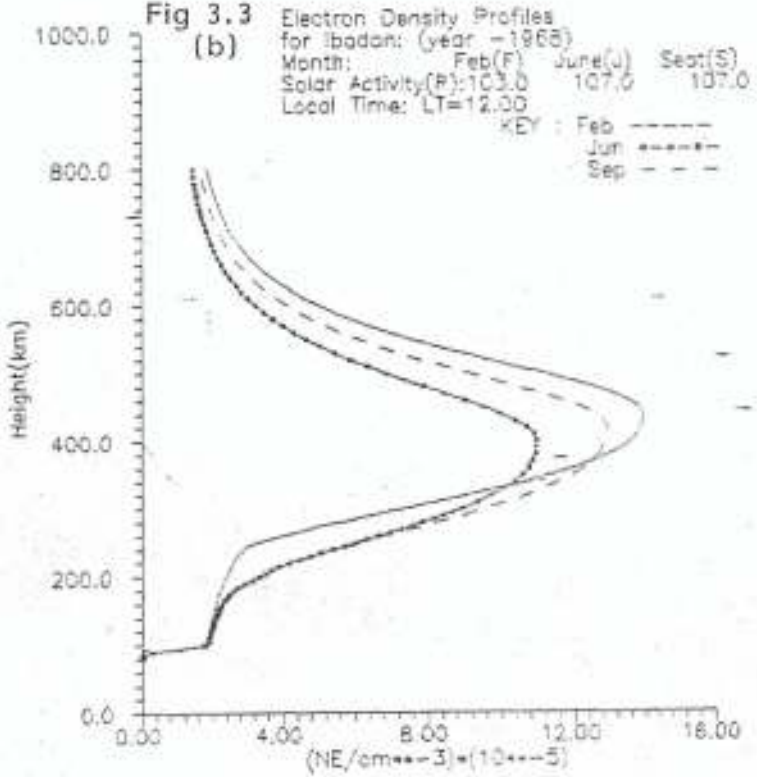
Fig 3.3 (b)
Electron Density Profiles
for Ibadan: (year -1968)
Month: Feb(F) June(J) Sept(S)
Solar Activity(R): 103.0 107.0 107.0
Local Time: LT=12.00
KEY : Feb ------
Jun *-*-*-
Sep - - -
Height(km)
1000.0
800.0
600.0
400.0
200.0
0.0
0.00
4.00
8.00
12.00
16.00
(NE/cm**-3)*(10**-5)

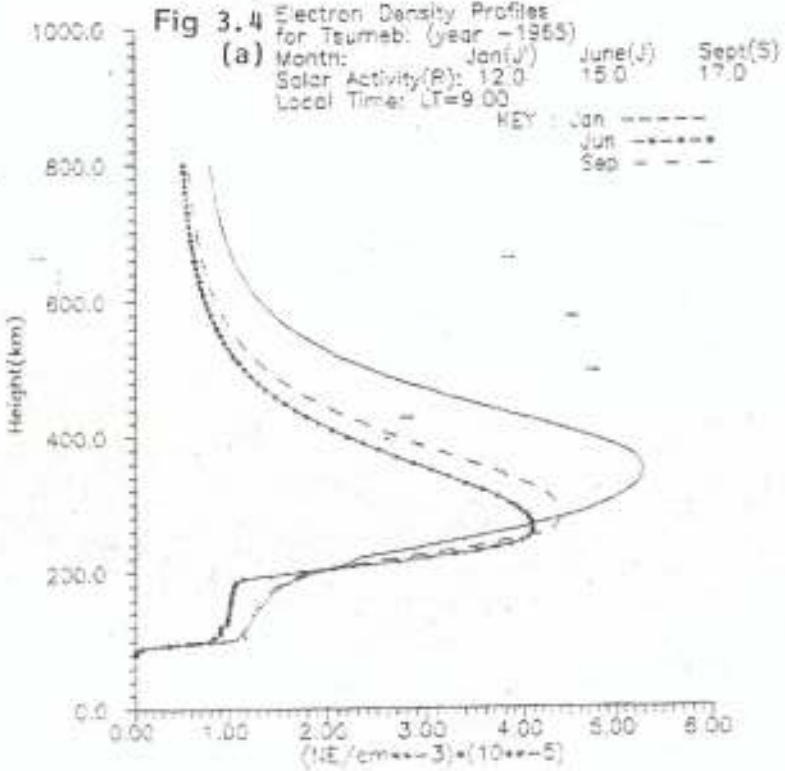
Fig 3.4 (a) Electron Density Profiles for Tsumeb: (year -1965)
Month: Jan(J') June(J) Sept(S)
Solar Activity(R): 12.0 15.0 17.0
Local Time: LT=9.00
KEY : Jan ------
Jun -*-*-*
Sep - - -
1000.0
800.0
600.0
400.0
200.0
0.0
Height(km)
0.00 1.00 2.00 3.00 4.00 5.00 6.00
(NE/cm**-3)*(10**-5)

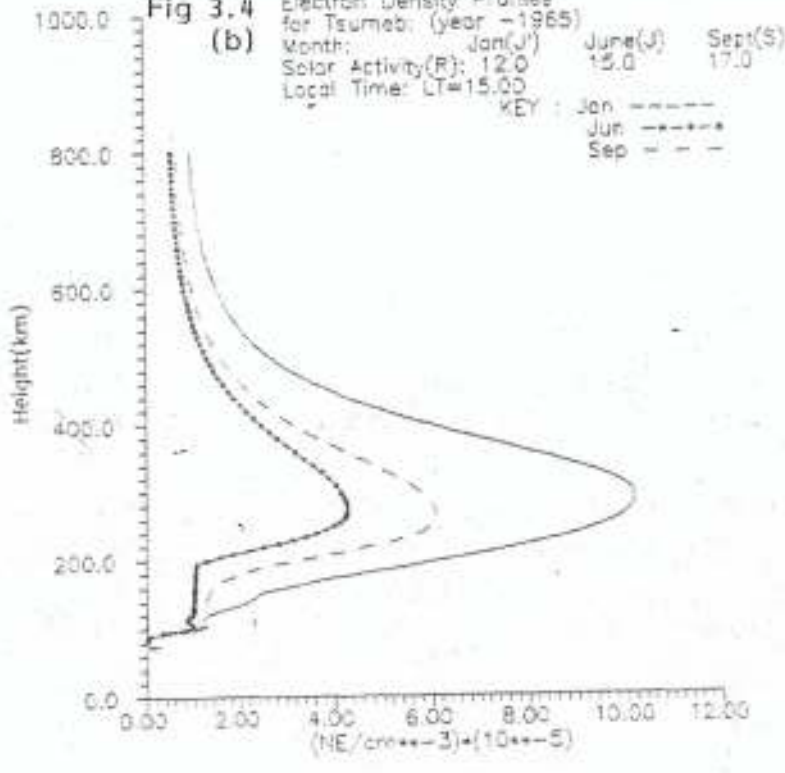
Fig 3.4 (b) Electron Density Profiles for Tsumeb: (year -1965)
Month: Jan(J') June(J) Sept(S)
Solar Activity(R): 12.0 15.0 17.0
Local Time: LT=15.00
KEY : Jan ------
Jun -*-*-*
Sep - - -
1000.0
800.0
600.0
400.0
200.0
0.0
Height(km)
0.00 2.00 4.00 6.00 8.00 10.00 12.00
(NE/cm**-3)*(10**-5)

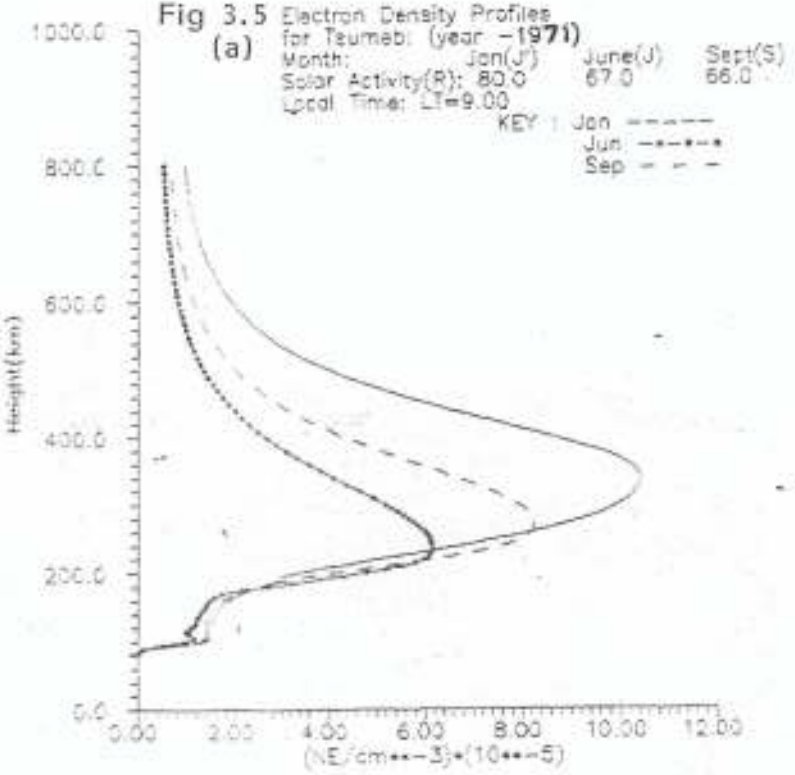
Fig 3.5 (a)
Electron Density Profiles
for Tsumeb: (year -1971)
Month: Jan(J') June(J) Sept(S)
Solar Activity(R): 80.0 67.0 66.0
Local Time: LT=9.00
KEY : Jan
Jun
Sep
1000.0
800.0
600.0
400.0
200.0
0.0
Height(km)
0.00 2.00 4.00 6.00 8.00 10.00 12.00
(NE/cm**-3)*(10**-5)

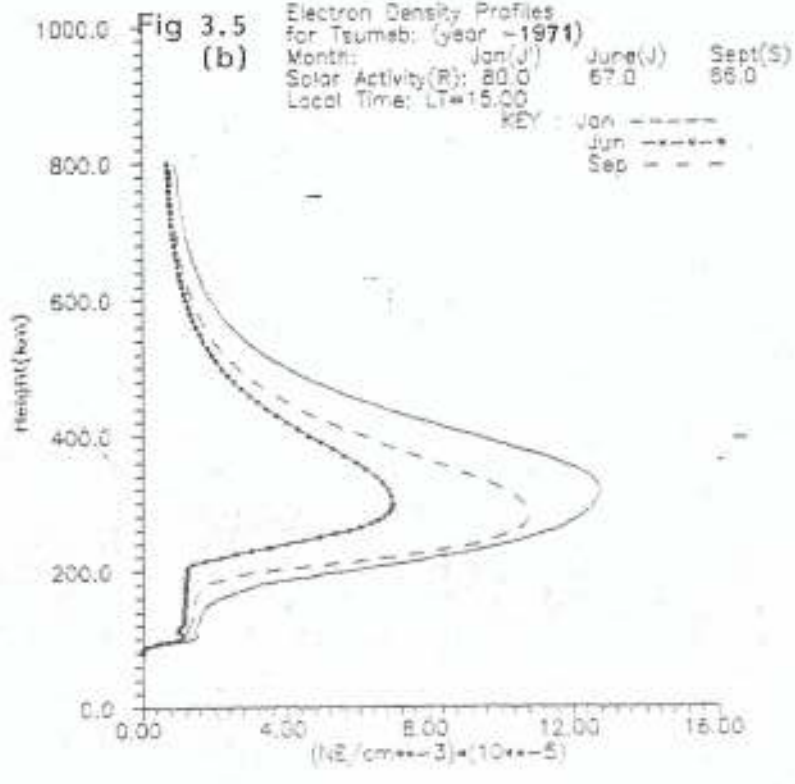
Fig 3.5 (b)
Electron Density Profiles
for Tsumeb: (year -1971)
Month: Jan(J') June(J) Sept(S)
Solar Activity(R): 80.0 67.0 66.0
Local Time: LT=15.00
KEY : Jan
Jun
Sep
1000.0
800.0
600.0
400.0
200.0
0.0
Height(km)
0.00 4.00 8.00 12.00 16.00
(NE/cm**-3)*(10**-5)

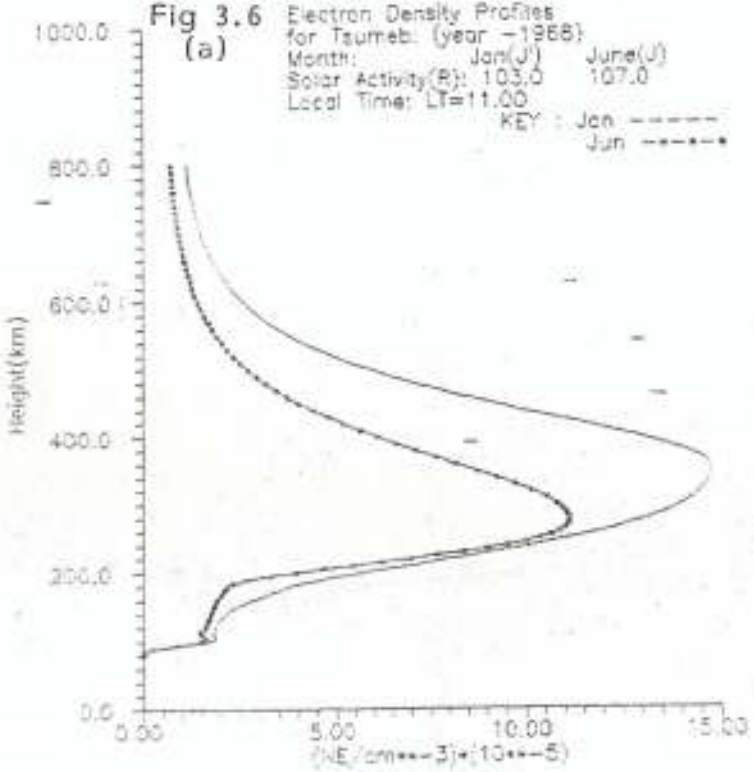
Fig 3.6 (a)
Electron Density Profiles
for Tsumeb: (year -1968)
Month: Jan(J') June(J)
Solar Activity(R): 103.0 107.0
Local Time: LT=11.00
KEY : Jan ------
Jun -*-*-*
1000.0
800.0
600.0
400.0
200.0
0.0
Height(km)
0.00
5.00
10.00
15.00
(NE/cm**-3)*(10**-5)

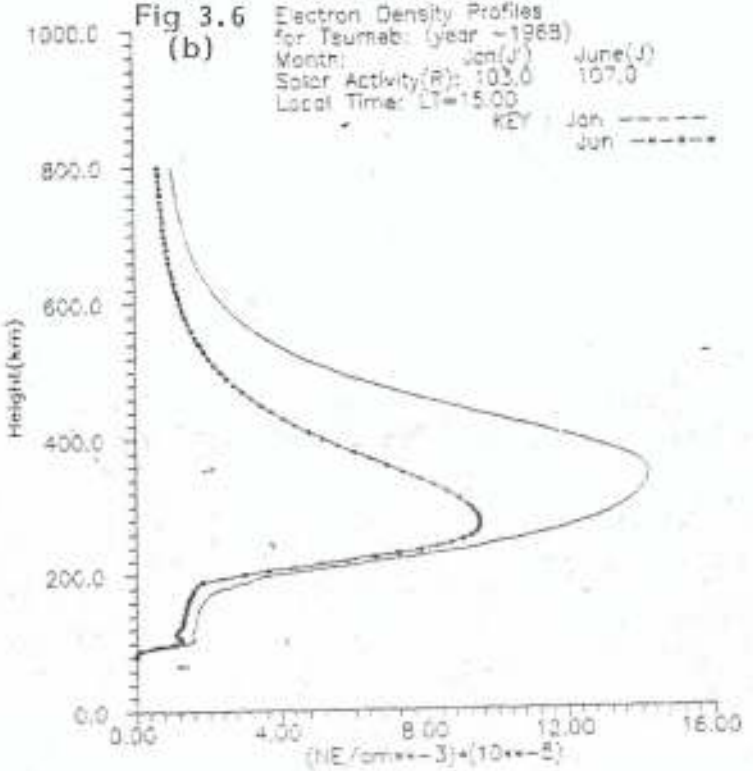
Fig 3.6 (b)
Electron Density Profiles
for Tsumeb: (year -1968)
Month: Jan(J') June(J)
Solar Activity(R): 103.0 107.0
Local Time: LT=15.00
KEY : Jan ------
Jun -*-*-*
1000.0
800.0
600.0
400.0
200.0
0.0
Height(km)
0.00
4.00
8.00
12.00
16.00
(NE/cm**-3)*(10**-5)

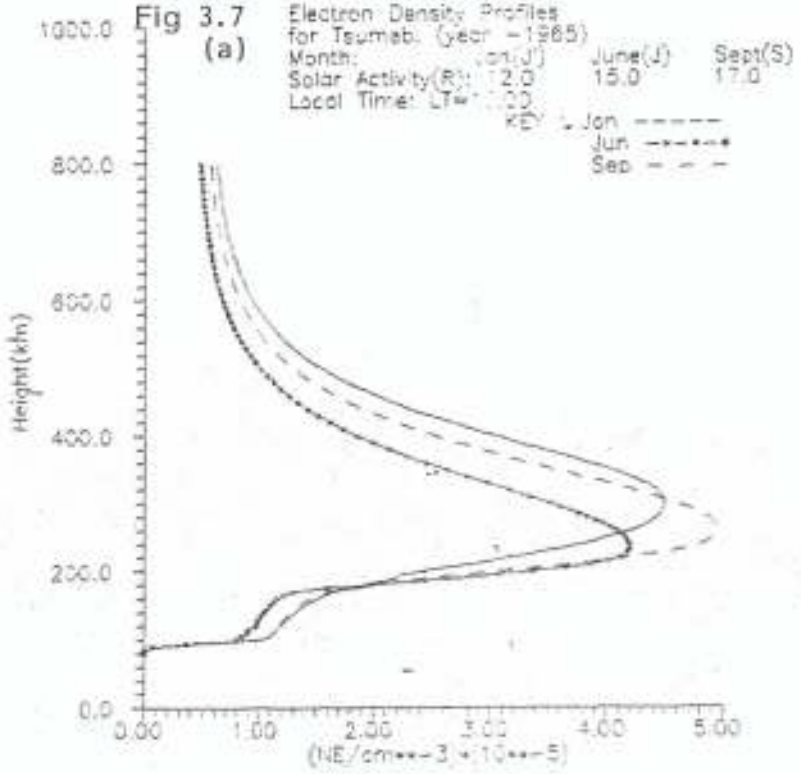
Fig 3.7
(a)
Electron Density Profiles
for Tsumeb: (year =1985)
Month: Jan(J') June(J) Sept(S)
Solar Activity(R): 12.0 15.0 17.0
Local Time: LT=15.00
KEY : Jan
Jun
Sep
1000.0
800.0
600.0
400.0
200.0
0.0
Height(km)
0.00
1.00
2.00
3.00
4.00
5.00
(NE/cm**-3)*(10**-5)

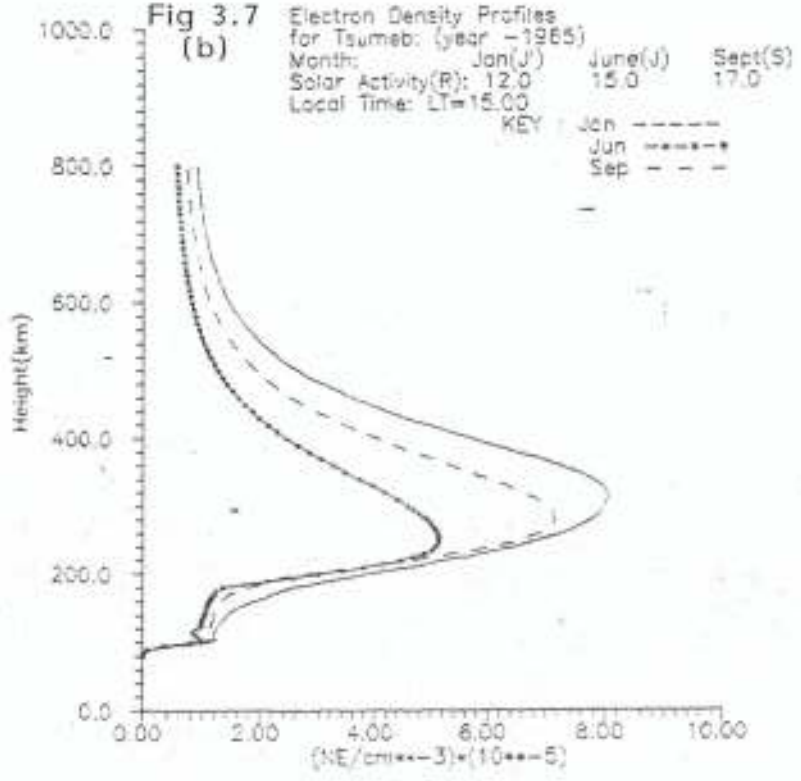
Fig 3.7
(b)
Electron Density Profiles
for Tsumeb: (year =1985)
Month: Jan(J') June(J) Sept(S)
Solar Activity(R): 12.0 15.0 17.0
Local Time: LT=15.00
KEY : Jan
Jun
Sep
1000.0
800.0
600.0
400.0
200.0
0.0
Height(km)
0.00
2.00
4.00
6.00
8.00
10.00
(NE/cm**-3)*(10**-5)

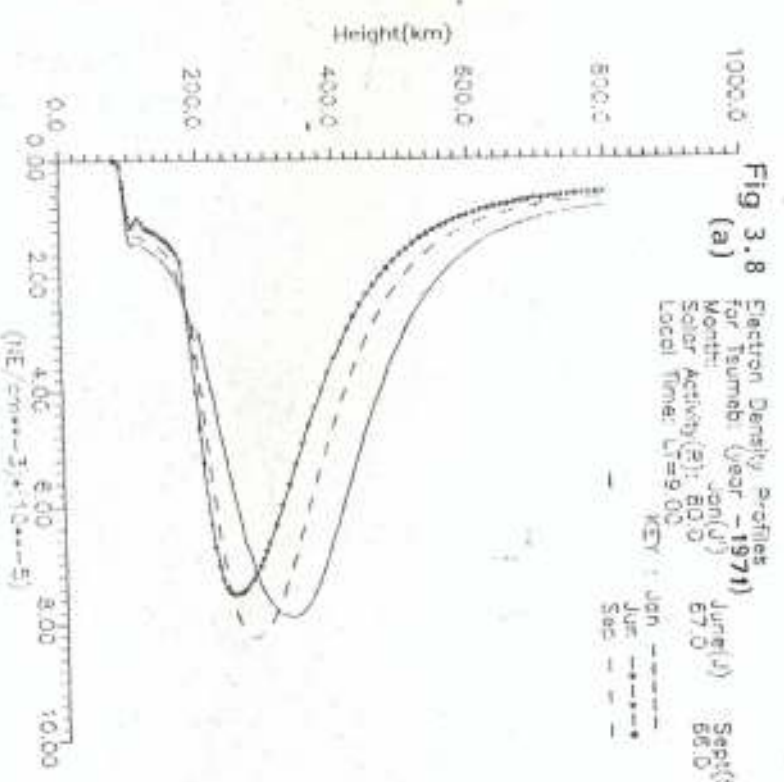

Fig 3.8 (a)

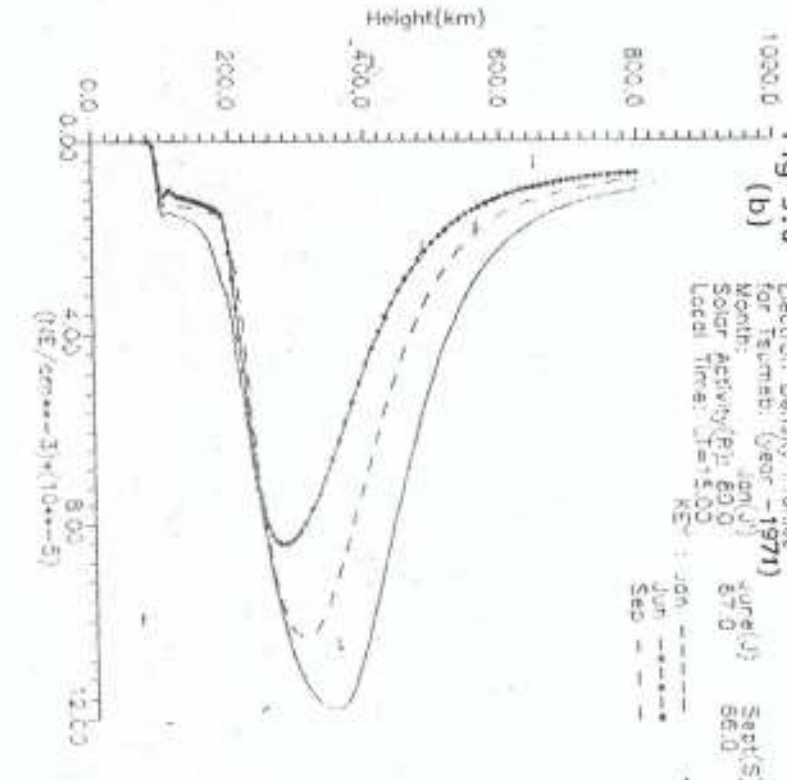

Fig 3.8 (b)

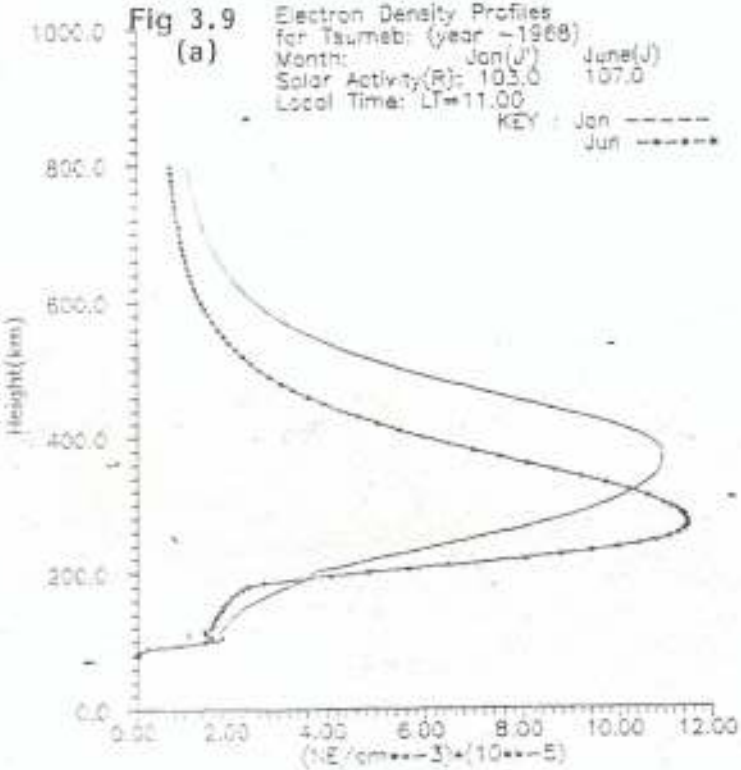
Fig 3.9
(a)
Electron Density Profiles
for Tsumeb: (year -1968)
Month: Jan(J) June(J)
Solar Activity(R): 103.0 107.0
Local Time: LT=11.00
KEY : Jan ------
Jun -*-*-*
1000.0
800.0
600.0
400.0
200.0
0.0
Height(km)
0.00
2.00
4.00
6.00
8.00
10.00
12.00
(NE/cm**-3)*(10**-5)

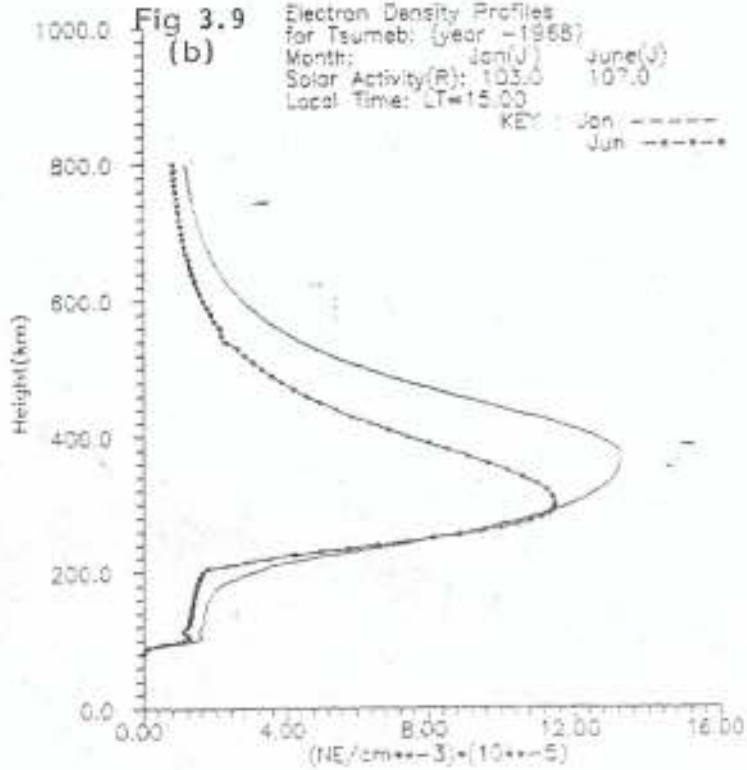
Fig 3.9
(b)
Electron Density Profiles
for Tsumeb: (year -1968)
Month: Jan(J) June(J)
Solar Activity(R): 103.0 107.0
Local Time: LT=15.00
KEY : Jan ------
Jun -*-*-*
1000.0
800.0
600.0
400.0
200.0
0.0
Height(km)
0.00
4.00
8.00
12.00
16.00
(NE/cm**-3)*(10**-5)

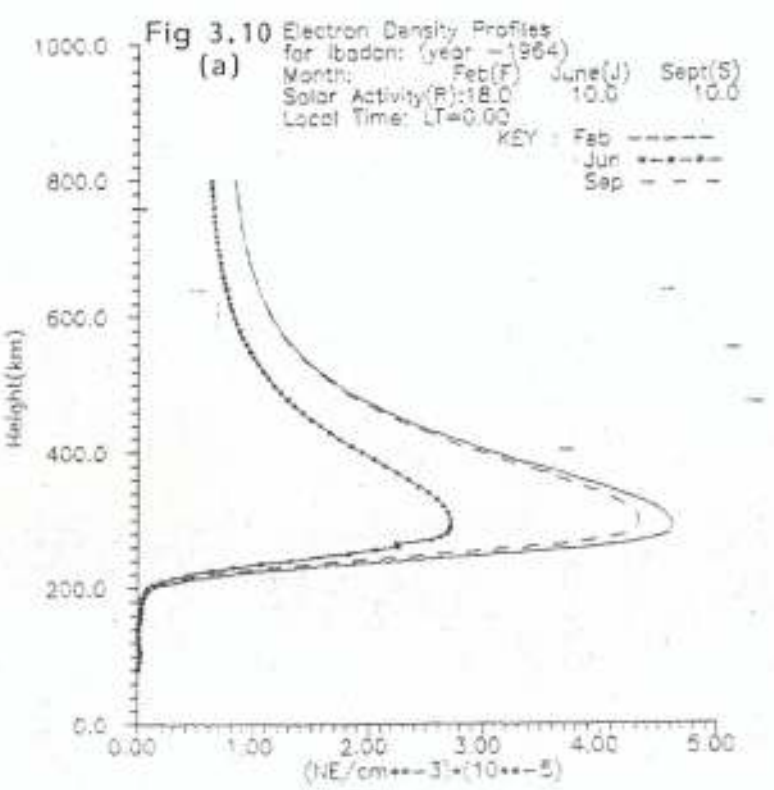
Fig 3.10 (a)
Electron Density Profiles
for Ibadan: (year -1964)
Month: Feb(F) June(J) Sept(S)
Solar Activity(R):18.0 10.0 10.0
Local Time: LT=0.00
KEY : Feb ------
Jun *-*-*-
Sep - - -
1000.0
800.0
600.0
400.0
200.0
0.0
Height(km)
0.00 1.00 2.00 3.00 4.00 5.00
(NE/cm**-3)*(10**-5)

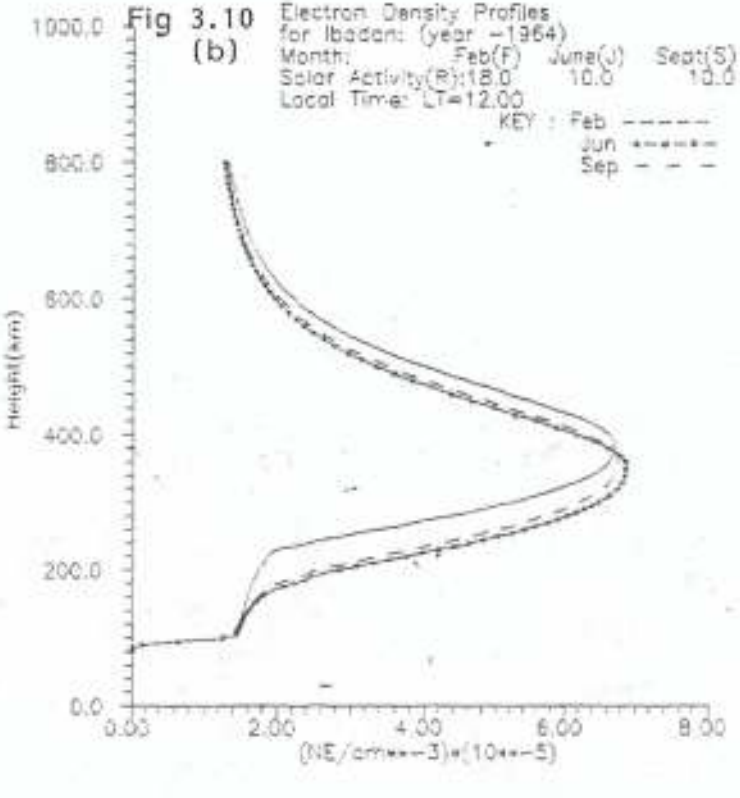
Fig 3.10 (b)
Electron Density Profiles
for Ibadan: (year -1964)
Month: Feb(F) June(J) Sept(S)
Solar Activity(R):18.0 10.0 10.0
Local Time: LT=12.00
KEY : Feb ------
Jun *-*-*-
Sep - - -
1000.0
800.0
600.0
400.0
200.0
0.0
Height(km)
0.00 2.00 4.00 6.00 8.00
(NE/cm**-3)*(10**-5)

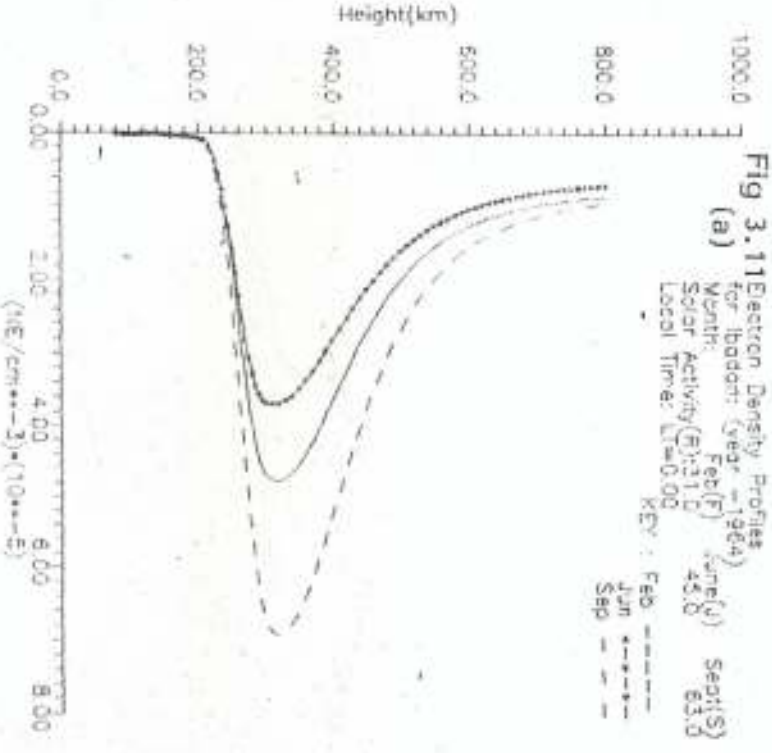

Fig 3.11 (a) Electron Density Profiles for Ibadan (year -1964)

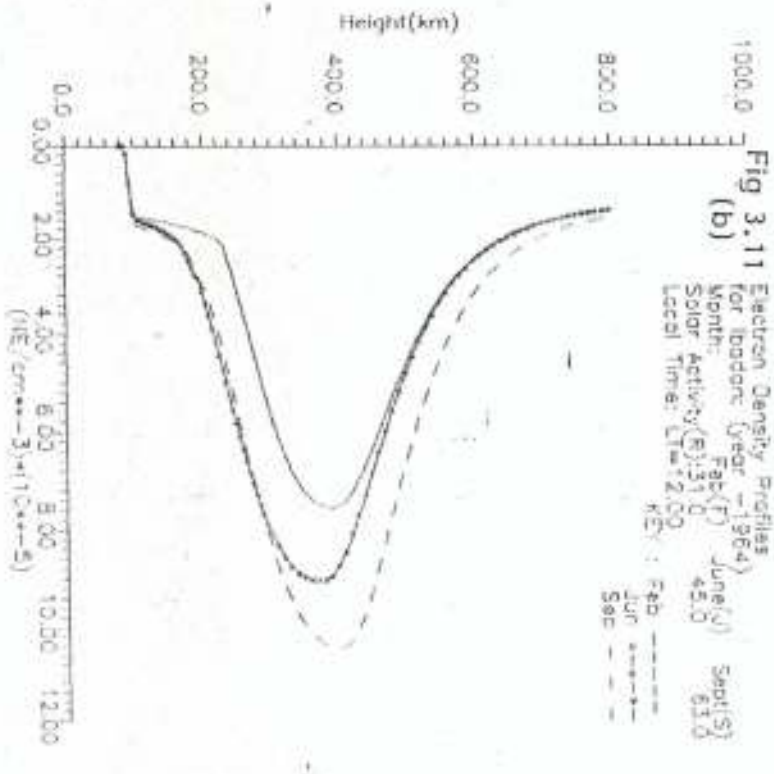

Fig 3.11 (b) Electron Density Profiles for Ibadan (year -1964)

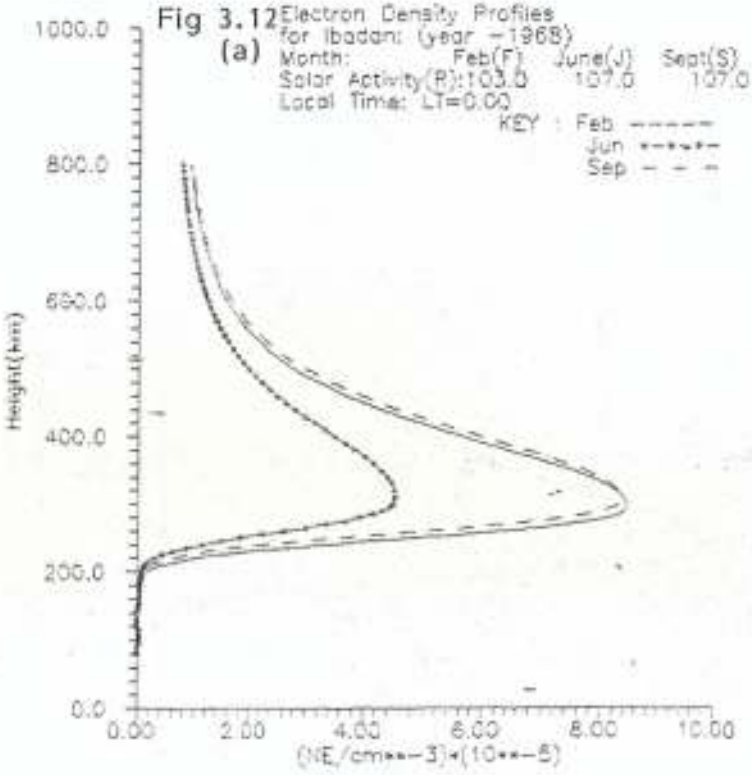
Fig 3.12 (a)
Electron Density Profiles for Ibadan: (year -1968)
Month: Feb(F) June(J) Sept(S)
Solar Activity(R): 103.0 107.0 107.0
Local Time: LT=0.00
KEY : Feb ------
Jun -*-*-*-
Sep - - - -
1000.0
800.0
600.0
400.0
200.0
0.0
Height(km)
0.00 2.00 4.00 6.00 8.00 10.00
(NE/cm**-3)*(10**-5)

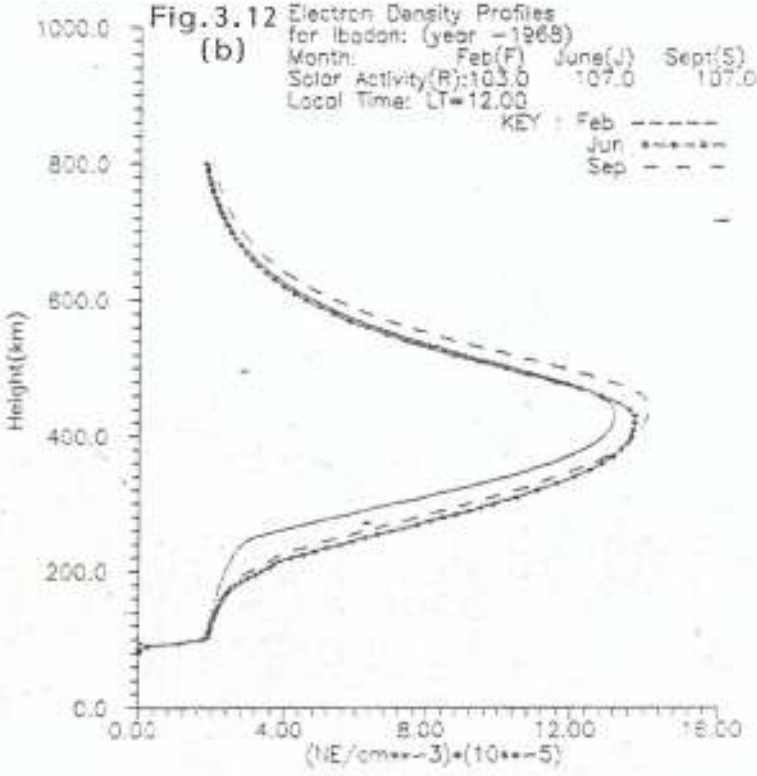
Fig. 3.12 (b)
Electron Density Profiles for Ibadan: (year -1968)
Month: Feb(F) June(J) Sept(S)
Solar Activity(R): 103.0 107.0 107.0
Local Time: LT=12.00
KEY : Feb ------
Jun -*-*-*-
Sep - - - -
1000.0
800.0
600.0
400.0
200.0
0.0
Height(km)
0.00 4.00 8.00 12.00 16.00
(NE/cm**-3)*(10**-5)

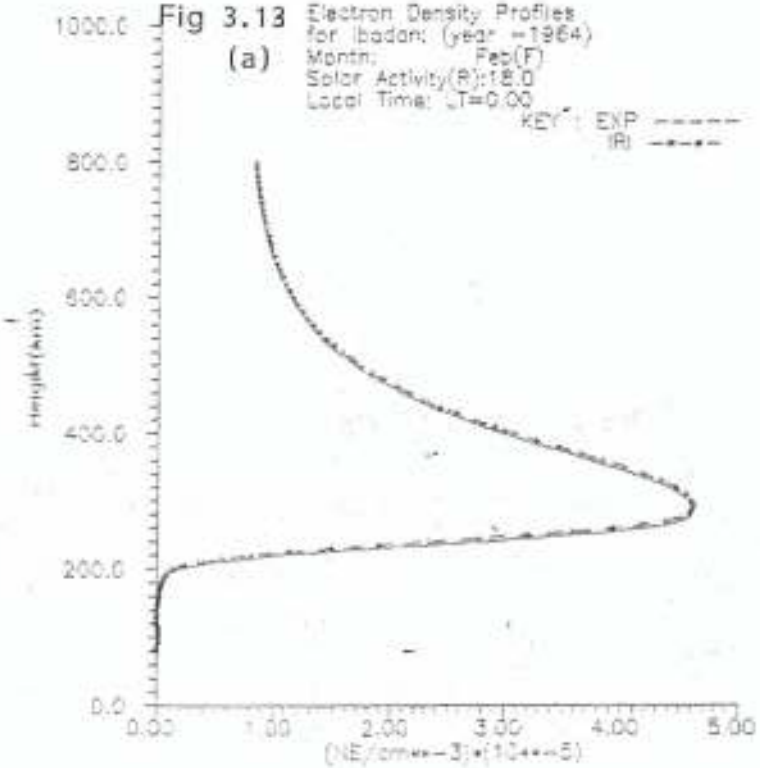
Fig 3.13 (a)
Electron Density Profiles
for Ibadan: (year =1964)
Month: Feb(F)
Solar Activity(R):18.0
Local Time: LT=0.00
KEY : EXP
(R)
1000.0
800.0
600.0
400.0
200.0
0.0
0.00
1.00
2.00
3.00
4.00
5.00
(NE/cm**-3)*(10**-5)

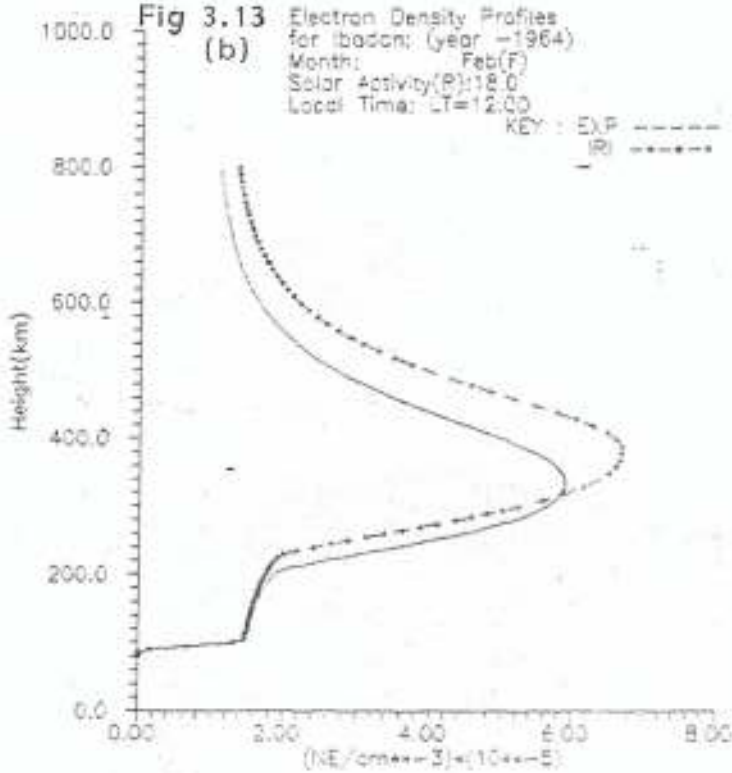
Fig 3.13 (b)
Electron Density Profiles
for Ibadan: (year =1964)
Month: Feb(F)
Solar Activity(R):18.0
Local Time: LT=12.00
KEY : EXP
(R)
1000.0
800.0
600.0
400.0
200.0
0.0
Height(km)
0.00
2.00
4.00
6.00
8.00
(NE/cm**-3)*(10**-5)

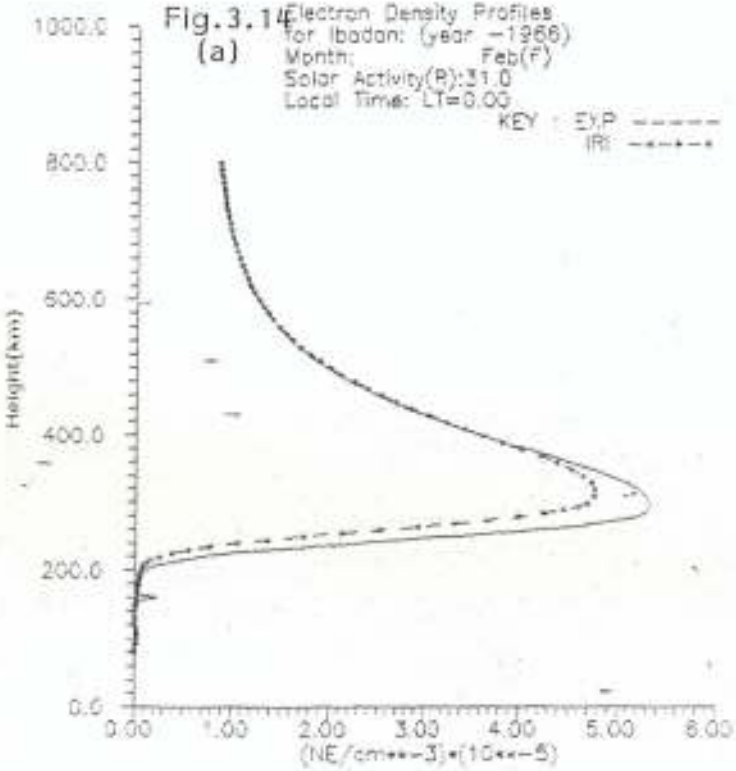
Fig.3.14 (a)
Electron Density Profiles
for Ibadan: (year -1966)
Month: Feb(F)
Solar Activity(R):31.0
Local Time: LT=0.00
KEY : EXP
IRI
1000.0
800.0
600.0
400.0
200.0
0.0
Height(km)
0.00
1.00
2.00
3.00
4.00
5.00
6.00
(NE/cm**-3)*(10**-5)

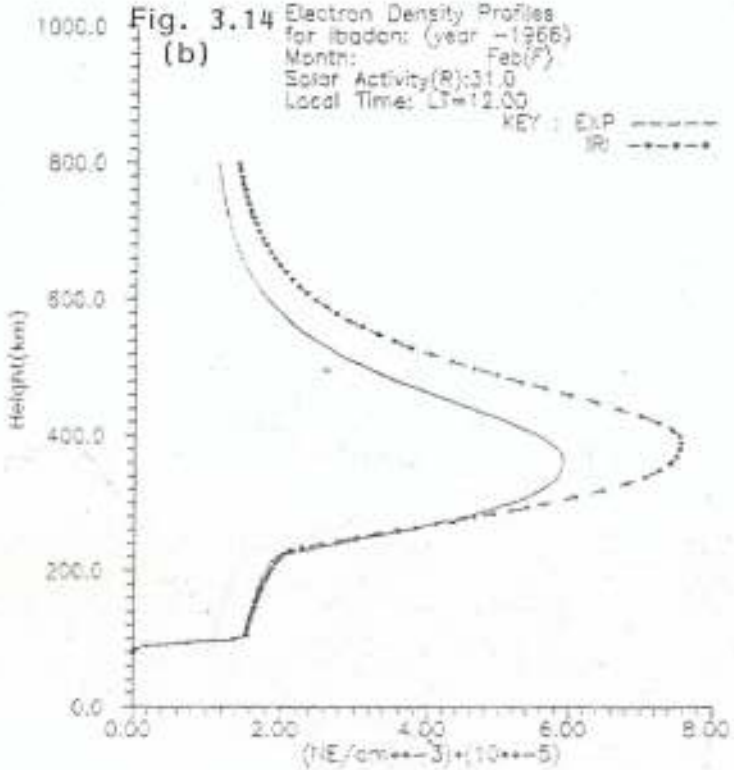
Fig. 3.14 (b)
Electron Density Profiles
for Ibadan: (year -1966)
Month: Feb(F)
Solar Activity(R):31.0
Local Time: LT=12.00
KEY : EXP
IRI
1000.0
800.0
600.0
400.0
200.0
0.0
Height(km)
0.00
2.00
4.00
6.00
8.00
(NE/cm**-3)*(10**-5)

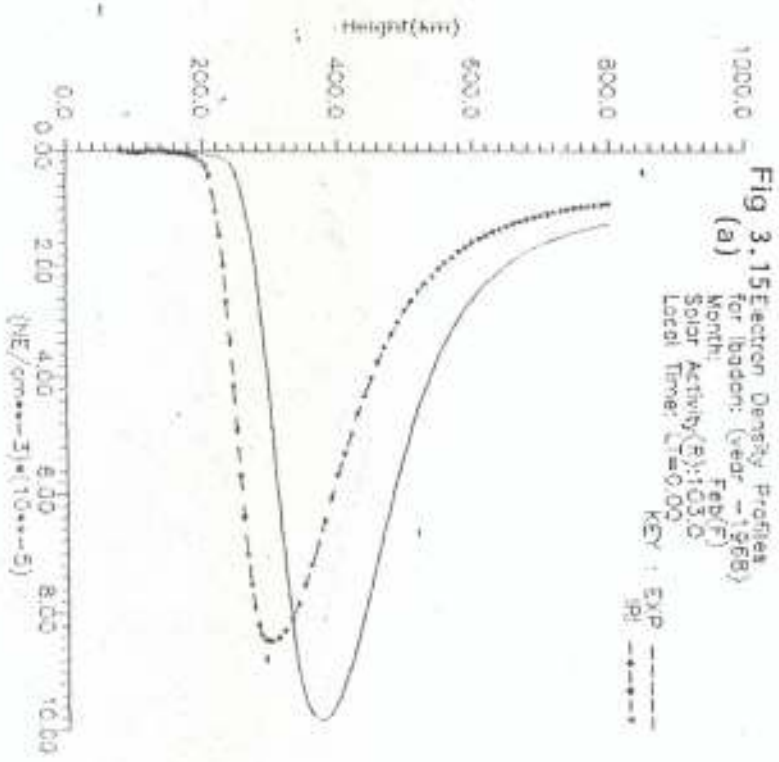

Fig 3.15 (a)

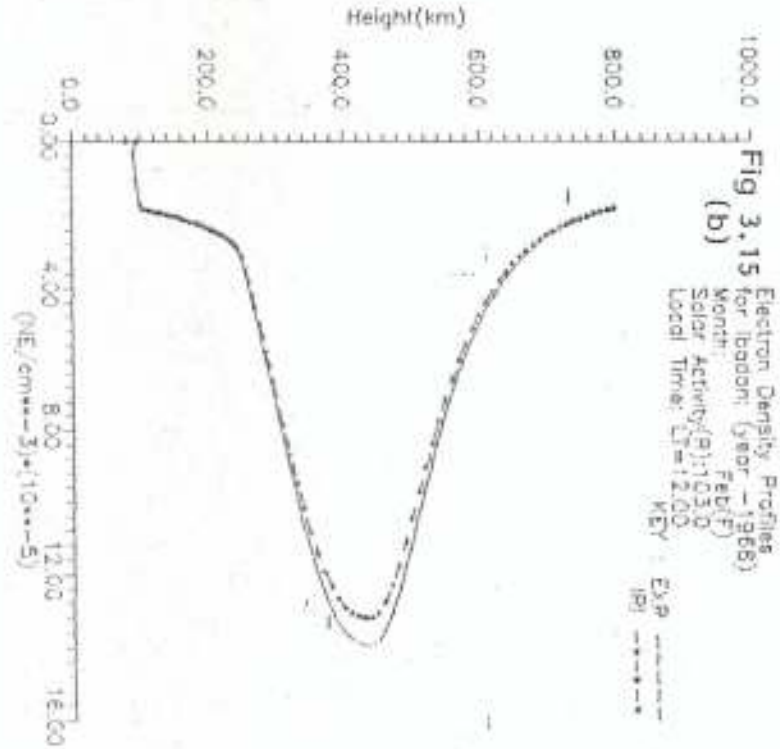

Fig 3.15 (b)

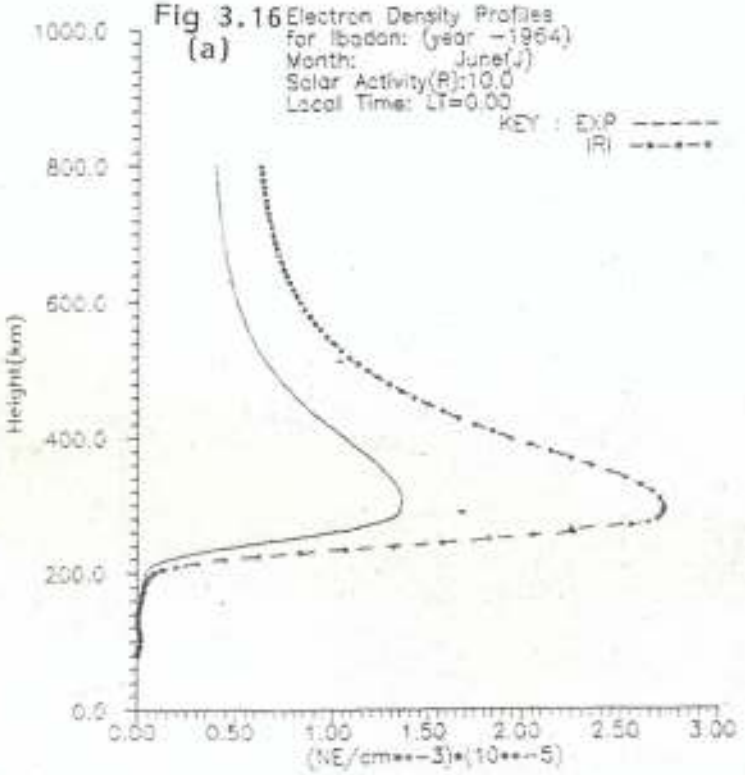
Fig 3.16 (a)
Electron Density Profiles
for Ibadan: (year -1964)
Month: June(J)
Solar Activity(R):10.0
Local Time: LT=0.00
KEY : EXP
(R)
1000.0
800.0
600.0
400.0
200.0
0.0
Height(km)
0.00
0.50
1.00
1.50
2.00
2.50
3.00
(NE/cm**-3)*(10**-5)

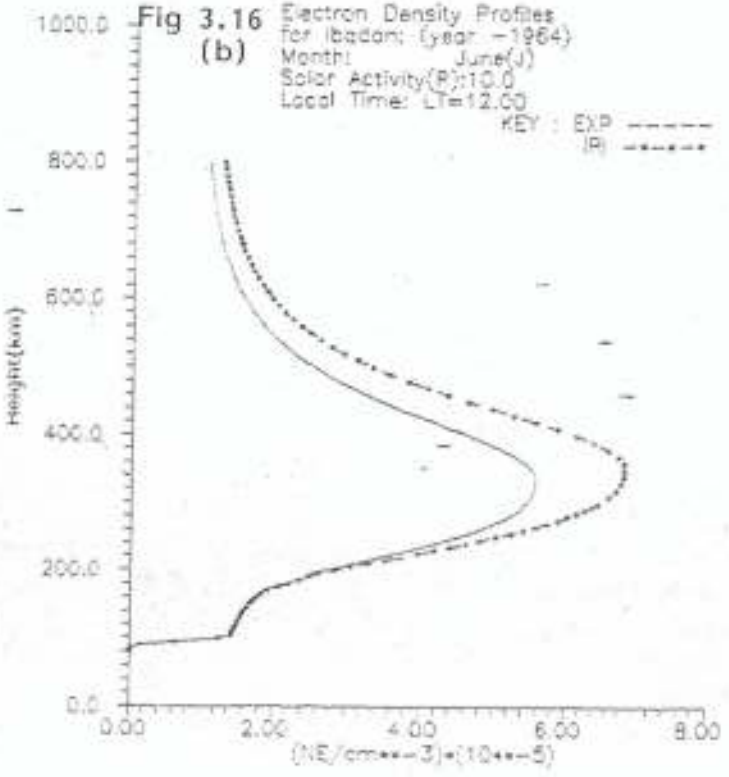
Fig 3.16 (b)
Electron Density Profiles
for Ibadan: (year -1964)
Month: June(J)
Solar Activity(R):10.0
Local Time: LT=12.00
KEY : EXP
(R)
1000.0
800.0
600.0
400.0
200.0
0.0
Height(km)
0.00
2.00
4.00
6.00
8.00
(NE/cm**-3)*(10**-5)

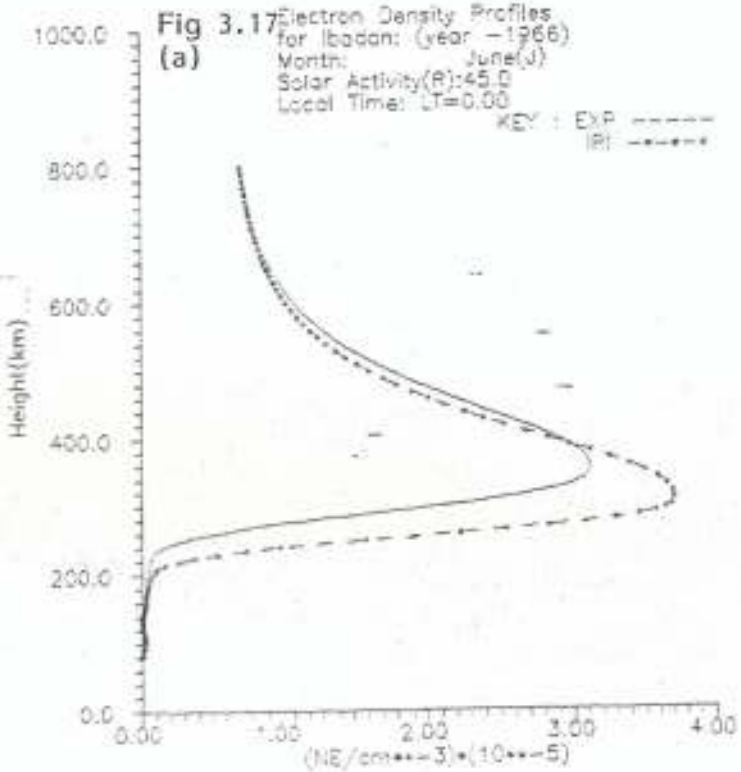
Fig 3.17 (a)
Electron Density Profiles
for Ibadan: (year −1966)
Month: June(J)
Solar Activity(R):45.0
Local Time: LT=0.00
KEY : EXP
IRI
1000.0
800.0
600.0
400.0
200.0
0.0
Height(km)
0.00
1.00
2.00
3.00
4.00
(NE/cm**-3)*(10**-5)

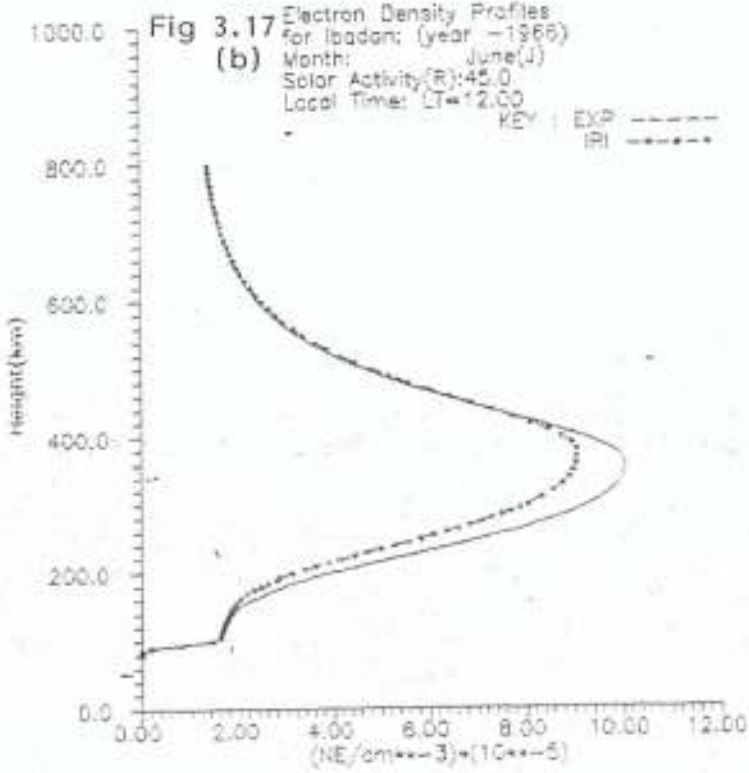
Fig 3.17 (b)
Electron Density Profiles
for Ibadan: (year −1966)
Month: June(J)
Solar Activity(R):45.0
Local Time: LT=12.00
KEY : EXP
IRI
1000.0
800.0
600.0
400.0
200.0
0.0
Height(km)
0.00
2.00
4.00
6.00
8.00
10.00
12.00
(NE/cm**-3)*(10**-5)

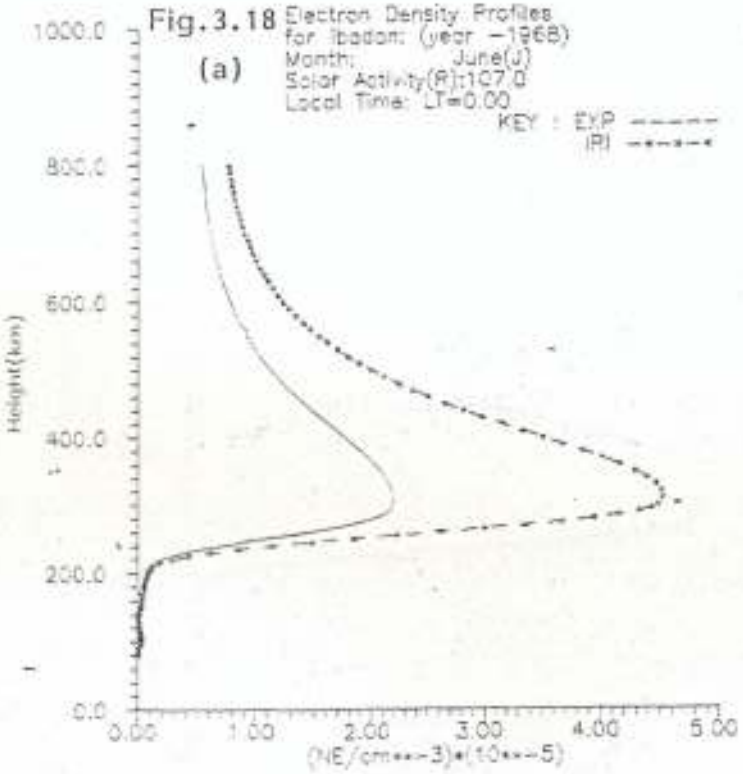
Fig. 3.18 Electron Density Profiles
for Ibadan: (year −1968)
(a)
Month: June(J)
Solar Activity(R):107.0
Local Time: LT=0.00
KEY : EXP
IRI
1000.0
800.0
600.0
400.0
200.0
0.0
Height(km)
0.00
1.00
2.00
3.00
4.00
5.00
(NE/cm**−3)*(10**−5)

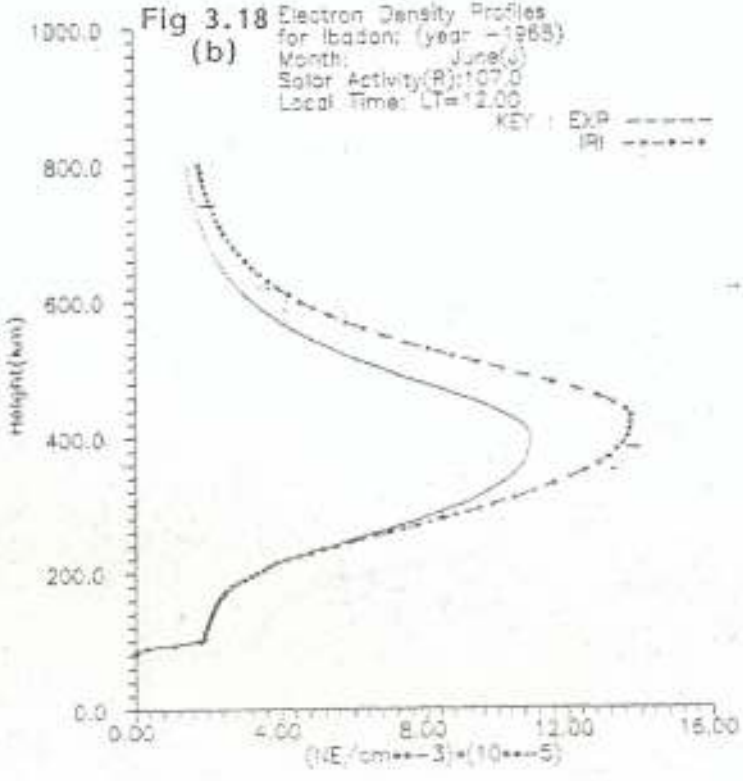
Fig 3.18 Electron Density Profiles
for Ibadan: (year −1968)
(b)
Month: June(J)
Solar Activity(R):107.0
Local Time: LT=12.00
KEY : EXP
IRI
1000.0
800.0
600.0
400.0
200.0
0.0
Height(km)
0.00
4.00
8.00
12.00
16.00
(NE/cm**−3)*(10**−5)

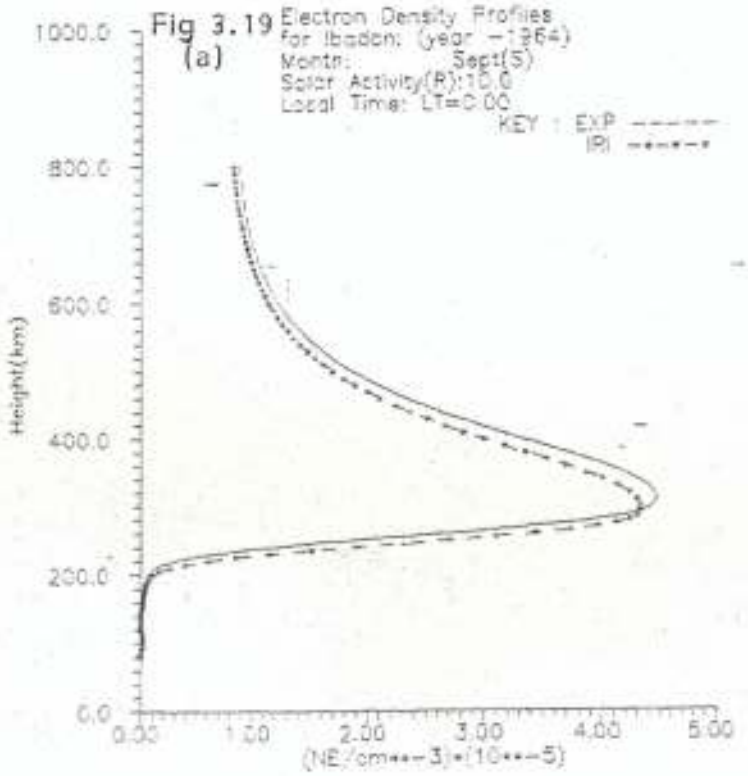
Fig 3.19 (a)
Electron Density Profiles
for Ibadan: (year -1964)
Month: Sept(5)
Solar Activity(R):10.0
Local Time: LT=0.00
KEY : EXP
(R)
1000.0
800.0
600.0
400.0
200.0
0.0
Height(km)
0.00
1.00
2.00
3.00
4.00
5.00
(NE/cm**-3)*(10**-5)

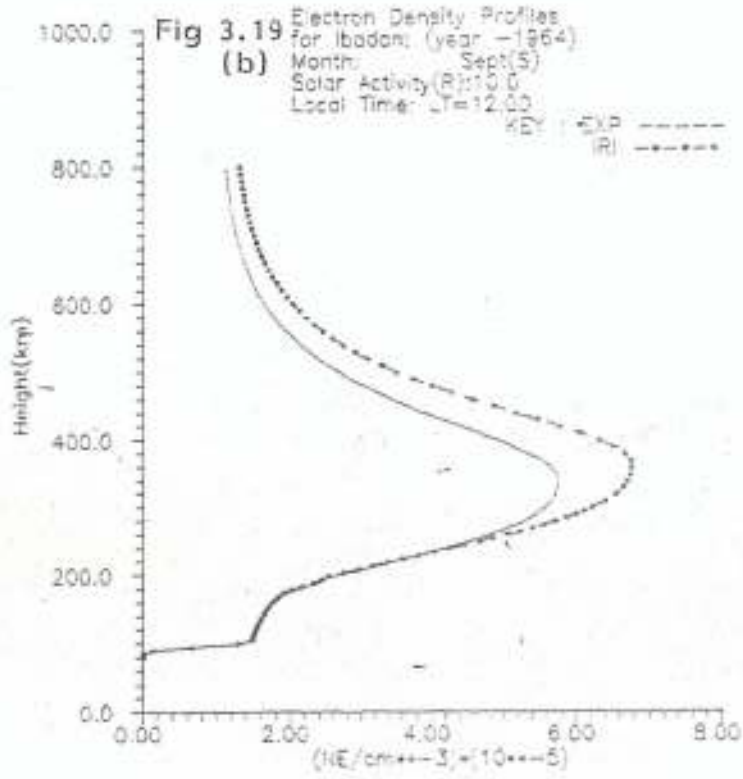
Fig 3.19 (b)
Electron Density Profiles
for Ibadan: (year -1964)
Month: Sept(5)
Solar Activity(R):10.0
Local Time: LT=12.00
KEY : EXP
(R)
1000.0
800.0
600.0
400.0
200.0
0.0
Height(km)
0.00
2.00
4.00
6.00
8.00
(NE/cm**-3)*(10**-5)

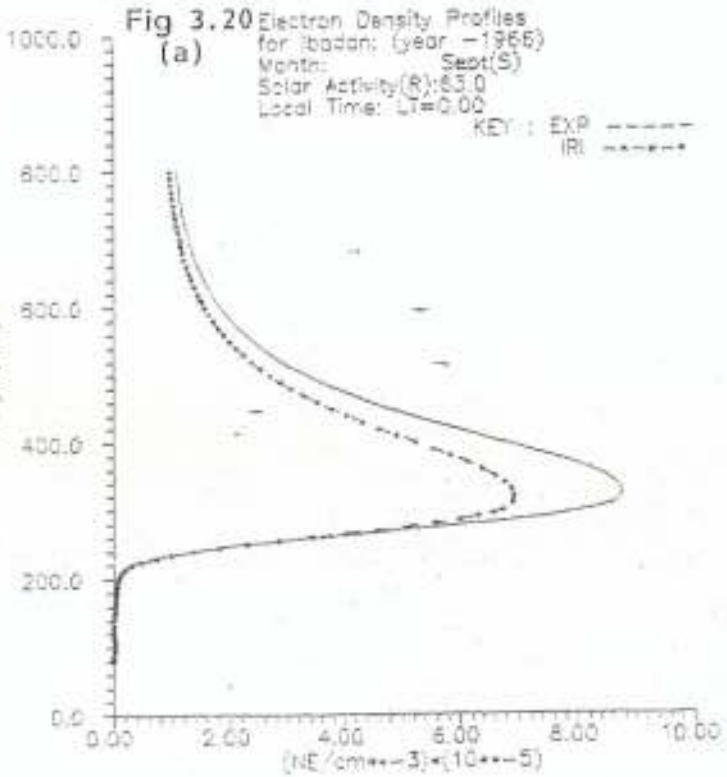
Fig 3.20 (a)
Electron Density Profiles
for Ibadan: (year -1966)
Month: Sept(S)
Solar Activity(R):63.0
Local Time: LT=0.00
KEY : EXP
IRI
1000.0
800.0
600.0
400.0
200.0
0.0
0.00
2.00
4.00
6.00
8.00
10.00
(NE/cm**-3)*(10**-5)

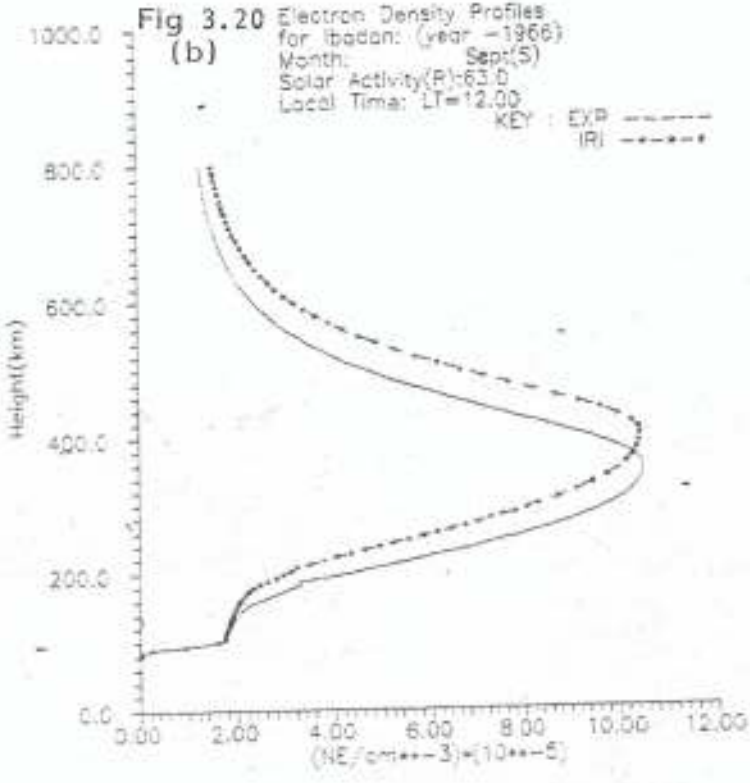
Fig 3.20 (b)
Electron Density Profiles
for Ibadan: (year -1966)
Month: Sept(S)
Solar Activity(R):63.0
Local Time: LT=12.00
KEY : EXP
IRI
1000.0
800.0
600.0
400.0
200.0
0.0
Height(km)
0.00
2.00
4.00
6.00
8.00
10.00
12.00
(NE/cm**-3)*(10**-5)

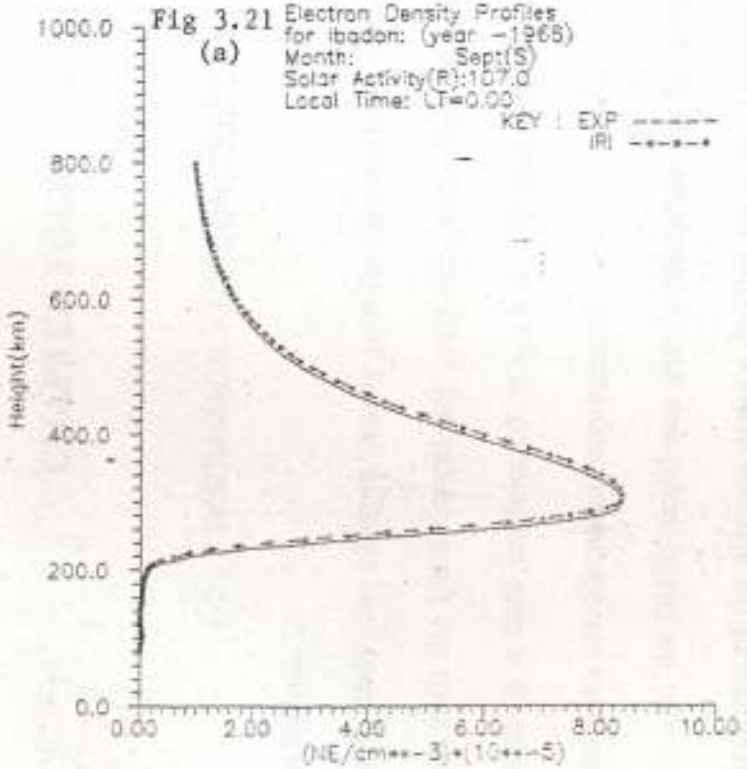
Fig 3.21 (a)
Electron Density Profiles
for Ibadan: (year -1965)
Month: Sept(S)
Solar Activity(R):107.0
Local Time: LT=0.00
KEY : EXP
IRI
1000.0
800.0
600.0
400.0
200.0
0.0
Height(km)
0.00
2.00
4.00
6.00
8.00
10.00
(NE/cm**-3)*(10**-5)

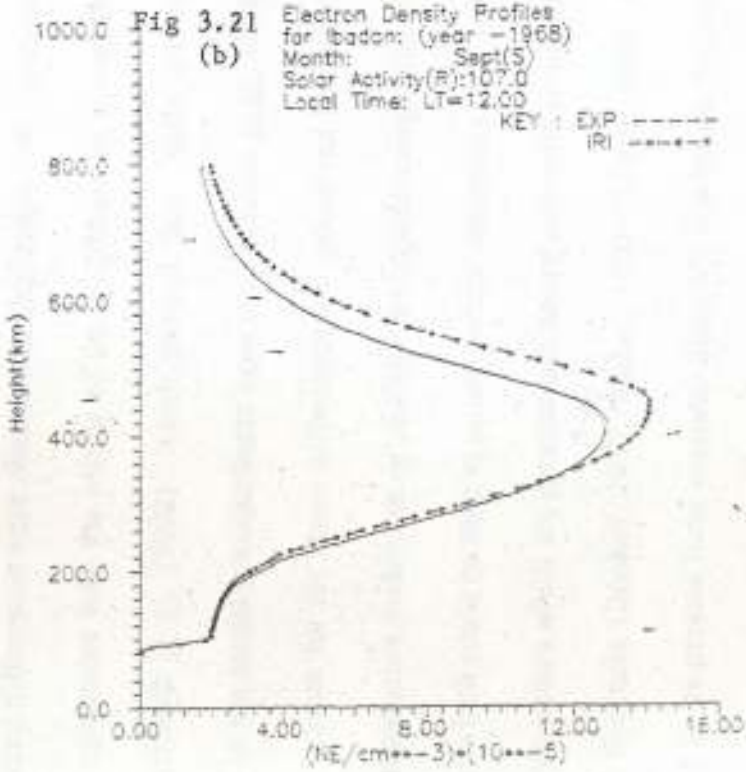
Fig 3.21 (b)
Electron Density Profiles
for Ibadan: (year -1968)
Month: Sept(S)
Solar Activity(R):107.0
Local Time: LT=12.00
KEY : EXP
IRI
1000.0
800.0
600.0
400.0
200.0
0.0
Height(km)
0.00
4.00
8.00
12.00
16.00
(NE/cm**-3)*(10**-5)

CHAPTER FOUR

4.0 DISCUSSION AND CONCLUSIONS.

4.1 Discussion.

In this study, the electron density profiles derived from observed data at Ibadan and Tsumeb with the IRI90 model are compared with those obtained from the CCIR predictions using a data set selected in such a way that diurnal, seasonal, and solar activity conditions are adequately represented.

Although, the IRI90 model was able to reproduce the features of the diurnal and seasonal variations of the electron density profiles for both observed and predicted data inputs, marked differences were observed in their respective representations. This result is quite in agreement with the results of the Validation of Ionospheric Models (VIM) study of Reinisch et al. (1992) which showed that, "there are significant seasonal differences in the model-measurements agreement" (Kecic et al, 1994).

The reasons for the above differences are indeed not far fetched. IRI90 electron density representation makes use of analytic description comprising of linear parameter (amplitudes) which could be used to satisfy certain constraints such as E and F peaks and non-linear parameters which are geometric in nature and could be interpreted as transition heights and thickness (Booker, 1977; Rawer, 1990; Bilitza, 1990). Furthermore, the IRI90 model in its present form excludes disturbed conditions (Bilitza, 1990; Benkova , 1990; Kecic et al, 1994).

In general, many phenomena observed in the equatorial and low-latitude E and F regions morphology have been explained in terms of the variations in the equatorial electrojet and the E x B drifts (Kolawole and Isherwood, 1980b; Rastogi et al, 1988;

Barbatsi, 1990; Adeniyi and Adimula, 1995). Also, the month to month variation in the E peak at low latitudes has been explained in terms of the geomagnetic control of the ionospheric E-region (Barbatsi, 1990). In addition, wind systems have also been considered to be one of the probable factors that influence ionospheric parameters in these regions (Barbatsi, 1990).

Therefore, there is the need to incorporate the results of studies on equatorial anomaly into the IRI model. For example, 'Noon bite-out' (a prenoon and postnoon peak with a minimum), during daytime and after sunset decay which is continuous at nighttime has been reported as some of the general features of equatorial F2 layer peak density at Ibadan (Kolawole and Isherwood, 1980a; Adeniyi and Adimula, 1995).

The investigations of ionospheric phenomena cannot be over emphasized considering its enourmous importance to radio propagation studies. In the study of empirical models of electron concentrations of the ionosphere and their values for communication purposes, the importance and relevance of ionospheric parameters f_0F2, h_mF2, f_0F1 and f_0E has been stressed (Dudeney and kressman, 1986).

However, in the study to investigate the significance of the various assumptions made in deriving simple equations for determining h_mF2 from the scaled ionospheric parameters f_0F2, f_0E and M(3000)F2, the effect of neglecting the spatial variations in the geomagnetic field has been shown to be small (Dudeney, 1983).

4.2 Conclusions.

Based on the findings of this study, it is necessary that further studies be carried out on the dependence of N_mF2 and h_mF2 on earth's magnetic dip angle, season and solar cycle. Example of further work would be an expansion of this study to 1.) cover more

ionospheric stations in the African sector and 2.) test larger sets of electron density profiles under different solar-geophysical conditions most especially during geomagnetically quiet and disturbed conditions.

In conclusion, it is expected that, with time, the IRI topside model would be considerably improved and the results of ionospheric drifts at low latitudes for diurnal, seasonal, and solar cycle variations would be updated and incorporated into the comprehensive IRI model. Such additional information and data would enhance the prediction and planning of the operational parameters for hf circuits in regions where there are dearths of ionosonde data.

Furthermore, if the peak values of the CCIR/IRI model are updated to higher solar activity above the present IRI validity level, a more profound improvement in the profile shape close to the peak would be achieved.

REFERENCES.

Adeniyi, J.O and I.A Adimula, (1995), Comparing the F2-layer model of IRI with observations at Ibadan, Advances in Space Research, Vol. 15, No. 2, pp 141 - 144.

Anderson D.N, M. Mendilo and B. Herniter (1987), A Semi-empirical low - latitude ionospheric model, Radio Science, Vol. 22, No. 2, pp 292- 306.

Anderson D.N, J.M Forbes and M. Codrescu (1989), A fully analytic low and middle latitude ionospheric model, Journal of GeophysicalResearch, Vol. 94, No. A2, pp 1520 - 1524.

Anderson D.N, A.J Preble, B.G Fejer, and P.H Patricia (1994), Comparison between calculated and observed F region electron density profiles at Jicamarca Peru, Vol. 29, No. 4, pp 857 - 866.

Barbatsi, K.K (1990), Geomagnetic control of the ionospheric E-region at three different latitudes in the European-African sector, Advances in Space Research, Vol. 10, No. 11, pp 89 - 92.

Beker, W. (1967), On the manual and digital computer methods used at Lindau for the conversion of multi-frequency ionograms to electron density-height profiles, Radio Science, vol. 2, No. 10, pp 1205 - 1232.

Benkova, N.P (1990), Comparison of topside electron density profiles in the subauroral ionosphere with IRI and SMI-85 models, Advances in space Research, Vol. 10, No. 11, pp 79 - 82.

Bent R.B, S.K Llewellyn and M.K Walloch (1972), Description and Evaluation of the Bent Ionospheric Model, Space and Missile Syst. Organ., Los Angeles California, Vol. 1, Rep. SAMSO TR-72-239.

Bilitza, D. (1986), International Reference Ionosphere: Recent developments, Radio Science, Vol. 21, No. 3, pp 343 - 346.

Bilitza, D. (1990), Progress Reports on IRI status, Advances in Space Research, Vol. 10, No. 11 pp (11)3 -(11)5.

Bilitza D., K. Rawer, L. Bossy, I. Kutiev, K. Oyama, R. Leitinger, and E. Kazimirovsky (1990), International Reference Ionosphere, National Space Science Data Centre / World Data Centre A for Rockets and Satellites, Boulder, Colorado, 156pp.

Booker, H.G (1977), Fitting the multi-region ionospheric profiles of the electron density by a single analytic function of height, Journal of Atmospheric and Terrestial Physics, Vol. 39, pp 619 - 623.

Bowman G.G, D.W Hainsworth and G.S Dunne (1986), A research oriented ionosonde with directional capabilities, Radio Science, Vol. 21, No. 3, pp 297 - 303.

Bradley, P.A and J.R Dudeney, (1973), A simple model of the vertical distribution of electron concentration in the ionosphere, Journal of Atmospheric and Terrestial Physics, Vol. 35, pp 2131 - 2146.

Bradley, P.A (1994), Further study of the f_0F2 and M(3000)F2 in different solar cycles, Annali Di Geofisica, Vol.37, No. 2, pp 201 - 207.

Budden, K.G. (1955), A method for determining the variation of electron density with height from curves of equivalent height against frequency, "The Physics of the Ionosphere", PP 332 - 339

Chiu, T. (1975), An improved phenomenological model of ionospheric density, Journal of Atmospheric and Terrestial Physics, Vol. 37, pp 1563 - 1570.

Davies, K. (1969), Ionospheric Radio Waves, Blaisdell Publishing Company, Colorado, 459pp.

Dudeney, J.R (1978), An improved model of the variation of electron concentration with height in the ionosphere, Journal of Atmospheric and Terrestial Physics, Vol. 40, pp 195 - 203.

Dudeney, J.R (1983), The accuracy of simple methods for determining the height of the maximum electron concentration of the F2-layer from scaled ionospheric characteristics, Journal of Atmospheric and Terrestial Physics, Vol. 45, No. 8/9, pp 629 - 640.

Dudeney, J.R and R.I Kressman, (1986), Empirical models of the electron concentration of the ionosphere and their value for radio communication purposes, Radio Science, Vol. 21, No. 3, pp 319 - 330.

Forbes J.M, D.N Anderson, M. Codrescu and P. Batista (1989), An analytic/ empirical model of middle and low latitude ionosphere, Tech. Report, Air Force Geophys. Labs.,Bedford,Massachusetts.

Kecic Z.J, P.A Bradley, L.R Cander, Dick M.I, and B. Zolezi (1994), Further test of the IRI and DGR model ionospheres, Annali Di Geofisica, Vol. 37, No. 2, pp 221 - 232.

Kolawole, L.B and M.C Isherwood, (1980a), Diurnal variations and semi-annual periodicities on F-region ionization at Ibadan over a solar cycle, Journal of Atmospheric and Terrestial Physics, Vol. 42, pp 257 - 260.

Kolawole, L.B and M.C Isherwood, (1980b), Low-latitude Model Electron Density Profiles Obtained by Empirical Procedures, Nigeria Journal of Science, Vol. 14, pp 114 - 124.

McNamara, L.F (1991), The Ionosphere: Communications, Surveillance and Direction Finding, Krieger Publishing Company, Florida, 237 pp.

Oyama, K. (1994), International Reference Ionosphere, URSI/COSPAR News Buletin, Vol. 1, No. 2, 8pp.

Oyinloye, J.O (1978), Radio Propagation Studies in Nigeria: Applications to Communications, Proceedings of the National symposium on Broadcasting in Nigeria, Ile - Ife, Nigeria, pp 143 - 177.

Paul, A.K (1967), Ionospheric electron density profiles with continuous gradients and underlying ionization convections, I , The mathematical-physical problems of real height determination from ionograms, Radio Science, Vol. 2, No. 10, pp 1127 - 1133.

Piggott, W.R and K. Rawer, (1978), URSI Handbook of ionogram interpretation and deduction, World Data Centre for Solar-Terrestial Physics Report UAG-23A, 2nd edition, 136 pp.

Rastogi R.G, S. Alex and M. Roy (1988), Effects of the electric field on Equatorial ionospheric plasma distribution, Journal of Atmospheric and Terrestial Physics, Vol. 50, pp 613 - 622.

Rawer, K. (1990), Proposed improvement of the IRI topside formular, Advances in Space Research, Vol. 10, No. 11, pp 75 - 78.

Reinisch B.W, D.A Anderson, R.R Gemache, X. Haung, C.F Chen and D.T Deker (1992), Validating ionospheric model with measured electron density profiles, Memoria -publicaciones del Observatorio del Ebro Roquetes, Vol.16, pp 41 - 52.

Rishbeth, H. and O.K Garrott, (1969), Introduction to ionospheric Physics, International Geophysics Series, Academic Press, New York, Vol. 14, 331 pp.

Titheridge, J.E (1961), A new method for the analysis of ionospheric h'(f) records, Journal of Atmospheric and Terrestial Physics, No. 28,pp1135 - 1150.

Titheridge, J.E (1967), The overlapping-polynomial analysis of ionograms, Radio Science, Vol. 2, No. 10, pp 1169 - 1175.

Wernik, A.W (1991), Ionospheric Modeling and Ionospheric Irregularities, conference on major scientific problems of the Atmospheric system and the developing countries, ICTP, Trieste, Italy, 28pp.